Infocommunications Journal

A PUBLICATION OF THE SCIENTIFIC ASSOCIATION FOR INFOCOMMUNICATIONS (HTE)

September 2019 Volume XI Number 3 ISSN 2061-2079

Technically Co-Sponsored by
IEEE ComSoc IEEE Communications Society
hte
IEEE HUNGARY SECTION
HTE for 70 years

Indexing information

Infocommunications Journal is covered by Inspec, Compendex and Scopus.

Infocommunications Journal is also included in the Thomson Reuters – Web of ScienceTM Core Collection, Emerging Sources Citation Index (ESCI)

Infocommunications Journal

Technically co-sponsored by IEEE Communications Society and IEEE Hungary Section

Supporters

FERENC VÁGUJHELYI – president, National Council for Telecommunications and Information Technology (NHIT)

GÁBOR MAGYAR – president, Scientic Association for Infocommunications (HTE)

Editorial Office (Subscription and Advertisements)**:**
Scientic Association for Infocommunications
H-1051 Budapest, Bajcsy-Zsilinszky str. 12, Room: 502
Phone: +36 1 353 1027
E-mail: info@hte.hu • Web: www.hte.hu

Articles can be sent also to the following address:
Budapest University of Technology and Economics
Department of Telecommunications and Media Informatics
Phone: +36 1 463 4189, Fax: +36 1 463 3108
E-mail: pvarga@tmit.bme.hu

Subscription rates for foreign subscribers: 4 issues 10.000 HUF + postage

Publisher: PÉTER NAGY

HU ISSN 2061-2079 • Layout: PLAZMA DS • Printed by: FOM Media

Indexing current advances with DOI – at the Infocommunications Journal

Pal Varga

THE vast domain of Infocommunications reach from the physics of wireless and wired communication channels, through traversing the information – in a secure way – to its destination(s) to analyzing the characteristics of that transmission.

Since the area is huge, categorizing advances is hard. We operate with keywords – index terms –, text-mining of research papers, and creating clusters based on similar set of areas involved in these papers. The survey papers that keep appearing in our journal is useful in this sense as well: connecting and summarizing the current knowledge of a field – even if it has just emerged. In order to help indexing of our journal papers and the ones cited inside, we encourage our authors to reference the DOI – Document Object Identifier – of their cited articles, and we make sure these DOIs point to the source of the document, making it easier for the readers to reach it directly. This activity is animated by DOI commissioners such as the Hungarian Academy of Sciences, who helps us assigning DOIs through the original DOI provider, CrossRef.

The six papers of this issue includes an invited survey and five papers that arrived to the open call. Let us have a brief overview of these papers.

In their survey paper on cellular MIMO systems, Fodor, Pap and Telek discussed recent advances in the field of Channel State Information (CSI) acquisition and managing the inherent tradeoff between using time, frequency and power resources for CSI acquisition and transmitting data symbols. As they describe, managing this tradeoff has a large impact on the achievable spectral efficiency in cellular systems, in which the number of transmit and receive antennas grows large. They make the point that the joint allocation of frequency, time and power resources is subject to constraints that depend on the specific pilot pattern, described in the paper.

In their study, Çiftlikli et. al. considers the transceiver design for multi-user MIMO (MU-MIMO) communications, in which a single transmitter adopts beamforming to simultaneously transmit information at the first time-slot. beamforming to simultaneously transmit information at first During the second time-slot, receivers cooperate to share specific results of OSIC detection in each user. They propose the maximum-likelihood (ML) approach to estimate the received symbols, claiming that their solution does not increase the system complexity significantly.

In his paper, Roman Ipanov describes, sythesizes, and discusses the various characteristics of the polyphase (p-phase, where p is the prime integer number) radar signal. This signal has an area of zero side lobes in a vicinity of the central peak of autocorrelation function. He shows that this signal represents a train from p coherent phase-code-shift keyed pulses, which are coded by complementary sequences of the p-ary D-code.

Our distinguished author, Sergey M. Smolskiy teamed up with Dmitrii I. Popov in their recent article on non-recursive rejection filters (RF) in the transient mode. They achieved RF modernization by its structure adjustment according to results of clutter edge detection, which leads to its effectiveness increase in the transient mode sequentially from one pulse to another.

Alawadi, Zaher and Molnar introduce novel methods for predicting behavior of elephant flows in Data Center Networks. In their paper, they empirically designed, implemented, and analyzed a new performance evaluation model for flow scheduling and flow congestion control algorithms used in data center networks based on multiple stochastic workloads to predict the value at risk of the elephant flows loss rate.

In their paper, Li, Wu and Wang propose a Deep Web data source classification method based on text feature extension and extraction. The experimental results not only show that their model has significant advantages over the previous methods, but also prove that the use of the Attention mechanism can improve the precision without a huge increase in the cost of training time.

Let us again stop for awhile and think of the seventy years that has passed since our HTE, the Scientific Association for Infocommunications, has born. It must be hard for most of us, since we have not been involved in research those times – so let us remember the ten years for our Journal. In both cases, this is a year for celebration: remembering some legendary achievements, and aiming for new challenges.

Pal Varga received the M.Sc. and Ph.D. degrees from the Budapest University of Technology and Economics, Hungary, in 1997 and 2011, respectively. He is currently an Associate Professor at the Budapest University of Technology and Economics. Besides, he is also the Director at AITIA International Inc. Earlier, he was working for Ericsson, Hungary, and Tecnomen, Ireland. His main research interests include communication systems, network performance measurements, root cause analysis, fault localisation, traffic classification, end-to-end QoS and SLA issues, as well as hardware acceleration. Recently he has been actively engaged with research related to Cyber-Physical Systems and Industrial Internet of Things. He has been involved in various industrial as well as European research and development projects in these topics. Besides being a member of HTE, he is a member of both the IEEE ComSoc (Communication Society) and IEEE IES (Industrial Electronics Society) communities, and the Editor-in-Chief of the Infocommunications Journal.

DOI: 10.36244/ICJ.2019.3.1

Recent Advances in Acquiring Channel State Information in Cellular MIMO Systems

Gábor Fodor[1,2], László Pap[3] and Miklós Telek[3,4]

Abstract— **In cellular multi-user multiple input multiple output (MU-MIMO) systems the quality of the available channel state information (CSI) has a large impact on the system performance. Specifically, reliable CSI at the transmitter is required to determine the appropriate modulation and coding scheme, transmit power and the precoder vector, while CSI at the receiver is needed to decode the received data symbols. Therefore, cellular MUMIMO systems employ predefined pilot sequences and configure associated time, frequency, code and power resources to facilitate the acquisition of high quality CSI for data transmission and reception. Although the trade-off between the resources used for pilot and user data transmission has been known for long, the near-optimal configuration of the available system resources for pilot and data transmission is a topic of current research efforts. Indeed, since the fifth generation of cellular systems utilizes heterogeneous networks in which base stations are equipped with a large number of transmit and receive antennas, the appropriate configuration of pilot-data resources becomes a critical design aspect. In this article, we review recent advances in system design approaches that are designed for the acquisition of CSI and discuss some of the recent results that help to dimension the pilot and data resources specifically in cellular MU-MIMO systems.**

Index Terms— **Multi-antenna systems, channel state information, estimation techniques, receiver algorithms.**

I. INTRODUCTION

In the uplink of cellular MU-MIMO systems, the base station (BS) typically acquires CSI of the uplink by means of uplink pilot or reference signals that are orthogonal in the code domain. Mobile stations (MSs) in long term evolution (LTE) systems, for example, use cyclically shifted Zadoff-Chu sequences to form demodulation reference signals allowing the BS to acquire CSI at the receiver (CSIR), which is necessary for uplink data reception [1]. By contrast, to acquire CSI at the transmitter (CSIT), BSs rely either on downlink pilots and quantized information fed back by MSs [2] or assume channel reciprocity [3]. It has been pointed out by several related works that in systems employing pilot aided channel estimation the number of pilot symbols and the pilot-to-data power ratio (PDPR) play a crucial role in optimizing the inherent trade-off of sharing the available resources between pilot and data symbols [3]–[6].

The early work in [4] determined lower and upper bounds on the difference between the mutual information when the receiver has an estimate of the CSI and when it has perfect knowledge of the channel. It also determined upper and lower bounds – as functions of the variance of the channel measurement error – on this difference. Subsequently, the results in [5] showed how pilot-based channel estimation affects the capacity of the fading channel, emphasizing that training imposes a substantial information-theoretic penalty, especially when the coherence interval T (expressed in terms of the number of symbols available for pilot and data transmission) is only slightly larger than the number of transmit antennas M, or when the signal-to-noise ratio (SNR) is low. In these regimes, learning the entire channel is highly suboptimal. Conversely, if the SNR is high, and T is much larger than M, training-based schemes can come very close to achieving capacity. Therefore, the power that should be spent on training and data transmission depends on the relation between T and M. Specifically in MIMO orthogonal frequency division multiplexing (OFDM) systems that employ minimum mean squared error (MMSE) channel estimation, references [6] and [7] computed lower bounds. It was also shown that the optimal PDPR that maximizes this lower bound or minimizes the average symbol error rate can significantly increase the capacity compared with a system that uses a suboptimal PDPR setting. More recently, specifically for MU-MIMO systems, the trade-off between pilot and data symbols was analyzed in [8].

While the above references focused on a single cell system, a series of other works developed models for multi-cell MU-MIMO systems and proposed multi-cell pilot and/or data power control schemes that aim to maximize suitable system-wide utility functions [9]–[11]. In particular, the results in [9] and [10] indicate that in multi-cell MU-MIMO systems controlling the transmit power of both the pilot and data symbols can drastically improve the spectral and energy efficiency of the system. These papers assume the availability of a central control entity, which is hardly feasible in practice. Likewise, [10] demonstrates that multi-cell power control for the pilot and data symbols is necessary to maximize the system sum-rate, but it does not propose a decentralized algorithm that could be used for this purpose in practice. Therefore, suitable multi-cell schemes are actively researched by the academic and industrial communities.

In this direction, the work by [11] proposes a multi-cell game-theoretic approach for pilot contamination avoidance, although it does not consider the power control problem and that of setting the PDPR. The purpose of the present article is to survey recent advances and to point at some open problems in acquiring CSI in cellular MU-MIMO systems. Since understanding the inherent trade-offs of CSI acquisition is necessary to appreciate recent system design approaches and results, Section II provides a brief overview of the evolution of multi-

G. Fodor is partially supported by the joint Ericsson-KTH project Machine Learning for Spectrum Sharing in Massive MIMO Networks (SPECS II). M. Telek is partially supported by the OTKA K-123914 and the TUDFO/51757/2019-ITM grants.

[1,2] Ericsson Research, Stockholm, Sweden. E-mail: Gabor.Fodor@ericsson.com

[2] KTH Royal Institute of Technology, Stockholm, Sweden. E-mail: gaborf@kth.se

[3] Budapest University of Technology and Economics, Budapest, Hungary. E-mail: {pap,telek}@hit.bme.hu

[4] MTA-BME Information Systems Research Group, Budapest, Hungary.

DOI: 10.36244/ICJ.2019.3.2

antenna systems specifically in cellular networks. Next, Section III describes the two fundamental inherent trade-offs associated with CSI acquisition (related to the number of pilot symbols and the applied pilot power respectively). Section IV surveys recent papers related to CSI at the transmitter acquisition, that is of fundamental importance for downlink transmissions. Section V discusses advancements in CSI acquisition at the receiver, that is important for uplink reception and downlink transmission when reciprocity between the uplink and downlink channels holds. Reference signal design and channel estimation are discussed in Section VI. Next, Section VII provides an overview of recent papers that develop decentralized schemes that ease the burden on the base station by involving the mobile stations in the power control, resource allocation and channel estimation tasks. Finally, Section VIII discusses recent advances in mmWave systems, that are promising candidates for accommodating large scale MIMO systems and for taking advantage of underutilized spectrum resources. Section IX offers concluding remarks and provides an outlook on CSI acquisition in future cellular systems.

II. The Evolution of Multi-Antenna Systems: From Single User to Massive Multi-user Multiple Input Multiple Output Systems

Conventional communication systems equipped with a single transmit antenna and a single receive antenna are called single input single output (SISO) communication systems (Figure 1, upper left). This intuitively clear terminology explicitly refers to a signal model that involves the convolution of the complex impulse response of the wireless channel (typically represented as a random variable h) and the single input x to model the single output y:

$$y = h \star x + n, \tag{1}$$

where n is complex baseband additive white Gaussian noise (AWGN). The above equation is for a single realization of the complex single output y [12].

The value of multiple antenna systems as a means to improve communications, including improving the overall system capacity and transmission reliability, was recognized in the early ages of wireless communications. Specifically, adaptive transmit or receive beamforming by means of employing multiple antennas either at the transmitter or the receiver roots back to classic papers that appeared in the 1960s and 1970s [13]–[15]. In particular, Widrow *et al.* described a least mean square (LMS) adaptive antenna array, which is a technique to adaptively determine the weights that are derived from the received signal to minimize the mean squared error (MSE) between the received signal and a reference (pilot) signal [13], [15]. Applebaum proposed a multiple antenna array structure that adaptively suppresses sidelobe energy when the desired signal's angle of arrival (AoA) is known, such as in a radar system.

Starting from the 1980's, there has been a renewed and increased interest in employing multiple antenna techniques in commercial systems, particularly mobile and cellular systems, where multipath and unintentional interference from simultaneously served users were the main concern [16]. However, it was not until the cost of digital signal processing was dramatically reduced and commercial wireless systems matured in the late 1990s that adaptive beamforming became commercially feasible, and large scale industrial interest has started to take off.

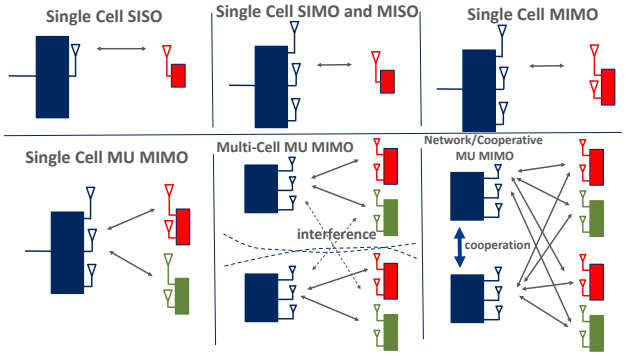

Figure 1. The evolution of multiple antenna systems from single cell single input single output transmissions to cooperative network multiple input multiple output transmissions.

While traditional SISO systems exploit time- or frequency-domain processing and decoding of the transmitted and received data [17], [18], the use of additional antenna elements at the cellular BS or user equipment (UE) side opens up the extra spatial dimension to signal precoding and detection. Depending on the availability of multiple antennas at the transmitter and the receiver, such techniques are classified as Single Input Multiple Output (SIMO), Multiple Input Single Output (MISO) or MIMO (Figure 1, upper middle and upper right). Specifically, space-time and space-frequency processing methods in SIMO, MISO and MIMO systems make use of the spatial dimension with the aim of improving the link's performance in terms of error rate, data rate or spectral and energy efficiency [15].

In the context of cellular networks, for example, in the scenario of a multi-antenna enabled BS communicating with a single antenna UE, the uplink (UL) and downlink (DL) are referred to as SIMO and MISO respectively. When a multi-antenna terminal is involved, a full MIMO link may be obtained, although the term MIMO is sometimes also used in a collective sense including SIMO and MISO as special cases.

A MIMO system, in which the transmitter and receiver are equipped with M and N antennas respectively, is conveniently characterized by the multi-dimensional version of (1) as follows:

$$\mathbf{y} = \underbrace{\mathbf{H}}_{N\times M}\underbrace{\mathbf{x}}_{M\times 1} + \underbrace{\mathbf{n}}_{N\times 1} \quad \in \mathcal{C}^{N\times 1}, \tag{2}$$

where $\mathbf{x}$ and $\mathbf{y}$ represent the complex M and N dimensional input and output vectors of the MIMO system respectively and $\mathbf{n}$ is complex baseband AWGN vector.

While a point-to-point multiple-antenna link between a BS and a UE is referred to as Single-User Multiple Input Multiple Output (SU-MIMO), MU-MIMO features several UEs communicating simultaneously using the same frequency- and time-domain resources (Figure 1, lower left). By extension, considering a multi-cell system, neighboring BSs sharing their

antennas and forming a virtual MIMO system to communicate with the same set of UEs in different cells are called cooperative multi-point (CoMP) or network MIMO transmission/reception (Figure 1, lower middle and lower right).

Multiple antenna techniques, as illustrated by Figure 1 offer (the combinations of) three advantages over traditional SISO systems:

- Diversity gain: The diversity gain corresponds to the mitigation of the effect of multipath fading, by means of transmitting and/or receiving over multiple wireless channels created by the multiple antennas on the transmit and/or receive sides of the communication link.
- Array gain: The array gain corresponds to a spatial version of the well-known matched-filter gain achieved by time-domain receivers.
- Spatial multiplexing gain: The spatial multiplexing gain refers to the ability to send multiple data streams in parallel and to separate them on the basis of their spatial signature. The spatial multiplexing gain is a particularly attractive gain of MIMO systems over SISO systems, because MIMO data stream multiplexing does not come at the cost of bandwidth expansion and can therefore yield drastic spectral efficiency gains.

As we shall see, the gains associated with multi-antenna systems strongly depend on the availability of CSI – the matrix $\mathbf{H}$ in (2) – at the transmitter and the receiver, which motivated the research and standardization communities to develop resource efficient techniques that enable the acquisition of CSIT and CSIR. Due to their great impact on the achievable gains, these acquisition techniques form an important part of MIMO systems, as discussed in more detail in the next section.

Due to the advances in digital signal processing, antenna theory and the commercial success of MIMO, and in particular, MU-MIMO systems, the research community has been investigating the characteristics of large scale antenna systems, in which the cellular BS is equipped with a great number of antennas. Indeed, evolving wireless standards are expected to support the deployment of several tens or even hundreds of transmit and receive antennas at infrastructure nodes and over ten transmit and receive antennas at commercial UEs. It is worth noting that in the asymptotic regime of such large scale or massive MIMO systems, it turns out that the lack of accurate CSI is the main cause of performance saturation, besides hardware impairments. Therefore, scalable and resource efficient CSI acquisition techniques have been and continues to be in the focus of the MIMO community ever since the large commercial deployments of such systems have started.

III. Channel State Information Acquisition and Transceiver Design: Challenges and Trade-offs in Multi-user Multiple Input Multiple Output Systems

As noted, the spectral and energy-efficient operation of wireless systems in general, and multiple antenna systems in particular, relies on the acquisition of accurate CSIT and CSIR [19]. The main reasons for this are that (i) transmitters of modern wireless systems adapt the transmitted signal characteristics to the prevailing channel conditions and (ii) the effect of the channel on the transmitted signal must be estimated in order to recover the transmitted information. As long as the receiver accurately estimates how the channel modifies the transmitted signal, it can recover the signal from the impacts of the wireless channel. In practice, pilot signal-based data-aided techniques are used not only due to their superior performance in fast fading environments, but also due to their cost efficiency and inter-operability in commercial systems. Consequently, channel estimation methods have been studied extensively and a large number of schemes, including blind, data-aided, and decision-directed non-blind techniques, have been evaluated and proposed in the literature [20]–[22].

As the number of antennas at the BS and the simultaneously served users grow large, it is desirable to have pilot based schemes that are scalable in terms of the required pilot symbols and provide high quality CSI for UL data detection and DL precoding. To this end, MU-MIMO systems employing a large number of antennas typically rely on channel reciprocity and employ uplink pilots to acquire CSI at BSs. Although solutions for non-reciprocal systems (such as systems operating in frequency division duplexing (FDD) mode) are available [23], it is generally assumed that massive MIMO systems can advantageously operate in time division duplexing (TDD) mode exploiting channel reciprocity [3], [24].

Pilot reuse generally causes contamination of the channel estimates, which is known as pilot contamination (PC) or pilot pollution. As there are a large number of channels to be estimated in MU-MIMO and massive MIMO systems, accurate CSI acquisition scaling with the number of BS antennas becomes a significant challenge due to the potentially limited number of pilots available. Indeed, PC limits the performance gains of non-cooperative MU-MIMO systems [3], [25]. Specifically, PC is known to cause a saturation effect in the signal-to-interference-plus-noise ratio (SINR) as the number of BS antennas increases to a very large value. This is in contrast to the PC exempt scenario where the SINR increases almost linearly with the number of antennas [25]. It is therefore clear that the trade-offs associated with the resources used for pilot signals and those reserved for data transmission is a key design aspect of modern wireless communication systems.

Although pilot-based CSI acquisition is advantageous in fast fading environments, its inherent trade-offs must be taken into account when designing channel estimation techniques for various purposes. These purposes include demodulation, precoding or beamforming, spatial multiplexing and other channel-dependent algorithms such as frequency selective scheduling or adaptive modulation and coding scheme (MCS) selection [6]–[8]. The inherent trade-offs between allocating resources to pilot and data symbols include the following, as illustrated in Figure 2:

- Increasing the power, time, or frequency resources to pilot signals improves the quality of the channel estimate, but leaves fewer resources for uplink or downlink data transmission [6]–[8].
- Constructing long pilot sequences (for example, employing orthogonal symbol sequences such as those based on the well-known Zadoff-Chu sequences in LTE systems) helps to avoid tight pilot reuse in multi-cell systems), helps to reduce or avoid inter-cell pilot interference. This is because

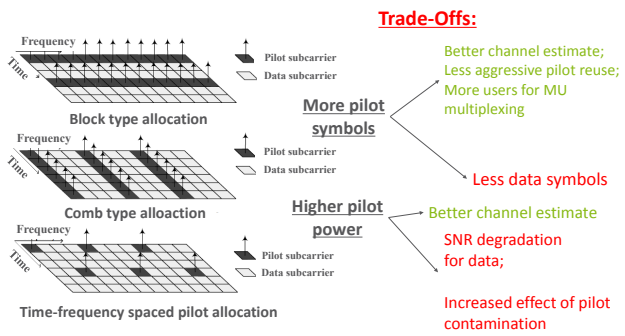

Figure 2. Trade-offs associated with channel estimation, reference (pilot) signal design in MU-MIMO systems

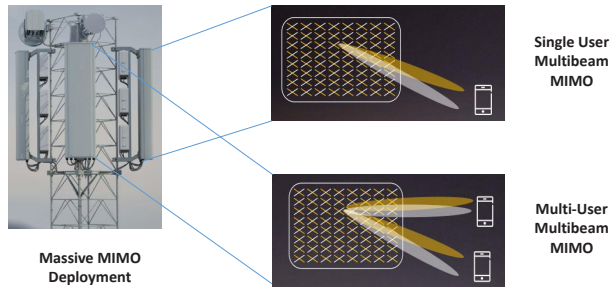

Figure 3. Massive MIMO deployments at the base station can support a large number of (up to several hundred) of possibly cross-polarized antenna elements. When high quality CSI is available at the BS, the system supports single and multi-user transmissions.

long pilot sequences enable to construct a great number of orthogonal sequences and, consequently, help to avoid pilot reuse in neighbor cells, and thereby address the root cause of PC. On the other hand, spending a greater number of symbols on pilots increases the pilot overhead and might violate the coherence bandwidth [8], [26].

- Specifically in MU-MIMO systems, increasing the number of orthogonal pilot sequences may increase the number of spatially multiplexed users at the expense of spending more symbols when creating the orthogonal sequences [6], [7].

In particular, increasing the pilot power increases the SNR of the received pilot signal, and thereby improves the quality of channel estimation in terms of the MSE of the channel estimate [27]. Unfortunately, increasing the pilot power may also lead to the SNR degradation of the data signals, and may exacerbate the PC problem in multi-cell scenarios [9]. In addition to these inherent trade-offs, the arrangement of the pilot symbols in the time, frequency, and spatial domains have been shown to have a significant impact on the performance of MU-MIMO and massive MIMO systems in practice, see for example [6], [7], [28].

IV. Recent Advances in CSIT Acquisition Techniques

Recent research results and experiments with practical implementations have identified the key challenges that must be overcome in order to realize the potential benefits of massive MIMO [29]. One of the real-world challenges is given by the need of accurate CSI at the BS side. In principle, CSI may be obtained through transmitting orthogonal reference signals from each transmit antenna element, and then feeding back the observed spatial channel at the UE to the BS. This approach has the drawback that the reference signal overhead in terms of required CSI grows linearly with the number of transmit antennas. More specifically, CSIT at the transmitter in cellular systems employing FDD requires a feedback channel to the cellular BS, since reciprocity between the downlink and uplink channels cannot be assumed. When the number of antennas deployed at the BS is large, feedback-based CSIT acquisition is a challenge, because the number of pilot sequences as well as feeding back information about the entire vector channel increases linearly with the number of antennas. For this reason, massive MU-MIMO systems are expected to be deployed in TDD systems, although valuable spectrum resources are allocated to FDD systems. Therefore, CSIT acquisition techniques that do not rely on channel reciprocity is of large interest by the research and standardization communities.

Indeed, one of the main technical goals of the 5th generation of cellular systems is to provide a system concept that supports 1000 times higher system spectral efficiency as compared with current LTE deployments but with a similar cost and energy dissipation per area as in today's cellular systems [30]. Historically, the 3rd Generation Partnership Project (3GPP) standard for the LTE has been designed with MU-MIMO as a goal to increase capacity. To this end, LTE has adopted various MU-MIMO technologies. Specifically, in LTE Release 8, the downlink transmission supports up to four antenna ports at the BS. There is an option for performing antenna switching with up to two transmit antennas. Furthermore, Release 10 (also known as LTE-Advanced or LTE-A) provides enhanced MIMO technologies. A new codebook and feedback design are implemented to support spatial multiplexing with up to eight independent spatial streams and enhanced MU-MIMO transmissions. The LTE Release 13 enables high-order MIMO systems with up to 64 antenna ports at the BS, which enables deployments in higher frequencies by supporting high-precision beamforming solution.

In a similar manner, massive or large MIMO systems are considered essential for meeting 5G capacity goals [24]. Massive MIMO systems generally have a large number of antennas at the BS consisting of 100 or more multiple antenna elements with associated large code books and scalable CSI acquisition techniques. An example of massive MIMO at the BS is shown in Figure 3. Clearly, these systems impose much more demanding requirements on CSI acquisition, precoding and receiver design in terms of scalability than the early release of LTE. Therefore, massive MIMO provides a suitable solution for substantially increasing the spectral efficiency and thereby the capacity for a given spectrum allocation. Massive MU-MIMO networks exploit the additional spatial degrees of freedom

(DoF) to spatially multiplex the complex data symbols for several UEs scheduled on the same time-frequency resources in order to focus the radiated energy towards the intended receivers and to minimize the intracell and intercell interference [3], [24], [31].

As mentioned, the original massive MIMO downlink implementation is based on TDD operation, which allows to design near-optimal linear precoders, as CSIT for the downlink channels can be acquired through orthogonal uplink sounding exploiting channel reciprocity [32]. In contrast, in FDD operating mode, acquiring CSIT is more complex, since the channel estimation has to be carried out through downlink reference symbols (RSs) and subsequent uplink feedback. Therefore, in FDD systems, there exists a one-to-one correspondence between RSs and antenna elements. Consequently, in FDD systems, training and feedback overhead are often associated with *unfeasibility* in the massive MIMO regime, where a few resource elements (REs) are left for data transmission [33].

Nevertheless, operating in FDD remains appealing to mobile network operators for several reasons, including i) most radio bands below 6 GHz are paired FDD bands, ii) the BSs have higher transmit power available for RSs than the UEs, and, as pointed out in [33], iii) overall deployment, operation and maintenance costs are reduced as fewer BSs are required in FDD networks. Moreover, as the number of UEs increases, longer orthogonal RSs are needed to avoid the so-called pilot contamination [32] – which increases power consumption at the UEs and the overall resource overhead.

To facilitate CSIT acquisition, in a way that scales well with the increasing number of antennas, the grid of beams (GoB) approach has been proposed in evolving 5G specifications [33], [34]. According to the GoB concept, a set of precoding vectors (that is a set of possible beams) is predefined, and the UEs see low-dimensional virtual *(effective)* channels instead of the actual ones, where the effective channels incorporate the precoding vectors. In particular, one orthogonal RS is allocated to each beam in the GoB codebook. Thus, estimating such effective channels reduces the overhead, as it becomes proportional to the codebook size (the number of possible beams) rather than to the number of antenna elements [35]. Unfortunately, the reduction in training overhead due to coarse granularity of the codebook, typically incurs some performance degradation [36], as the digital precoder for data transmission is based on a reduced channel representation, rather than a per-antenna complex channel coefficient.

Another option for CSIT acquisition consists of designing the GoB with a large number of beams, and training a small subset of the available beams, which contains the dominant channel (multi-path) components of those beams [33], [37]. The number of such components depends on several factors, including the frequency band and the radio scattering environment, which are in general beyond the designer's control. Nevertheless, when multi-antenna UEs are deployed, statistical beamforming at the UE side can be exploited to let the UEs excite a suitable channel subspace, with the aim to further reduce the number of relevant components to be estimated [38], [39].

V. Recent Advances in CSIR and Reciprocity-based CSIT Acquisition Techniques

In fact, in 5G systems MSs are expected to have multiple antennas. Therefore, in 5G systems, the cost of utilizing reciprocity is that CSI acquisition requires array calibration in order to take the differences in the transmit/receive radio frequency (RF) chains of the different antenna elements at the BS and MS into account. In time varying channels, the delay between training and data transmission also represents an effect that should be further studied. For example, recent results indicate that channel prediction techniques can be used to mitigate this delay which would degrade the performance of massive MIMO systems [30].

In multi-cell and multi-tier cellular networks operating in TDD and utilizing channel reciprocity, reusing the pilot sequences leads to uplink pilot interference, often referred to as pilot contamination [3], [40]. In multi-cell MU-MIMO systems, the pilot-data resource allocation trade-off is intertwined with the management of intercell interference (contamination) both on the pilot and data signals and calls for rethinking the reference signal design of classical systems such as the 3GPP LTE system. Recent works provide valuable insights into the joint design of pilot and data channels in multi-cell massive MU-MIMO systems [41].

Some of the problems related to PDPR setting in MU-MIMO systems have been addressed by [8], [9], [26], [42]–[46]. Reference [8] considers a MU-MIMO scenario with time-division duplex operation, and a coherence interval of T symbols spent for channel training, channel estimation, and precoder computation for DL transmission. The optimum number of pilot symbols is determined for maximizing the lower bound of the sum-throughput. However, receiver design and the PDPR-setting are out of the scope of that paper. The problem of joint power loading of data and pilot symbols for the purpose of maximizing sum spectral efficiency is addressed in [42], but the impact of PDPR setting at the MU-MIMO receiver is not considered. In contrast, the problem of optimal training period and update interval for maximizing the UL sum-rate is addressed in [44], whereas the receiver structure at the BS is not considered. Reference [26] considers single-user wireless fading channels, and optimizes the pilot overhead. That paper also identifies that the pilot overhead, as well as the spectral efficiency penalty, depends on the square root of the normalized Doppler frequency. More recently, uplink power control and the PDPR-setting problem in MU-MIMO systems have been addressed in references [9], [43], [47], [48], assuming practical (zero-forcing (ZF) and MMSE based) multi-antenna receiver structures. However, the papers mentioned above focus on centralized approaches, and may not scale well in multi-cell multi-user systems in practice. Scalable decentralized schemes with low complexity are appealing for PDPR setting in multi-cell MU-MIMO systems, and have been proposed in [28], [49]–[51].

VI. Reference Signal Design and Channel Estimation in Cellular MIMO Systems

Due to the importance of CSI acquisition for data transmission and reception, it is natural, that designing reference (pilot)

signals and employing accurate channel estimation techniques are of particular importance in cellular MIMO systems. The design of the uplink demodulation reference signals (DMRS) specifically in 3GPP Long Term Evolution Advanced (LTE-A) systems is described in [52]. In the LTE uplink, DMRS are used to facilitate channel estimation for the coherent demodulation of the physical uplink shared and control channels. The LTE DMRS occupies specific OFDM symbols within the uplink subframe according to the block type arrangement and supports a large number of user equipment utilizing cyclic extensions of the well known Zadoff-Chu sequences [53]. Because of its importance in practical systems, in this section we elaborate on the interplay between reference signal design and channel estimation in cellular MIMO systems, and refer to related works for further details.

To illustrate the design of reference signals in cellular MIMO systems, let us consider the uplink transmission of a multi-antenna single cell wireless system, in which users are scheduled on orthogonal frequency channels. In cellular MIMO systems, each MS employs an orthogonal pilot sequence, so that no interference between pilots within any given cell is present in the system. (Note that due to pilot reuse across neighbor cells, pilot contamination may still cause pilot interference.) This is a common practice in massive MU-MIMO systems in which a single MS may have a single antenna. The BS estimates the channel $\mathbf{h}$ (column vector of dimension N_r, where N_r is the number of receive antennas at the BS) by either least squares (LS) or MMSE channel estimation to initialize an MMSE equalizer for uplink data reception. Since we employ orthogonal pilot sequences, the channel estimation process can be assumed independent for each MS within any given cell of the cellular system. Let us consider a time-frequency resource of T time slots in the channel coherence time, and F subcarriers in the coherence bandwidth, with a total number of symbols $\tau = F \cdot T$. We denote by τ_p the number of symbols allocated to pilots, and by τ_d the number of symbols allocated to data ($\tau_p+\tau_d = \tau$). Moreover, we consider a transmission power level P_p and P for each pilot and data symbol, respectively. With this setup, we consider two pilot symbol allocation methods, namely block type and comb type, which we discuss in the following subsections. In practice, both of these schemes, and, in fact, a combination of these are often used to construct uplink and downlink reference signals [52].

A. Block Type Pilot Allocation

The block type pilot arrangement consists of allocating one or more time slots for pilot transmission, by using all subcarriers in those time slots. This approach is a suitable strategy for slow time-varying channels. Given T slots, a fraction of T_p slots are allocated to the pilot and $T_d = T - T_p$ slots are allocated to the data symbols. Note that a maximum transmission power P_{tot} is allowed in each time slot, among all F subcarriers. This power constraint is then identical for both the pilot (P_p) and data power (P), i.e.,

$$FP_p \leq P_{tot} \qquad FP \leq P_{tot}. \tag{3}$$

The power cannot be traded between pilot and data, but the *energy* budget can be distributed by tuning the number of time slots T_p and T_d, i.e., $\tau_p = FT_p$ and $\tau_d = FT_d$.

B. Comb Type Pilot Allocation

In the comb type pilot arrangement a certain number of subcarriers are allocated to pilot symbols, continuously in time. This approach is a suitable strategy for non-frequency selective channels. Given F subcarriers in the coherence bandwidth, a fraction of F_p subcarriers are allocated to the pilot and $F_d = F - F_p$ subcarriers are allocated to the data symbols.

Each MS transmits at a constant power P_{tot}, however, the transmission power can be distributed unequally in each subcarrier. In particular, if we consider a transmitted power P_p for each pilot symbol and P for each data symbol transmission, the following constraint is enforced:

$$F_pP_p + F_dP = P_{tot}. \tag{4}$$

The total number of symbols for pilots is $\tau_p = TF_p$ and for data is $\tau_d = TF_d$. However, with comb type pilot arrangement, the trade-off between pilot and data signals includes the trade-offs between the number of frequency channels *and* between the transmit power levels, which is an additional degree of freedom compared with the block type arrangement.

C. Channel Estimation

Let us consider a MS that transmits an orthogonal pilot sequence $\mathbf{s} = [s_1, ..., s_{\tau_p}]^T$, where each symbol is scaled as $|s_i|^2 = 1$, for $i = 1, .., \tau_p$, and ^{T}, *, and ^{H} denote the transpose, the conjugate and the conjugate transpose, respectively. Thus, the $N_r \times \tau_p$ matrix of the received pilot signal at the BS from the MS is:

$$\mathbf{Y}^p = \alpha\sqrt{P_p}\mathbf{h}\mathbf{s}^T + \mathbf{N}, \tag{5}$$

where we assume that $\mathbf{h}$ is a circular symmetric complex normal distributed vector of r.v. with mean vector $\mathbf{0}$ and covariance matrix $\mathbf{C}$ (of size N_r), denoted as $\mathbf{h} \sim \mathcal{CN}(\mathbf{0}, \mathbf{C})$, α accounts for the propagation loss, $\mathbf{N} \in \mathbb{C}^{N_r \times \tau_p}$ is the spatially and temporally AWGN with element-wise variance σ^2.

In this paper, we consider two techniques, i.e., the LS and the MMSE channel estimation.

1) LS Estimation: Conventional LS estimation relies on correlating the received signal with the known pilot sequence. The BS estimates the channel based on assuming

$$\hat{\mathbf{h}}_{LS} = \mathbf{h} + \tilde{\mathbf{h}}_{LS} = \frac{1}{\alpha\sqrt{P_p}}\mathbf{Y}^p\mathbf{s}^*(\mathbf{s}^T\mathbf{s}^*)^{-1} = \mathbf{h} + \frac{1}{\alpha\sqrt{P_p}\tau_p}\mathbf{N}\,\mathbf{s}^*. \tag{6}$$

Note that $\mathbf{N}\,\mathbf{s}^* = \left[\sum_{i=1}^{\tau_p} s_i^* n_{i,1}, ..., \sum_{i=1}^{\tau_p} s_i^* n_{i,N_r}\right]^T$, then $\mathbf{N}\,\mathbf{s}^* \sim \mathcal{CN}(\mathbf{0}, \tau_p\sigma^2\mathbf{I}_{N_r})$.

By considering $\mathbf{h} \sim \mathcal{CN}(\mathbf{0}, \mathbf{C})$, it follows that the estimated channel $\hat{\mathbf{h}}_{LS}$ is a circular symmetric complex normal distributed vector $\hat{\mathbf{h}}_{LS} \sim \mathcal{CN}(\mathbf{0}, \mathbf{R}_{LS})$, with

$$\mathbf{R}_{LS} = \mathcal{E}\{\hat{\mathbf{h}}_{LS}\hat{\mathbf{h}}_{LS}^H\} = \mathbf{C} + \frac{\sigma^2}{\alpha^2 P_p\tau_p}\mathbf{I}_{N_r}. \tag{7}$$

The channel estimation error is defined as $\tilde{\mathbf{h}}_{LS} = \mathbf{h} - \hat{\mathbf{h}}_{LS}$, so that $\tilde{\mathbf{h}}_{LS} \sim \mathcal{CN}(\mathbf{0}, \mathbf{W}_{LS})$ with

$$\mathbf{W}_{LS} = \frac{\sigma^2}{\alpha^2 P_p\tau_p}\mathbf{I}_{N_r}$$

and the estimation MSE is derived as

$$\varepsilon_{LS} = \mathcal{E}\{||\tilde{\mathbf{h}}_{LS}||_F^2\} = \mathrm{tr}\{\mathbf{W}_{LS}\} = \frac{N_r\sigma^2}{\alpha^2 P_p \tau_p}, \quad (8)$$

where $||\cdot||_F^2$ is the Frobenius norm.

2) MMSE Estimation: We define a training matrix $\mathbf{S} = \mathbf{s} \otimes \mathbf{I}_{N_r}$ (of size $\tau_p N_r \times N_r$), so that $\mathbf{S}^H\mathbf{S} = \tau_p \mathbf{I}_{N_r}$. The $\tau_p N_r \times 1$ vector of received signal can be conveniently rewritten as

$$\tilde{\mathbf{Y}}^p = \alpha\sqrt{P_p}\mathbf{S}\mathbf{h} + \tilde{\mathbf{N}}, \quad (9)$$

where $\tilde{\mathbf{Y}}^p, \tilde{\mathbf{N}} \in \mathbb{C}^{\tau_p N_r \times 1}$. The MMSE equalizer aims at minimizing the MSE between the estimate $\hat{\mathbf{h}}_{MMSE} = \mathbf{H}\tilde{\mathbf{Y}}^p$ and the actual channel realization $\mathbf{h}$. More precisely,

$$\begin{aligned}\mathbf{H} &= \arg\min_{\mathbf{H}} \mathcal{E}\{||\mathbf{H}\tilde{\mathbf{Y}}^p - \mathbf{h}||_F^2\} \\ &= \alpha\sqrt{P_p}(\sigma^2\mathbf{I}_{N_r} + \alpha^2 P_p \mathbf{C}\mathbf{S}^H\mathbf{S})^{-1}\mathbf{C}\mathbf{S}^H; \quad \mathbf{H} \in \mathbb{C}^{N_r \times \tau_p N_r}.\end{aligned} \quad (10)$$

The MMSE estimate is then expressed as

$$\begin{aligned}\hat{\mathbf{h}}_{MMSE} &= \alpha\sqrt{P_p}(\sigma^2\mathbf{I}_{N_r} + \alpha^2 P_p\tau_p\mathbf{C})^{-1}\mathbf{C}\mathbf{S}^H(\alpha\sqrt{P_p}\mathbf{S}\mathbf{h} + \tilde{\mathbf{N}}) \\ &= \left(\frac{\sigma^2}{\alpha^2 P_p\tau_p}\mathbf{I}_{N_r} + \mathbf{C}\right)^{-1}\mathbf{C}\left(\mathbf{h} + \frac{1}{\alpha\sqrt{P_p}\tau_p}\mathbf{S}^H\tilde{\mathbf{N}}\right).\end{aligned} \quad (11)$$

Notice that $\mathbf{S}^H\mathbf{N} \sim \mathcal{CN}(\mathbf{0}, \tau_p\sigma^2\mathbf{I}_{N_r})$, and therefore the estimated channel $\hat{\mathbf{h}}_{MMSE}$ is also a circular symmetric complex normal distributed vector $\hat{\mathbf{h}}_{MMSE} \sim \mathcal{CN}(\mathbf{0}, \mathbf{R}_{MMSE})$, that is

$$\hat{\mathbf{h}}_{MMSE} = \mathbf{h} + \tilde{\mathbf{h}}_{MMSE},$$

and

$$\mathbf{R}_{MMSE} = \mathbf{C}^2\left(\frac{\sigma^2}{\alpha^2 P_p\tau_p}\mathbf{I}_{N_r} + \mathbf{C}\right)^{-1}, \quad (12)$$

where we considered $\mathbf{C} = \mathbf{C}^H$ and applied the commutativity of $\mathbf{C}$ and $\mathbf{I}_{N_r}$ to substitute

$$\left(\frac{\sigma^2}{\alpha^2 P_p\tau_p}\mathbf{I}_{N_r} + \mathbf{C}\right)^{-1}\mathbf{C} = \mathbf{C}\left(\frac{\sigma^2}{\alpha^2 P_p\tau_p}\mathbf{I}_{N_r} + \mathbf{C}\right)^{-1}.$$

The channel estimation error is $\tilde{\mathbf{h}}_{MMSE} = \mathbf{h} - \hat{\mathbf{h}}_{MMSE}$ so that $\tilde{\mathbf{h}}_{MMSE} \sim \mathcal{CN}(\mathbf{0}, \mathbf{W}_{MMSE})$ with

$$\mathbf{W}_{MMSE} = \mathbf{C}\left(\mathbf{I}_{N_r} + \frac{\alpha^2 P_p\tau_p}{\sigma^2}\mathbf{C}\right)^{-1} \quad (13)$$

and the estimation MSE simply follows as

$$\varepsilon_{MMSE} = \mathrm{tr}\left\{\mathbf{C}\left(\mathbf{I}_{N_r} + \frac{\alpha^2 P_p\tau_p}{\sigma^2}\mathbf{C}\right)^{-1}\right\}. \quad (14)$$

Notice that for both LS and MMSE channel estimation, the estimation MSE is a monotonically decreasing function of the pilot energy per antenna $P_p\tau_p$. Building on the characteristics of LS and MMSE channel estimation techniques, several research contributions characterize the receiver and the uplink signal MSE and spectral efficiency based on $\tilde{\mathbf{h}}$, which is computed for LS ($\hat{\mathbf{h}}_{LS}$) and MMSE estimation ($\hat{\mathbf{h}}_{MMSE}$) [54], [55].

VII. Decentralized Approaches to CSI Acquisition

As the number of antennas and the number of simultaneously served users by a single BS increase, decentralized algorithms for MU-MIMO systems become important, because they help to reduce the required processing power at a single entity such as the cellular base station. Therefore, there is an increasing interest in decentralized optimization schemes for MU-MIMO systems, see for example [28], [49]–[51]. These papers either assume the availability of perfect CSI, or incorporate CSI errors, but do not address the joint optimization of setting the pilot and the data power. A different line of work proposed a game theoretic approach for decentralized power control and resource allocation in multi-user (MU) systems in which some form of "performance coupling" [56] exists among the users, as the increase of one user's performance degrades the performance of others, e.g., [57] and [58]. These references suggest that game theoretic approaches in MU systems are appealing, because they naturally admit decentralized algorithms that can be easily deployed by both network nodes and MSs. It is, however, unclear whether a game theoretic treatment could be used for designing low complexity decentralized algorithms for setting the PDPR in MU cellular systems.

Due to its central role in the performance of MIMO systems, many recent work investigated the performance impact of the PDPR and proposed optimal or near-optimal schemes for setting the PDPR. The MU-MIMO scenario is analyzed in [8], in which the coherence interval of T symbols is spent for channel training, channel estimation, and precoder computation for DL transmission. Specifically, the optimum number of terminals in terms of the DL spectral efficiency is determined for a given coherence interval, number of base station antennas, and SINR. There is no receiver design involved and the pilot-to-data power trade-off is out of the scope of the considered optimization problem. The joint power loading of data and pilot symbols for the purpose of acquiring CSIT for precoding is considered in [42], but the impact of setting the PDPR at the MU-MIMO receiver is not considered. In contrast, the UL sum-rate maximization problem by tuning the training period in a frequency-flat fading channel is considered in [44], without modeling the receiver structure at the BS. Reference [45] proposes a pilot design that maximizes the spectral efficiency of high mobility wireless communication systems that use pilot-assisted MMSE channel estimation. That work does not explicitly model the impact of CSI errors on MU-MIMO receivers, such as an MMSE receiver. Reference [26] investigated the optimization of the pilot overhead for single-user wireless fading channels, and the dependencies of this pilot overhead on various system parameters of interest (e.g. fading rate, SNR) were quantified. By finding an expansion of the spectral efficiency for the overhead optimization in terms of the fading rate around the perfect-CSI point, the square root dependence of both the overhead and the spectral efficiency penalty was clearly identified.

Another set of related papers develop decentralized optimization schemes for MIMO systems, either assuming the availability of perfect channel state information, or incorporating channel state information errors, but do not address the joint optimization of pilot and data power setting, see for example [28], [49]–[51].

Also, a number of recent work proposed a game theoretic approach for power control and resource allocation in MU systems in which performance coupling exists among the users, as the increase of one user's performance degrades the performance of others [56], [59], [57], [58], [60], [61] and [62]. The MU power control problem for the Gaussian frequency-flat relay channel is modelled as a Gaussian interference relay game (GIRG) in [56]. In the GIRG, instead of allocating the power budget across the set of sub-channels, each player aims to decide the optimal power control strategy across a set of hops. For cooperative cognitive radio networks, a coalitional game theoretic approach is proposed in [59]. The coalitional game model captures a cooperative secondary spectrum access scenario, and involves primary and secondary spectrum users such that the secondary users can act as cooperative relays for the primary users. A non-cooperative feedback-rate control game with pricing is considered in [57], as a model of the downlink transmission of a closed-loop wireless network, in which a multi-antenna BS utilizes CSI feedback to properly set linear precoders to communicate with multiple users. Reference [58] proposes a distributed power splitting scheme for simultaneous wireless information and power transfer in relay interference channels, where multiple source-destination pairs communicate through energy harvesting relays. The authors in [60] model power control as a non-cooperative game between transmitter-receiver pairs and show the existence of equilibria using quasi-variational inequality theory. Reference [61] formulates the problem of downlink power control of small cell base stations under a total power constraint as a generalized Nash equilibrium problem and proves the existence of equilibria. The authors in [62] consider a game theoretical formulation of the improper graph multi-coloring problem as a model of resource allocation between transmitter-receiver pairs, prove the existence of equilibria and provide polynomial complexity algorithms for computing equilibria.

A powerful game theoretic framework for the non-cooperative maximization of mutual information assuming Gaussian interference channels in MU-MIMO systems is developed in [63]. As it is pointed out by [63], the main difficulty in the MIMO case as compared with SISO systems is that the optimal transmit directions of each MS change with the strategies of the other users, as opposed to the SISO case, where only the power allocation depends on the strategies of the other MSs. However, this framework assumes the availability of perfect CSI and does not address the trade-off between data transmission and channel estimation. In contrast, the work reported in [64] develops a game theoretic approach to maximizing the own information rates subject to transmit power and robust interference constraints allowing for non-perfect CSI availability at the transmitters and receivers specifically in a cognitive radio environment. However, the aspect of tuning the pilot and data power levels subject to a sum power constraint is not considered. For the DL, reference [65] assumes perfect CSIT at the BS and proposes a partially asynchronous distributed algorithm based on a non-cooperative game to find the DL precoders in MU-MIMO systems.

The MIMO scheme proposed in [46] considers the problem of joint pilot and data power control for the MU-MIMO UL. However, the model of [46] uses a receiver that minimizes the MSE of the estimated data symbols only when perfect CSI is available. As it has been shown in our previous work [47], the performance of this *naive* receiver can be significantly improved by regularizing the receiver with respect to the statistics of the CSI estimation errors.

Recognizing the importance of scalable CSI acquisition approaches, in our recent work we propose a game theoretic approach to setting the PDPR in the UL of MU-MIMO systems and proposed decentralized algorithms that can be implemented in practice and converge to a unique Nash equilibrium [66], [67]. The contribution of those papers is a decentralized MU (pilot and data) power allocation algorithm, which we refer to as Best PDPR Algorithm (BPA). The numerical results obtained by testing BPA in a MU-MIMO system employing an increasing number of receive antennas yield several unique insights. Our results showed that BPA performs close to the globally optimal solution, which minimizes the sum of MSEs in MU-MIMO systems, and outperforms the traditional pilot power setting scheme that uses a fixed, predefined PDPR [66].

VIII. TOWARDS MMWAVE FREQUENCY BANDS

As discussed in this paper, Large-scale MIMO (LS-MIMO) systems involving an order of magnitude greater number of antenna elements than in the early releases of wireless standards are key enablers of next generation cellular systems and providing mobile broadband services [32]. Theoretically, a fully digital LS-MIMO beamforming architecture employing a large number of digital transmit and receiver chains, combined with resource efficient CSI acquisition techniques, near-optimal receiver design and employing decentralized power control schemes can yield near-optimal performance in terms of energy and spectral efficiency [68].

However, deploying LS-MIMO systems in traditional cellular frequency bands is also problematic due to the large physical size of the antenna arrays and related environmental concerns of the general public. Therefore, higher frequency bands, including the millimeter-wave (mmWave) bands have recently emerged as an appealing alternative for the commercial deployment of LS-MIMO systems [69]. Indeed, in mmWave bands, the physical array size can be greatly reduced, and, as an additional advantage, vast amount of unused spectrum can be utilized for attractive and bandwidth-demanding services [70], [71].

Deploying a large number of antennas with the associated fully digital beamforming architecture incurs high cost and increased power consumption, due to the excessive demand for a large number of transceiver chains. Therefore, LS-MIMO systems with hybrid analog and digital beamforming for mmWave deployment have attracted much attention from the research and engineering communities, and a great number of promising hybrid architectures and associated technologies such as training sequence and codebook designs have been proposed and tested in practice [72]–[76]. The results of the marriage of LS-MIMO and hybrid beamforming include significant gains in terms of spectral and energy efficiency, and a cost-efficient technology for accessing large amount of unused spectrum [68], [75], [77].

Specifically, in the framework of mmWave communications, [78]–[80] have studied the effect of hardware impairments on the performance of MIMO systems. The results of [78]

show that single-carrier frequency domain equalization is more robust against impairments from nonlinear power amplifiers than OFDM in typical mmWave system configurations. On the other hand, the results reported in [79] show a slight bit error rate performance advantage of OFDM over single-carrier frequency domain equalization under nonlinear RF distortions, and suggest that subcarrier spacing is a crucial parameter in mmWave massive MIMO systems.

IX. Concluding Remarks

In this survey paper, we discussed recent advances in the field of CSI acquisition and managing the inherent the trade-off between using time, frequency and power resources for CSI acquisition and transmitting data symbols. Managing this trade-off has a large impact on the achievable spectral efficiency in cellular systems, in which the number of transmit and receive antennas grows large. We made the point that the joint allocation of frequency, time and power resources is subject to constraints that depend on the specific pilot pattern, such as the pattern used by the block or comb type arrangements of pilot (reference) symbols.

Recent research results suggest that with a large number of antennas, exploiting the engineering freedom of tuning *both* the number of pilot symbols and the pilot transmit power levels become increasingly important, especially if the relatively simple LS estimator is used at the base station. Also, the gain of using MMSE estimation (preferably with optimized pilot power allocation) increases over LS estimation. Interestingly, the optimal amount of pilot and data resources is different when using MMSE and LS estimators and the gain in terms of spectral efficiency when optimizing *both* the number of pilot symbols and the transmit power levels increases as the number of antennas increases. In practical systems, decentralized schemes in which mobile stations and base stations participate in finding near optimal resource allocations become important, because decentralized schemes scale well with the number of served users and the number of antennas. A new field of research deals with resource allocation and CSI acquisition in millimeter-wave systems.

References

[1] Stefania Sesia, Issam Toufik, and Matthew Baker. *LTE - The UMTS Long Term Evolution: From Theory to Practice*. WILEY, 2nd edition, 2011. ISBN-10: 0470660252.

[2] D. Gesbert, M. Kountouris, R. W. Heath Jr., C.-B. Chae, and T. Salzer. Shifting the MIMO paradigm: From single-user to multiuser communications. *IEEE Signal Processing Magazine*, 24(5):36–46, October 2007, DOI: 10.1109/MSP.2007.904815.

[3] T. Marzetta. Noncooperative cellular wireless with unlimited numbers of base station antennas. *IEEE Trans. Wireless Comm.*, 9(11):3590–3600, 2010, DOI: 10.1109/TWC.2010.092810.091092.

[4] M. Médard. The effect upon channel capacity in wireless communications of perfect and imperfect knowledge of the channel. *IEEE Trans. on Information Theory*, 46(3):933–946, May 2000, DOI: 10.1109/18.841172.

[5] B. Hassibi and B. M. Hochwald. How much training is needed in multiple-antenna wireless links? *IEEE Trans. on Information Theory*, 49(4):951–963, April 2003, DOI: 10.1109/TIT.2003.809594.

[6] T. Kim and J. G. Andrews. Optimal pilot-to-data power ratio for MIMOOFDM. In *IEEE Globecom*, pages 1481–1485, St. Louis, MO, USA, Dec. 2005. DOI: 10.1109/GLOCOM.2005.1577897.

[7] T. Kim and J. G. Andrews. Balancing pilot and data power for adaptive MIMO-OFDM systems. In *IEEE Globecom*, San Francisco, CA, USA, Dec 2006. DOI: 10.1109/GLOCOM.2006.47.

[8] T. Marzetta. How much training is needed for multiuser MIMO? *IEEE Asilomar Conference on Signals, Systems and Computers (ACSSC)* , pages 359–363, June 2006, DOI: 10.1109/ACSSC.2006.354768.

[9] K. Guo, Y. Guo, G. Fodor, and G. Ascheid. Uplink power control with MMSE receiver in multi-cell MU-Massive-MIMO systems. *In Proc. of IEEE International Conference on Communications (ICC)*, pages 5184–5190, Jun. 2014, DOI: 10.1109/ICC.2014.6884144.

[10] X. Li, E. Björnsson, E. G. Larsson, S. Zhou, and J. Wang. Massive MIMO with multi-cell MMSE processing: Exploiting all pilots for interference suppression. arXiv:*1505.03682v2 [cs.IT]*, May 2015.

[11] H. Ahmadi, A. Farhang, N. Marchetti, and A. MacKenzie. A game theoretic approach for pilot contamination avoidance in massive MIMO. *IEEE Wireless Communications Letters*, 5(1):12–15, February 2016, DOI: 10.1109/LWC.2015.2487261.

[12] Iana Siomina, Anders Furuskär, and Gabor Fodor. A mathematical framework for statistical QoS and capacity studies in OFDM networks. *In Personal, Indoor and Mobile Radio Communications (PIMRC)*, pages 2772 – 2776, 10 2009, DOI: 10.1109/PIMRC.2009.5450287.

[13] B. Widrow, P. E. Mantey, L. J. Griffiths, and B. B. Goode. Adaptive antenna systems. *Proceedings of the IEEE*, 55(12):2143–2159, December 1967, DOI: 10.1109/PROC.1967.6092.

[14] S. R. Applebaum. Adaptive arrays. *IEEE Transactions on Antennas and Propagation*, 24(5):585–598, September 1976, DOI: 10.1109/TAP.1976.1141417.

[15] J. Winters. *Space-Time Wireless Systems – From Array Processing to MIMO Communications*. Number ISBN:9780511279942. Cambridge University Press, 2006.

[16] J. H. Winters. Optimum combining in digital mobile radio with cochannel interference. *IEEE Journal on Selected Areas in Communications,* 2(4):528–539, April 1984, DOI: 10.1109/T-VT.1984.24001.

[17] Ádám Knapp and László Pap. General performance analysis of binary fading channels with measurement based feedback channel equalization. *Infocommunications Journal,* 1:1–9, 2014.

[18] Ádám Knapp and László Pap. Statistical based optimization of number of pilot signals in LTE/LTE-A for higher capacity. In *IEEE EUROCON 2015 - International Conference on Computer as a Tool (EUROCON)*, pages 1–5, Sep. 2015, DOI: 10.1109/EUROCON.2015.7313768.

[19] A. Goldsmith, S. A. Jafar, N. Jindal, and S. Vishwanath. Capacity limits of MIMO channels. *IEEE Journal on Selected Areas of Communications*, 21(5):684–702, June 2003, DOI: 10.1109/JSAC.2003.810294.

[20] M. K. Ozdemir and H. Arslan. Channel estimation for wireless OFDM systems. *IEEE Communications Surveys and Tutorials*, 9(2):18–48, 2007, DOI: 10.1109/COMST.2007.382406.

[21] S. Coleri, M. Ergen, A. Puri, and A. Bahai. Channel estimation techniques based on pilot arrangement in OFDM systems. *IEEE Transactions on Broadcasting*, 48(3):223–229, September 2002, DOI: 10.1109/TBC.2002.804034.

[22] Y-H Nam, Y. Akimoto, Y. Kim, M i. Lee, K. Bhattad, and A. Ekpenyong. Evolution of reference signals for LTE-advanced systems. *IEEE Communications Magazine*, 5(2):132–138, February 2012, DOI: 10.1109/MCOM.2012.6146492.

[23] J. Choi, T. Kim, D. J. Love, and J-Y. Seol. Exploiting the preferred domain of FDD massive MIMO systems with uniform planar arrays. In *IEEE International Conference on Communications*, pages 3068–3073, London, UK, June 2015. DOI: 10.1109/ICC.2015.7248530.

[24] F. Rusek, D. Persson, B. K.Lau, E. G. Larsson, T. L. Marzetta, O. Edfors, and F. Tufvesson. Scaling Up MIMO - Opportunities and Challenges with Very Large Arrays. *IEEE Signal Processing Magazine*, 30(1):40 – 60, January 2013, DOI: 10.1109/MSP.2011.2178495.

[25] B. Gopalakrishnan and N. Jindal. An analysis of pilot contamination on multiuser MIMO cellular systems with many antennas. In *International Workshop on Signal Processing Advances in Wireless Communications*, pages 381–385, San Francisco, June 2011. DOI: 10.1109/SPAWC.2011.5990435.

[26] N. Jindal and A. Lozano. A unified treatment of optimum pilot overhear in multipath fading channels. *IEEE Trans. on Communications*, 58(10):2939–2948, October 2010, DOI: 10.1109/TCOMM.2010.083110.090696.

[27] G. Fodor and M. Telek. On the pilot-data power trade off in single input multiple output systems. *European Wireless '14*, Barcelona, Spain(ISBN: 978-3-8007-3621-8), May 2014.

[28] H. Yin, D. Gesbert, M. Filippou, and Y. Liu. A Coordinated Approach to Channel Estimation in Large-Scale Multiple-Antenna Systems. *IEEE Journal on Selected Areas in Communications*, 31(2):264–273, February 2013, DOI: 10.1109/JSAC.2013.130214.

[29] L. Lu, G. Li, A. Swindlehurst, A. Ashikhmin, and R. Zhang. An overview of massive MIMO: Benefits and challenges. *IEEE Journal 9 of Selected Topics in Signal Processing*, 8(5):742–758, October 2014, DOI: 10.1109/JSTSP.2014.2317671.

[30] Nandana Rajatheva, Satoshi Suyama, Wolfgang Zirwas, Lars Thiele, Gabor Fodor, Antti Tölli, Elisabeth Carvalho, and Jesper Hemming Sörensen. *5G Mobile and Wireless Communications Technology*. Cambridge University Press, 2016.

[31] J. Hoydis, S. T. Brink, and M. Debbah. Massive MIMO: How many antennas do we need? *49th Annual Allerton Conference on Communication, Control and Computing*, pages 545–550, 2011, DOI: 10.1109/Allerton.2011.6120214.

[32] E. G. Larsson, O. Edfors, F. Tufvesson, and T. L. Marzetta. Massive MIMO for next generation wireless systems. *IEEE Commun. Mag.*, Feb. 2014, DOI: 10.1109/MCOM.2014.6736761.

[33] W. Zirwas, M. B. Amin, and M. Sternad. Coded CSI reference signals for 5G - exploiting sparsity of FDD massive MIMO radio channels. In Proc. *IEEE WSA,* number ISBN:978-3-8007-4177-9, Mar. 2016.

[34] 3GPP. NR; physical layer procedures for data - Rel. 15, TS 38.214. Dec. 2018.

[35] F. Maschietti, G. Fodor, D. Gesbert, and P. de Kerret. Coordinated beam selection for training overhead reduction in FDD massive MIMO. Proc. *IEEE International Symposium on Wireless Comm. Systems*, ISWCS, Aug. 2019.

[36] J. Flordelis, F. Rusek, F. Tufvesson, E. G. Larsson, and O. Edfors. Massive MIMO performance – TDD vs FDD: What do measurements say? *IEEE Trans. Wireless Commun.*, Apr. 2018, DOI: 10.1109/TWC.2018.2790912.

[37] F. Maschietti, D. Gesbert, P. de Kerret, and H. Wymeersch. Robust location-aided beam alignment in millimeter wave massive MIMO. *Proc. IEEE GLOBECOM*, Dec. 2017, DOI: 10.1109/GLOCOM.2017.8254901.

[38] N. N. Moghadam, H. Shokri-Ghadikolaei, G. Fodor, M. Bengtsson, and C. Fischione. Pilot precoding and combining in multiuser MIMO networks. *IEEE J. Sel. Areas Commun.*, Jul. 2017, DOI: 10.1109/JSAC.2017.2699398.

[39] P. Mursia, I. Atzeni, D. Gesbert, and L. Cottatellucci. Covariance shaping for massive MIMO systems. In *Proc. IEEE GLOBECOM*, Dec. 2018, DOI: 10.1109/GLOCOM.2018.8647861.

[40] J. Jose, A. Ashikhmin, T. Marzetta, and S. Vishwanath. Pilot contamination and precoding in multi-cell TDD systems. *IEEE Transactions on Wireless Communications*, 10(8):2640–2651, August 2011, DOI: 10.1109/TWC.2011.060711.101155.

[41] M. Kurras, L. Thiele, and G. Caire. Interference mitigation and multiuser multiplexing with beam-steering antennas. In *19th International ITG Workshop on Smart Antennas*, number ISBN:978-3-8007-3662-1, pages 1–5, Ilmenau, Germany, March 2015.

[42] C. P. Sukumar and R. MerR. Merched. Eltawil. Joint power loading of data and pilots in OFDM using imperfect channel state information at the transmitter. In *IEEE Global Communications Conference*, pages 1–5, Nov. 2008, DOI: 10.1109/GLOCOM.2008.ECP.872.

[43] K. Min, M. Jung, T. Kim, Y. Kim, J. Lee, and S. Choi. Pilot power ratio for uplink sum-rate maximization in zero-forcing based MUMIMO systems with large number of antennas. In *IEEE Vehicular Technology Conference (VTC-Fall)*, pages 1–5, 2-5 September 2013, DOI: 10.1109/VTCFall.2013.6692364.

[44] Kien T. Truong, A. Lozano, and R. W. Heath Jr. Optimal training in continuous block-fading massive MIMO systems. *20th European Wireless*, Barcelona, Spain, May 2014.

[45] N. Sun and J. Wu. Maximizing spectral efficiency for high mobility systems with imperfect channel state information. *IEEE Trans. Wireless Communication*, 13(3):1462–1470, March 2014, DOI: 10.1109/TWC.2014.012314.130772.

[46] K. Guo, Y. Guo, and G. Ascheid. Energy-efficient uplink power allocation in multi-cell MU-Massive-MIMO systems. In *Proc. of European Wireless,* number ISBN:978-3-8007-3976-9, pages 1–5, Budapest, Hungary, May 2015.

[47] G. Fodor, P. Di Marco, and M. Telek. On the impact of antenna correlation and CSI errors on the pilot-to-data power ratio. *IEEE Transactions on Communications*, 64(6):2622 – 2633, April 2016, DOI: 10.1109/TCOMM.2016.2549536.

[48] M. Sajadieh, A. Esswie, A. Fouda, H. Shirani-Mehr, and D. Chatterjee. Progressive channel state information for advanced multi-user mimo in next generation cellular systems. In 2016 *IEEE Wireless Communications and Networking Conference,* pages 1–6, April 2016, DOI: 10.1109/WCNC.2016.7564830.

[49] M. Ding and S. D. Blostein. Relation between joint optimizations for multiuser MIMO uplink and downlink with imperfect CSI. In *IEEE International Conference on Acoustics, Speech and Signal Processing (ICASSP)*, pages 3149 – 3152, Las vegas, NV, USA, March 31-April 4 2008. DOI: 10.1109/ICASSP.2008.4518318.

[50] J. Kron, D. Persson, M. Skoglund, and E. G. Larsson. Closed-form Sum-MSE minimization for the two-user gaussian MIMO broadcast channel. *IEEE Communications Letters,* 15(9):950–952, Sep. 2011, DOI: 10.1109/LCOMM.2011.070711.110571.

[51] J. Wang, M. Bengtsson, B. Ottersten, and D. Palomar. Robust MIMO precoding for several classes of channel uncertainty. *IEEE Trans. Signal Processing*, 61(12):3056–3070, April 2013, DOI: 10.1109/TSP.2013.2258016.

[52] B. Furht and S. A. Ahson. *Long Term Evolution: 3GPP LTE Radio and Cellular Technology. Auerbach Publications*, ISBN-10: 1420072102, April 2009.

[53] X. Hou, Z. Zhang, and H. Kayama. DMRS Design and Channel Estimation for LTE-Advanced MIMO Uplink. *70th IEEE Vehicular Technology Conference (Fall)*, pages 1–5, 2009, DOI: 10.1109/VETECF.2009.5378829.

[54] G. Fodor, P. Di Marco, and M. Telek. Performance analysis of block and comb type channel estimation for massive MIMO systems. In *First International Conference on 5G for Ubiquitous Connectivity (5GU),* pages 62–69, Nov. 2014, DOI: 10.4108/icst.5gu.2014.258076.

[55] G. Fodor, P. D. Marco, and M. Telek. On the impact of antenna correlation on the pilot-data balance in multiple antenna systems. In *IEEE International Conference on Communications (ICC)*, pages 2590–2596, London, UK, Jun. 2015. DOI: 10.1109/ICC.2015.7248715.

[56] Y. Shi, J. Wang, K. B. Letaief, and R. K. Mallik. A game-theoretic approach for distributed power control in interference relay channels. *IEEE Trans. On Wireless Communications*, 8(6):3151–3161, 2009, DOI: 10.1109/TWC.2009.080831.

[57] L. Song, Z. Han, Z. Zhang, and B. Jiao. Non-cooperative feedback-rate control game for channel state information in wireless networks. *IEEE Journal on Selected Areas in Communications,* 30(1):188–197, 2012, DOI: 10.1109/JSAC.2012.120117.

[58] H. Chen, Y. Li, Y. Jiang, Y. Ma, and B. Vucetic. Distributed power splitting for SWIPT in relay interference channels using game theory. *IEEE Transactions On Wireless Communications*, 14(1):410–420, 2015, DOI: 10.1109/TWC.2014.2349892.

[59] D. Li, Y. Xu, X. Wang, and M. Guizani. Coalitional game theoretic approach for secondary spectrum access in cooperative cognitive radio networks. *IEEE Trans. On Wireless Communications*, 10(3):844–855, 2011, DOI: 10.1109/TWC.2011.011111.100216.

[60] I. Stupia, L. Sanguinetti, G. Bacci, and L. Vandendorpe. Power control in networks with heterogeneous users: A quasi-variational inequality approach. *IEEE Trans. Signal Process.*, 63(21):5691–5705, Nov. 2015, DOI: 10.1109/TSP.2015.2452231.

[61] J. Wang, W. Guan, Y. Huang, R. Schober, and X. You. Distributed optimization of hierarchical small cell networks: A GNEP framework. *IEEE J. Sel. Areas Commun.*, 35(2):249–264, Feb. 2017, DOI: 10.1109/JSAC.2017.2658999.

[62] V. Pacifici and G. Dán. Convergence in player-specific graphical resource allocation games. *IEEE J. Sel. Areas Commun.*, 30(11):2190–2199, Dec. 2012, DOI: 10.1109/JSAC.2012.121211.

[63] G. Scutari, D. P. Palomar, and S. Barbarossa. Competitive design of multiuser MIMO systems based on game theory: A unified view. *IEEE Journal on Selected Areas in Communications*, 26(7):1089–1103, Aug. 2008, DOI: 10.1109/JSAC.2008.080907.

[64] J. Wang, G. Scutari, and D. P. Palomar. Robust MIMO cognitive radio via game theory. *IEEE Trans. on Signal Processing*, 59(3):1183–1201, March 2011, DOI: 10.1109/TSP.2010.2092773.

[65] B. Fallah, B. X. Huang, and L. Tu. Distributed asynchronous game theoretic solutions for precoding strategies in multiuser MIMO systems. *International Journal of Distributed and Parallel Systems (IJDPS)*, 3(4):133–143, July 2012, DOI: 10.5121/ijdps.2012.3414.

[66] P. Zhao, G. Fodor, G. Dan, and M. Telek. A game theoretic approach to setting the pilot-to-data power ratio in MU-MIMO systems. *IEEE Transactions on Communications,* 19(9):1604 – 1607, September 2017, DOI: 10.1109/TCOMM.2017.2778094.

[67] P. Zhao, G. Fodor, G. Dan, and M. Telek. A game theoretic approach to uplink pilot and data power control in multi-cell MU-MIMO systems. *IEEE Transactions on Vehicular Technology*, 19(9):1604 – 1607, June 2019, DOI: 10.1109/TVT.2019.2927127.

[68] S. Han, C. l. I, Z. Xu, and C. Rowell. Large-scale antenna systems with hybrid analog and digital beamforming for millimeter wave 5G. *IEEE Commun. Mag.*, 53(1):186–194, Jan. 2015, DOI: 10.1109/MCOM.2015.7010533.

[69] S. Rangan, T. S. Rappaport, and E. Erkip. Millimeter-wave cellular wireless networks: Potentials and challenges. *Proc. IEEE*, 102(3):366–385, Mar. 2014, DOI: 10.1109/JPROC.2014.2299397.

[70] Z. Pi and F. Khan. An introduction to millimeter-wave mobile broadband systems. *IEEE Communications Magazine*, 49(6):101–107, 2011, DOI: 10.1109/MCOM.2011.5783993.10

[71] S. Hur, T. Kim, D. J. Love, J. V. Krogmeier, T. A. Thomas, and A. Ghosh. Millimeter wave beamforming for wireless backhaul and access in small cell networks. *IEEE Trans. Commun.*, 61(10):4391–4403, October 2013, DOI: 10.1109/TCOMM.2013.090513.120848.

[72] O. E. Ayach, S. Rajagopal, S. Abu-Surra, Z. Pi, and R. W. Heath. Spatially sparse precoding in millimeter wave MIMO systems. *IEEE Trans. Wireless Commun.*, 13(3):1499–1513, March 2014, DOI: 10.1109/TWC.2014.011714.130846.

[73] A. Alkhateeb, O. El Ayach, G. Leus, and R. W. Heath. Channel estimation and hybrid precoding for millimeter wave cellular systems. *IEEE J. Sel. Top. Signal Process.*, 8(5):831–846, October 2014, DOI: 10.1109/JSTSP.2014.2334278.

[74] S. Kutty and D. Sen. Beamforming for millimeter wave communications: An inclusive survey. *IEEE Communications Surveys Tutorials*, 18(2):949–973, September 2016, DOI: 10.1109/COMST.2015.2504600.

[75] S. Noh, M. D. Zoltowski, and D. J. Love. Training sequence design for feedback assisted hybrid beamforming in massive MIMO systems. *IEEE Trans. Commun.*, 64(1):187–200, Jan. 2016, DOI: 10.1109/TCOMM.2015.2498184.

[76] J. Song, J. Choi, and D. J. Love. Common codebook millimeter wave beam design: Designing beams for both sounding and communication with uniform planar arrays. *IEEE Trans. Commun.*, 65(4):1859–1872, Apr. 2017, DOI: 10.1109/TCOMM.2017.2665497.

[77] H. Shokri-Ghadikolaei, F. Boccardi, C. Fischione, G. Fodor, and M. Zorzi. Spectrum sharing in mmWave cellular networks via cell association, coordination, and beamforming. *IEEE J. Sel. Areas Commun.*, 34(11):2902–2917, November 2016, DOI: 10.1109/JSAC.2016.2615259.

[78] M. Wu, D. Wuebben, A. Dekorsy, P. Baracca, V. Braun, and H. Halbauer. Hardware impairments in millimeter wave communications using OFDM and SC-FDE. In *Proc. Smart Antennas (WSA), 2016 International ITG Workshop on*, number ISBN:978-3-8007-4177-9, pages 1–8, March 2016.

[79] A. Khansefid, H. Minn, Q. Zhan, N. Al-Dhahir, H. Huang, and X. Du. Waveform parameter design and comparisons for millimeterwave massive MIMO systems with RF distortions. In *Proc. IEEE Globecom Workshops (GC Wkshps)*, pages 1–6, Dec 2016, DOI: 10.1109/GLOCOMW.2016.7849081.

[80] H. Yan and D. Cabric. Digital predistortion for hybrid precoding architecture in millimeter-wave massive MIMO systems. In *Proc. 42nd IEEE Int. Conf. on Acoustics, Speech and Signal Process.*, Mar. 2017, DOI: 10.1109/ICASSP.2017.7952803.

Gábor Fodor [SM'08] (Gabor.Fodor@ericsson.com) received his Ph.D. degree in electrical engineering from the Budapest University of Technology and Economics in 1998, his Docent degree from KTH Royal Institute of Technology, Stockholm, Sweden, in 2019, and his D.Sc. degree from the Hungarian Academy of Sciences in 2019. He is currently a master researcher with Ericsson Research and an adjunct professor with KTH Royal Institute of Technology. He was a co-recipient of the IEEE Communications Society Stephen O. Rice Prize in 2018. He is serving as the Chair of the IEEE Communications Society Full Duplex Emerging Technologies Initiative and as an Editor for IEEE Transactions on Wireless Communications.

László Pap graduated from the Technical University of Budapest, Faculty of Electrical Engineering, Branch of Telecommunications. He became Dr. Univ. and Ph.D. in 1980, and Doctor of Sciences in 1992. In 2001 and 2007 he has been elected as a Correspondent and Full Member of the Hungarian Academy of Sciences. His main fields of the research are the electronic systems, nonlinear circuits, synchronization systems, modulation and coding, spread spectrum systems, CDMA, multiuser detection and mobile communication systems. His main education activity has covered the fields of electronics, modern modulation and coding systems, communication theory, introduction to mobile communication. Professor Pap had been Head of the Dept. of Telecommunications, the Dean of the Faculty of Electrical Engineering at Budapest University of Technology and Economics, and Vice Rector of the University.

Miklós Telek graduated as an electrical engineer at the Faculty of Electrical Engineering, Technical University of Budapest in 1987. He received the candidate of science and the MTA doctor degree from the Hungarian Academy of Sciences in 1995 and 2004, respectively. Since 1990 he has been with the Technical University of Budapest. Currently, he is a professor at Department of Networked Systems and Services. Since 2012, he is heading the MTA-BME Information Systems Research Group of the Hungarian Academy of Sciences. His current research interests include various aspects of stochastic performance modeling and analysis of computer and communication systems.

Cooperative OSIC System to Exploit the Leakage Power of MU-MIMO Beamforming based on Maximum SLR for 5G

Cebrail ÇiFTLiKLi, Musaab AL-OBAIDI, Mohammed FADHIL and Wael AL-OBAIDI

***Abstract*— This study investigated the crucial—but not well-discussed—issues involved in designing beamforming for all receivers, subject to leakage power constraints. Our assumption is that all users use ordered successive interference cancellation (OSIC) detection when the channel state information (CSI) is available. The problem of interest is to find beamforming that can improve OSIC performance of a multi-user scheme without significantly increasing the complexity. This study considers the transceiver design for multi-user MIMO (MU-MIMO) communications, in which a single transmitter adopts beamforming to simultaneously transmit information at first time-slot. During the second time-slot, receivers cooperate to share specific results of OSIC detection in each user. We propose the maximum-likelihood (ML) to estimate the received symbols. The estimated symbols will be used in OSIC detection to detect interference symbols. Promising results show that our cooperative OSIC scheme of the MU-MIMO beamforming system based on maximum signal-to-leakage ratio (SLR) realizes the diversity order of OSIC. Also, by utilizing leakage power as a useful power and not just as an interference power, the performance of the proposed scheme over Rayleigh and Rician channels is significantly better than the performance of classical MU-MIMO beamforming system based on SLR at a high signal-to-noise ratio (SNR).**

***Index Terms* — MU-MIMO, Beamforming, CSI, SLR, OSIC, ML.**

I. INTRODUCTION

Communication over MIMO channels has appealed to scientists because of its promising results and extraordinary performance. MIMO systems have the tremendous potential to achieve great throughput and high reliability in wireless communication systems [1]. Recently, especially since the discovery of the MIMO broadcast channel capacity, attention has shifted to the MU-MIMO wireless system [2]-[4], which is emerging wireless communication technology. It is highly expected that future 5G networks should achieve a 10-fold increase in connection density, i.e., 10^6 connections per square kilometers [5].

Beamforming scheme based on SLR technology enables the MU-MIMO system to provide good quality of service (QoS), thus absorbing more users and makes it promising to address the 5G requirement of massive connectivity. Specifically, in Internet of Things (IoT) scenario and massive machine-type communications (mMTC) scenario, which are considered as typical 5G application scenarios. In these scenarios, users may be low-cost sensors deployed in a small area, where both line-of-sight (LOS) and non-line-of-sight (NLOS) exist, which can be better modeled by the Rician fading channel. 4G and 5G cellular systems rely on MU-MIMO transmitters, which use linear precoding [6]-[9]. Although linear precoding is incapable of achieving the channel capacity in regions of MIMO broadcasts, it is an attractive choice because of its simplicity. In MU-MIMO systems, several users with an antenna array employ identical frequency bands and time slots to communicate with the base station (BS). Therefore, these systems are susceptible to co-channel interference (CCI) [10], which can decline the overall capacity of MU-MIMO systems. In [11], the system performance with regards to the Alamouti scheme undergoes both analysis and evaluation with block diagonalization precoding applied when there is the presence of CSI.

For optimized performance, it is extremely important to suppress CCI [12]. Although the transmitter can coordinate transmission from all of its antenna elements, users cannot coordinate with one another. Overcoming this inability of the user is the major challenge in MU-MIMO systems [13]. To ensure the complexity is lower at the receiving end, transmitter optimization must be addressed. The most commonly used techniques for transmission optimization include CSI at the transmission side to deal with the CCI. This technique will definitely reduce overhead due to channel feedback.

Numerous works have suggested such schemes for perfectly cancelling the CCI for each receiver [14]-[17]. Although these schemes lead to excellent performance, they tend to restrict the system configuration because it requires using a specific number of antennas. This approach also results in obvious system capacity cutbacks as the useful power of the received signals is significantly reduced at a low SNR [18].

This paper submitted in 12 Jan 2019.

Cebrail ÇiFTLiKLi, he joined Vocational College, Erciyes University, Kayseri, Turkey, as Professor where he is now principal (e-mail: cebrailc@erciyes.edu.tr).

Musaab AL-OBAIDI, he is Ph.D. student in Department of Electrical and Electronics Engineering, Erciyes University, Kayseri, Turkey (e-mail: musaab_sami2000@ yahoo.com).

Mohammed Fadhil, he is currently Ph.D. candidate at Universiti Kebangsaan Malaysia (UKM), Kuala Lumpur, Malaysia (e-mail: moh_fadhil77@yahoo.com).

Wael AL-OBAIDI, he is M.Sc. student in Department of Electrical and Electronics Engineering, Erciyes University, Kayseri, Turkey (e-mail: wael.s.ismaeel@gmail.com).

DOI: 10.36244/ICJ.2019.3.3

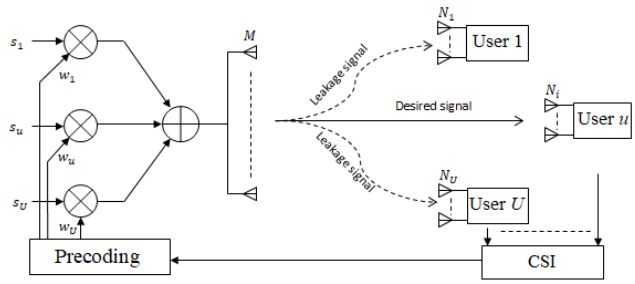

Fig. 1. Block diagram of the MU-MIMO beamforming system.

Other approaches rely on using algorithms to boost or maximize the useful power of received signals. However, these algorithms do not attempt to reduce multi-user interference. Hence, the systems based on these algorithms are also not perfect owing to their susceptibility to interference at high SNRs [19]. Broadly, all these systems either attempt to maximize the output of signal-to-interference-plus-noise ratio (SINR) or minimize the transmission power while satisfying the SINR targets for all the users. Owing to the coupled nature of both signals and interference, most of the solutions are typically iterative. Algorithm-based systems also lose the same power to keep these systems simple and uncomplicated. We actually are crawling from simplicity to little complexity in the BS and, in some cases, shifting gradually from little complexity to clear complexity.

This study proposes a novel MU-MIMO downlink scheme. This study considers an alternative approach based on the concept of SLR to design transmits beamforming vectors and uses OSIC [20] in each user to detect its own signal and then detect other users' signals. Our suggested system encourages cooperation between users to share the interference signal so that the benefit of leakage power can be realized. In our proposed system, the complexity in the BS will be reduced by giving very few tasks to the users to support the desired signal by reusing the leakage signal. In the MU-MIMO beamforming system based on SLR, the design procedure for precoding weight needs to use constantly of proportionality, which is chosen to normalize the norm of the precoding to unity [10]. Comparing this solution to the proposed scheme; there is no need to do this step in BS. Also, in our proposed scheme, a cooperative SLR transmission scheme did not use coding in the transmission process and thus did not use the decoding and recoding in the user. Extensive simulations in the MU-MIMO system have been carried out over Rayleigh (in the NLOS environment) and Rician fading channels (in the LOS environment).

The simulation results demonstrate that the proposed scheme outperforms classical schemes at high SNRs. Furthermore, it can significantly reduce the BS complexity. The rest of the paper is organized as follows. The system model is introduced in Section II. In Section III, we review the SLR precoding. Section IV provides proposed scheme. In Section V we provide and discuss the simulation. In section VI concludes the paper. Finally, in section IX we provide the contribution of this paper. The superscripts$(\cdot)^{\mathrm{T}}$, $(\cdot)^{*}$, $(\cdot)^{\mathrm{H}}$, and $(\hat{\cdot})$ denote transpose, complex conjugate, Hermitian operations, and noisy version of $(\cdot)$, respectively.

II. SYSTEM MODEL

We considered an environment of downlink MU-MIMO broadcast channel consisting of U geographically sparse mobile stations communicating with the BS that has M antennas. In such an environment system, each user is independent. Let user i employing N_i antennas. This user will receive its own signal, as shown in Fig. 1. This user will receive its own signal, while the other users will receive the leakage signal of user i. We define $N_T=\sum_{u=1}^{U} N_u$ as the total number of users' antennas for $u = \{1, \ldots, U\}$. For a typical wireless communication network, we imagine that $N_T \geq M$ with the independent channels of flat fading. Suppose that the intended message signal for user i is the scalar s_i [10]. Therefore, the transmitted symbol vector to U users is:

$$S = [\, s_1, \ldots, s_U]^T \tag{1}$$

In the precoding step, the matrix of precoding is denoted as follows:

$$W = [\, w_1, \ldots, w_U] \tag{2}$$

where $w_i \in C^{M \times 1}$ is the joint precoding vector (beamforming coefficients) for the user i. After the joint precoding step, the symbol is multiplied by beamforming vector and then the transmitted vector will be:

$$X = \sum_{u=1}^{U} w_u s_u = WS \tag{3}$$

It is assumed that signals $WS \in C^{M \times 1}$ are broadcast over the channels denoted as:

$$H = [H_1^T, \ldots, H_U^T]^T \tag{4}$$

where $H_i \in C^{N_i \times M}$ describes the channel coefficients between the N_i receiver antenna at the user i and BS antennas as follows:

$$H_i = \begin{bmatrix} h_i^{(1,1)} & \ldots & h_i^{(1,M)} \\ \vdots & \ddots & \vdots \\ h_i^{(N_U,1)} & \ldots & h_i^{(N_U,M)} \end{bmatrix} \tag{5}$$

where $h_i^{(n,m)}$ denotes the channel coefficient between the BS, which has the m transmitter antenna, and the user i, which has the n receiver array antenna. Thus, the received signals at the receivers' antennas are:

$$\boldsymbol{y} = [\, y_1{}^T, \ldots, \, y_U{}^T]^T = HWS + no \tag{6}$$

where $y_i \in C^{N_i \times 1}$ represents the signal received at the recipient i, while that for the additive noise is denoted by $no \in C^{UN_i \times 1}$.

When each user has been carefully considered separately, we will find the received signal at a recipient i as:

$$\begin{aligned} y_i &= H_i \sum_{u=1}^{U} w_u s_u + no_i \\ &= H_i w_i s_i + H_i \sum_{u=1, u \neq i}^{U} w_u s_u + no_i \end{aligned} \tag{7}$$

The H_i vector has complex Gaussian variable components with unit variance and zero mean. Moreover, the components of the additive noise no_i have a distribution as $N(0,\sigma_i^2)$ and are temporarily and spatially white. To describe the proposed scheme clearly, the original SLR-based precoding scheme [10] is reviewed in the next section.

III. SLR PRECODING

The original SLR-based precoding scheme is reviewed in [10]. Recall that SLR is defined as the ratio of received signal power at the desired user to received signal power at the other terminals (the leakage power) plus noise power without considering receive matrices. This scheme computes the maximum beamforming precoding (w_i^o) of each user from the maximum SLR of these users [10] as follows:

$$SLR = \frac{||H_i w_i||^2}{\sum_{u=1.\ u\neq i}^{U} ||H_u w_i||^2} \quad (8)$$

Then

$$w_i^o = arg \ \ max \ \frac{||H_i w_i||^2}{\sum_{u=1.\ u\neq i}^{U} ||H_u w_i||^2} \quad (9)$$

where $||H_i w_i||^2$ represents the required signal power of user *i*, while $\sum_{u=1.\ u\neq i}^{U} ||H_u w_i||^2$ represents the total leakage power from the total power of user *i* as an interference to the other users. By substituting $\widetilde{H}_i = \sum_{u=1.\ u\neq i}^{U} H_u$ into (8), we can obtain

$$SLR = \frac{||H_i w_i||^2}{||\widetilde{H}_i w_i||^2} = \frac{w_i^* H_i^* H_i w_i}{w_i^* \widetilde{H}_i^* \widetilde{H}_i w_i} \quad (10)$$

As in [10] we can solve (9) as

$$\frac{w_i^* H_i^* H_i w_i}{w_i^* \widetilde{H}_i^* \widetilde{H}_i w_i} \leq \lambda_{max}\left(H_i^* H_i, \widetilde{H}_i^* \widetilde{H}_i\right) \quad (11)$$

where λ_{max} is the largest generalized eigenvalue. According to the SLR criterion, the precoding matrix w_i is designed based on the following metric:

$$w_i^o \propto max\ gen.eigenvector\left(H_i^* H_i, \widetilde{H}_i^* \widetilde{H}_i\right) \quad (12)$$

Depending on [10], the proportionality constant is chosen to normalize the norm of w_i^o to unity. At user *i*, the maximum-likelihood detection scheme will be used to estimate s_i from the received signal as follows [10]:

$$\hat{s}_i = \frac{w_i^* H_i^*}{||H_i w_i||^2} y_i \quad (13)$$

Then

$$\hat{s}_i = s_i + \frac{w_i^* H_i^* \sum_{u=1.\ u\neq i}^{U} H_i w_u s_u}{||H_i w_i||^2} + \frac{w_i^* H_i^*}{||H_i w_i||^2}\ no_i \quad (14)$$

IV. COOPERATIVE ALGORITHM

Considerable limited network resources such as energy can be saved through cooperation, which also increases the reliability and quality of services. Quality and reliability are measured by parameters such as bit error rate and outage probability. Hence, cooperation can extend the coverage range and data throughput.

1. Amplify-And-Forward (AAF)

A simple form of wireless cooperative communication is the AAF method. In this method, the signal received by each relay is a noise signal. It suffers from attenuation. Therefore, the noisy version of the original signal needs to be amplified before it can be sent again by the partner or relay. In doing so, the noise in the signal is also amplified. At the destination, the information transmitted by the user and partner will be combined. Although the AAF method amplifies the signal, it also amplifies the noise. Laneman and Wornell [21] present and analyze the AAF method.

2. Decode-And-Forward (DAF)

This method involves two sub-steps. First, the partner decodes the user's information, and second, the decoded information is retransmitted to the destination. Therefore, there is no amplified noise in the sent signal. The DAF is the most preferred method in a relay. This method can only be meaningfully provided the relay can decode the original message completely. Sendonaris employed the DAF signaling in a simple code-division multiple access (CDMA) system with two users [22].

V. PROPOSED SCHEME

In this section, a novel MU-MIMO system is proposed aimed at fully benefiting from the transmission power to each user. In practice, in MU-MIMO beamforming based on maximum SLR system, the power leaked from one user to the others is different. Power control in BS is usually applied to design a beamforming coefficient for each user.

From the literature on SLR precoding described in Section III, we consider an appropriate combination of three algorithms.

1. Precoding Design

Based on [19], the drawback of [10] is that when each user has multiple data streams, the effective channel gain for each stream can be severely unbalanced. If power control or adaptive modulation and coding cannot be applied, then the overall error performance of each user will suffer a significant loss. Therefore, unlike the original SLR scheme in [10], which gives the solution in Equation (12) dependent on *subject to* $\|w_u\|^2 = 1$, we apply total transmission power constraints (P_u) at the transmitter, which can be described as $E(\|w_u s_u\|^2) \leq P_u$. The symbol s_u satisfies the power constraint as $E_u = E(|s_u|^2) = 1$. Therefore, the same solution is chosen in Equation (12) but depends on [23]:

$$subject\ to\ \|w_u\|^2 = {w_u}^H w_u \leq P_u / E_u \quad (15)$$

Note that the norm of w_u is irrelevant to the final solutions; in other words, the norm of w_u can be forced to be any value to achieve the best value for w_u under the power constraints.

2. OSIC Detection Algorithm

Linear detection methods require a low complexity of hardware implementation. The OSIC method helps to improve performance without increasing complexity. In OSIC, based on the received signal at all the antennas, the symbols are selected to remove the effect from the others. To reduce the interference, the detected signal in each stage is subtracted from the received signal [20]. Suppose that the ML detection scheme will be used to estimate s_i from the received signal. After estimation, the remaining signal in the first stage is formed by subtracting it from the received signal y_i. After estimation s_i, the remaining signal in the first stage is formed by subtracting it from the received signal as shown in Fig. 2, that is,

$$\hat{y}_i = y_i - H_i s_i \tag{16}$$

then the interference is successfully canceled in the course of estimating s_u , $u=1, \ldots, i-1, i+1, \ldots, U$. After estimating all s_u in each user, all users cooperate with one another to share the interference signal only to benefit from the leakage power.

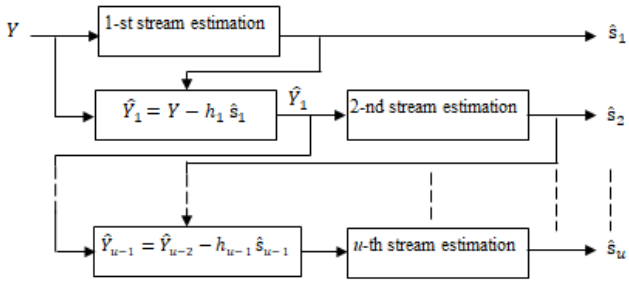

Fig.2 Illustration of OSIC-MU signal detection for u-th spatial streams of user 1

3. Hybrid Relaying Model

Our suggestion cooperative method is different from DAF as well as from AAF method. We produce a Hybrid Relaying model of DAF and AAF which does not depend on coding the signal in BS like DAF method, but it depends on the estimation of the leakage signal using OSIC (without decoding and recoding the leakage signal like DAF method) in the first user (or relay). Then the estimated leakage signals multiplies by control power parameter (β) and it transmits to the second user (or destination) without increasing the effect of noise as in AAF method. In this way, the complexity of BS will reduce based on dispense of using coding technique in BS. Also, the decoding and recoding the leakage signal in the relay was excluded, to reduce the processing latency, thus reducing the complexity load in real-time detection in the relay and depend on signal estimation and leakage power in the user side. In the proposed scheme, at the first interval, using ML estimation and OSIC detection, each user differentiates and identifies its own signal (desired signal) from other user signals known as the leakage signal. At the second interval, the leakage signals for other users are transmitted to them. By using this scheme, we can benefit from leakage power and turn it into a productive power by using the combiner in each user to combine the desired signal detected by each user as its own signal with the leakage signal detected by other users as an interference signal. When the inter-user channel (the channel between users) is appropriate, the control power (β) will be used for the interference signal cooperation. Simply put, to take advantage of the leaked signal, the signal leaked from the original signal will be reintroduced to its real destination. Total transmission power constraints exist at the transmitter, which can be described as $E(\|\beta_i s_i\|^2) \leq P_i$. β_i is a constant to meet the total transmitted power constraint and is given as follows [20]:

$$\beta = \sqrt{\frac{N_T}{Tr(H^{-1}(H^{-1})^H)}} \tag{17}$$

Therefore, the transmitted signal from u-th to i-th user at the second time slot is:

$$\hat{s}_{u-i-2nd} = \beta * \hat{s}_{u-i-1st} \tag{18}$$

where $\hat{s}_{u-i-1st}$ is the noisy version of the leakage signal ($s_{u-i-1st}$) from the i-th user who is detected by the u-th user at the first time slot. The received signal at the second time slot in i-th user is given by

$$y_{u-i-2nd} = H_{u-i-2nd} * \hat{s}_{u-i-2nd} + no_i \tag{19}$$

where $H_{u-i-2nd}$ is the inter-user channel between the user u and user i. no_i is the AWGN in user i. In user i, maximum ratio combiner (MRC) will be used to combine the desired signal ($\hat{s}_i$), which is detected as its own signal at the first time slot, with $\hat{s}_{u-i-2nd}$. By using MRC scheme, the signal of i-th user will be

$$\begin{aligned} s_i &= \hat{s}_i + \sum_{u=1,\ u\neq i}^{U} \hat{s}_{u-i-2nd} \\ &= \hat{s}_i + \sum_{u=1,\ u\neq i}^{U} \frac{H^*_{u-i-2nd}}{||H_{u-i-2nd}||^2} * y_{u-i-2nd} \end{aligned} \tag{20}$$

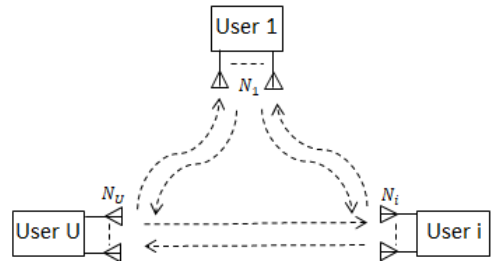

Fig.3 Cooperative of OSIC-MU signal detection for u-th spatial streams of u-th user

VI. DOWNLINK CHANNEL MODEL

Due to LOS propagation, the strongest propagation component of MIMO channel corresponds to the deterministic component (also referred to as specular components). On the other hand, all the other components are random components (due to NLOS also referred to as scattering components) [20].

VI. DOWNLINK CHANNEL MODEL

Due to LOS propagation, the strongest propagation component of MIMO channel corresponds to the deterministic component (also referred to as specular components). On the other hand, all the other components are random components (due to NLOS also referred to as scattering components) [20].

The broadcast channel distribution has been following the Rayleigh channel distribution which is Gaussian distribution with a variance of σ^2 and zero mean. That means there is no component of LOS (K= 0): $\sigma = \sqrt{\frac{1}{K+1}}$. On the other hand, when there is any component of LOS (For K > 0) the broadcast channel distribution has been following the Gaussian distribution with a variance of σ^2 and mean of q or Rician distribution when K increases as: $q = \sqrt{\frac{K}{K+1}}$, $\sigma = \sqrt{\frac{1}{K+1}}$. Therefore, in this work, the channel matrix of MIMO system is described as [24]:

$$H = \sqrt{\frac{K}{K+1}}\ H_d + \sqrt{\frac{1}{K+1}}\ H_r \qquad (21)$$

where H_d is representing the component of the normalized deterministic channel matrix, while H_r is representing the component of random channel matrix, with $||\ H_d\ ||^2 = N_T\ M$, $E\{\ |[H_r]_{i,j}|^2\}$= 1, i = 1: N_T, j = 1: M [24]. While K is known as a factor of the Rician channel which is the relation between the component of the specular power c^2 and the component of scattering power $2\sigma^2$, displayed as [20]:

$$K = \frac{\|H_d\|^2}{E\left\{\left|[H_r]_{i,j}\right|^2\right\}} = \frac{c^2}{2\sigma^2} \qquad (22)$$

VII. SIMULATION RESULTS AND EVALUATION

In this part, it was evaluated the signal-to-noise ratio (SNR) against the bit error rate (BER) as a scale of precoding efficiency. A typical MU-MIMO scheme is imitated to estimate the performance of the suggested MU-MIMO beamforming precoding scheme over the Rayleigh fading channel as a conventional channel in the first time slot (downlink channel) and Rician fading channel as a realistic channel in the second time slot (inter-user channel). For random Rayleigh and Rician fading channel case, the samples of these parameters are set up to 1000 with elements generated as zero-mean for Rayleigh fading channel while m-mean for Rician fading channel and unit-variance independent and identically distributed (i.i.d) complex Gaussian random variables. We simulate MU-MIMO system, where the average BER is taken of SLR-based precoding approach at BS while the receiver was using a ML with OSIC detection approach.

BS transmits by M antennas to each user over the noisy channel and flat fading channel while each user has employed N_u antennas to receive the signal. QPSK signal constellation has been used as a broadcast modulation in all simulations and the results are averaged through several channel investigations. For all receivers, the noise variance per receive antenna is supposed to be equal, $\sigma_1^2 = \ldots = \sigma_U^2 = \sigma^2$. As for the power constraints, $P_u = P_i = 1$ is considered. The typical values and simulation parameters are presented in Table 1.

Table 1.
Typical values and simulation parameters.

Parameters	Definition
Channel type	Rayleigh and Rician
SNR of inter user channel	15dB
Number of users (U)	3
Number of antenna for BS (M)	6
Number of antenna in each user (Ni)	3
Rician channel factor (K)	10 – 15dB
Beta (β)	0.075 – 0.15

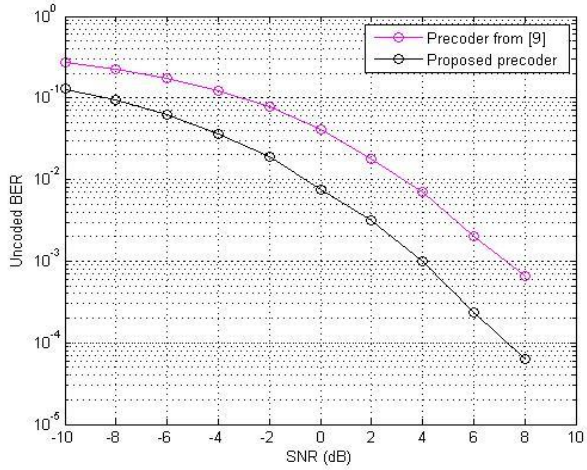

Fig.4 MU-MIMO system for M = 6, U = 3, Ni = 3.

Fig. 4 illustrates the comparison of the classical MU-MIMO beamforming system based on SLR and the proposed precoder. While the classical MU-MIMO beamforming system based on SLR, which maximizes the useful power of users and neglects the MU interference fails in a multi-user environment, to pass the proposed precoder, the proposed precoder provides an acceptable BER. For example in Figure 5, the classical MU-MIMO beamforming system based on SLR achieves 10^{-3} uncoded BER at a SNR of 7dB while the proposed precoder maintains an acceptable 10^{-3} uncoded BER for 3 simultaneously active users at a SNR of 4dB.

Figs. 5, 6 and 7 present the results based on the BS as a transmitter and three nodes as receivers. In the presented scheme, each one of these nodes will be a receiver in the first time slot and a relay node in the second time slot. These figures illustrate that the performance of the cooperative OSIC scheme for downlink channels has an equal value of SNR (from -10dB to 10dB), while the SNR of the inter-user channel equals 15dB.

Note that the results of this diversity are the outcome of cooperation between the users to share some results of OSIC detection. Another observation is the results of the cooperative OSIC scheme, which is indicated by the curve between the bit error rate (BER) in relation to SNR. These users must be able to identify a suitable partner to obtain optimal performance through their knowledge of the inter-user channel characteristics between each user and its' partner.

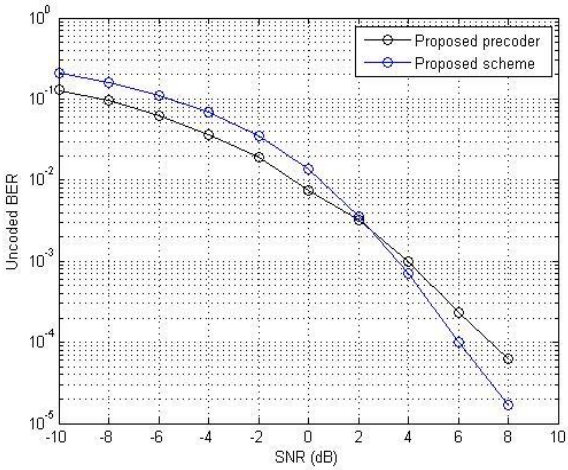

Fig.5 MU-MIMO system for $M = 6$, $U = 3$, $Ni = 3$, Rician inter user channel with $K = 15$ dB and $\beta = 0.15$.

As seen in Fig.5, in the case of the proposed scheme, the performance of the system gradually and continuously improved with increases in the values of SNRs. On the other hand, in the case of the proposed precoder, the performance of the system was dramatically improved at significantly lower values of SNRs.

Unfortunately, when the values of SNRs increased, performance improvement slowly stabilized even at high values of SNRs comparing to the proposed scheme.

That is because of noise and inter-user interference factors. For the proposed precoder, which supports inter-user interference but does not benefit from it, the system performed better than the proposed scheme at low SNR values because the effect of noise was bigger than the effect of inter-user interference. Therefore, at low SNR values, the major factor limiting the performance of the system was the noise.

On the other hand, the proposed scheme, which supports multi-user interference to take advantage of it, outperformed the proposed precoder at high values of SNRs because the effect of inter-user interference as the useful signal was greater than the effect of noise on the system. Therefore, at high values of SNRs, the major factor limiting the performance of the system was inter-user interference.

Fig. 6 illustrates the comparison of the proposed precoder and the proposed scheme to select the optimum value of β. In the proposed scheme, two scenarios are observed compared to the proposed precoder. In the first scenario, when $\beta = 0.15$, the proposed precoder has better performance than the proposed scheme for SNR values lower than 3dB.

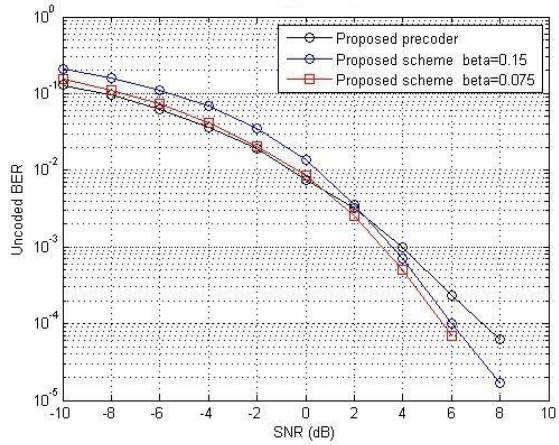

Fig.6 MU-MIMO system for $M = 6$, $U = 3$ and $Ni = 3$, Rician inter user channel with $K = 15$ dB.

This result is attributed to the high effect of noise and MU interference in the second time slot of the proposed scheme when the users will share the signals with high interference value. In the second scenario, when $\beta = 0.075$, the effect of the interference on sharing signals is reduced.

Therefore, the performance of the proposed scheme is improved when SNR > 0dB. Therefore, the interference is the main factor limiting the capacity of the system because the proposed scheme turns the interference signals into useful signals when it detects these signals using OSIC. Furthermore, it can benefit from the MU interference by sharing these signals among users. Therefore, the proposed scheme with $\beta = 0.075$ enjoys better performance than the proposed scheme with $\beta = 0.15$.

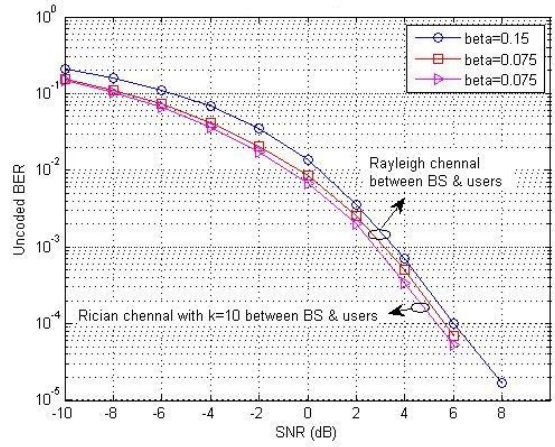

Fig.7 MU-MIMO system for $M = 6$, $U = 3$, $Ni = 3$, Rician channel between users with $K = 15$ dB.

Fig.7 shows the BER results for different system configurations. Although the performance of the proposed scheme significantly improved when the channel between BS and users is a Rician channel with K=10 dB.

VIII. CONCLUSION

This study proposed a novel MU-MIMO downlink scheme that appropriately combines an SLR-based beamforming precoding scheme (with different power constraints) and an OSIC-MU detection scheme to improve the performance of the MU-MIMO system.

To achieve the OSIC-MU detection of the proposed scheme, we also presented a Hybrid Relaying model of AAF and DAF cooperative algorithm to share the specific results of OSIC detection in each user. The signal that leaked from the original signal was reintroduced to its real destination to take advantage of it. In the proposed scheme, the complexity in the BS will be reduced by reducing the design procedure for beamforming precoding. Because in the conventional SLR-beamforming scheme the precoder procedure needs to the proportionality constant. The proportionality constant is chosen to normalize the norm of the precoder to be unity. Comparing this solution to the proposed scheme; there is no need for this step in BS.

On the other hand, the Hybrid Relaying cooperative SLR transmission scheme did not use coding in the BS and thus not using the decoding and recoding in the relay without increasing the effect of noise. In this way, the complexity of BS will be reduced. Also, the processing latency will be reduced, thus reducing the complexity load in real-time detection in the relay. Simulations were carried out over the Rayleigh fading downlink channel in the first time slot and then over the Rician fading inter-user channel in the second time slot.

Simulation results demonstrated that the proposed scheme outperforms the classical SLR-based beamforming precoding schemes. The performance of the proposed scheme with different numbers of users and numbers of antennas was also investigated. The critical parameters of the proposed scheme were likewise demonstrated.

IX. CONTRIBUTION OF THE WORK

The contribution of this paper is exploiting the leakage power of MU MIMO Beamforming, by applying the following model and scheme:

1-This study proposed a cooperative model for the downlink MU-MIMO Beamforming system.

2-This paper considers an alternative approach based on the concept of SLR to find a beamforming weight that can improve the OSIC performance of the MIMO scheme without significantly increasing the complexity of the system.

REFERENCES

[1] E. Telatar, "Capacity of multi-antenna Gaussian channels," Euro. Trans. Telecommun., vol. 10, no. 6, pp. 585-595, November 1999. DOI: 10.1002/ett.4460100604.

[2] Q. H. Spencer, C. B. Peel, A.L. Swindlehurst, and M. Haardt, "An Introduction to the Multi-user MIMO Downlink," *IEEE Commun. Mag.*, vol. 24, no. 10, pp. 60-67, October 2004. DOI: 10.1109/ MCOM. 2004.1341262.

[3] P. Viswanath and D. Tse, "Sum capacity of the vector Gaussian broadcast channel and uplink-downlink duality," *IEEE Trans. Inform. Theory*, vol. 49, no. 8, pp. 1912-1921, August 2003. DOI: 10.1109/TIT.2003.814483.

[4] W. Yu and J. Cioffi, "Sum capacity of Gaussian vector broadcast channels," *IEEE Trans. Inform. Theory*, vol. 50, no. 9, pp. 1875-1892, September 2004. DOI: 10.1109/TIT.2004.833336.

[5] F. Boccardi, R. W. Heath, A. Lozano, T. L. Marzetta, and P. Popovski, "Five disruptive technology directions for 5G," *IEEE Commun. Mag.*, vol. 52, no. 2, pp. 74–80, Feb. 2014. DOI: 10.1109/MCOM. 2014.6736746.

[6] M. Vu and A. Paulraj, "MIMO wireless linear precoding," *IEEE Signal Processing Magazine*, vol. 24, no. 5, pp. 86–105, Sept. 2007. DOI: 10.1109/MSP.2007.904811.

[7] E. L. Bengtsson, F. Rusek, S. Malkowsky, F. Tufvesson, P. C. Karlsson, and O. Edfors, "A simulation framework for multiple-antenna terminals in 5G massive MIMO systems," *IEEE Access*, vol. 5, no. 99, pp. 26819 - 26831, 2017. DOI: 10.1109/ACCESS.2017.2775210.

[8] A. Gupta and R. K. Jha, "A survey of 5G network: Architecture and emerging technologies," *IEEE Access*, vol. 3, pp. 1206–1232, 2015. DOI: 10.1109/ACCESS.2015.2461602.

[9] Cong Shen, "Downlink Multi-User MIMO Precoding Design Via Signal-Over-Leakage Capacity," *IEEE Access*, vol. 6, pp. 2812-2824, Dec. 2017. DOI: 10.1109/ACCESS.2017.2785347.

[10] A. Tarighat, M. Sadek, and A. H. Sayed, "A multiuser beamforming scheme for MIMO channels based on maximizing signal-to-leakage ratios," *IEEE International Conference on Acoustics, Speech, and Signal Processing*, pp. 1129–1132, March 2005. DOI: 10.1109/ICASSP.2005.1415913.

[11] C. ÇiFTLiKLi, M. AL-OBAIDI, "*Combining Alamouti STBC with Block Diagonalization for Downlink MU-MIMO System over Rician Channel for 5G*," Infocommunications Journal, vol. XI, no. 1, pp. 22-28, March 2019.

[12] H. Du and P. J. Chung, "A probabilistic approach for robust leakage-based MU-MIMO downlink beamforming with imperfect channel state information," *IEEE Trans. Wireless Commun.*, vol. 11, no. 3, pp. 1239–1247, Mar. 2012. DOI: 10.1109/TWC.2012.011012.111260.

[13] G. J. Foschini and M. J. Gans, "On limits of wireless communications in a fading environment when using multiple antennas," *Wireless Pers. Commun.*, vol. 6, pp. 311-335, March 1998. DOI: 10.1023/A: 1008889222784.

[14] Q. H. Spencer, A. L. Swindlehurst, and M. Haardt, "Zeroforcing methods for downlink spatial multiplexing in multiuser MIMO channels," *IEEE Transactions on Signal Processing*, vol. 52, pp. 461–471, Feb. 2004. DOI: 10.1109/TSP.2003.821107.

[15] M. Bengtsson, "A pragmatic approach to multi-user spatial multiplexing," *IEEE Sensor Array and Multichannel Signal Processing Workshop*, Rosslyn, VA, pp. 130–134, Aug. 2002. DOI: 10.1109/SAM. 2002.1191014.

[16] R. Chen, J. G. Andrews, and R. W. Heath, "Multiuser space-time block coded MIMO with downlink precoding," I*EEE International Conference on Communications*, Paris, France, pp. 2689–2693, June 2004. DOI: 10.1109/ICC.2004.1313019.

[17] K. Wong, R. D. Murch, and K. B. Letaief, "Performance enhancement of multiuser MIMO wireless communication systems," *IEEE Transactions on Communications*, vol. 50, pp. 1960–1970, Dec. 2002. DOI: 10.1109/TCOMM.2002.806503.

[18] H. Liu, X. Cheng, Z. Zhou, G. Wu, "*Block Diagonalization Eigenvalue Based Beamforming precoding design for Downlink Capacity Improvement in Multiuser MIMO channel,*" IEEE International Conference on Wireless Communications and Signal Processing (WCSP), November 2010. DOI: 10.1109/WCSP.2010.5633549.

[19] Y. Jiang, J. Li, and W. W. Hager, "*Joint Transceiver Design for MIMO communications using Geometric Mean Decomposition*," IEEE Trans. Signal Process., vol. 53, no. 10, pp. 3791-3803, October 2005. DOI: 10.1109/TSP.2005.855398.

[20] Y. S. Cho, J. Kim, W. Y. Yang, C. G. Kang, "*Wireless Communications with MATLAB*," John Wiley & Sons, New York, p.544, 25 Aug 2010.

[21] J. N. Laneman and G. W. Wornell, "Cooperative diversity in wireless networks: efficient protocols and outage behavior," *IEEE Trans. Inform. Theory*, vol. 50, no. 12, pp. 3062-3080, 2004. DOI: 10.1109/TIT .2004.838089

[22] A. Sendonaris, E. Erkip, and B. Aazhang, "User Cooperation Diversity Part I and Part II," *IEEE Trans. Commun.*, vol. 51, no. 11, pp. 1927–1948, Nov. 2003. DOI: 10.1109/TCOMM.2003.819238.

[23] E. Bjornson, M. Bengtsson, B. Ottersten, "Optimal multiuser transmit beamforming: A difficult problem with a simple solution structure," *IEEE Signal Process.* Mag., vol. 31, no. 4, pp. 142-148, Jul. 2014. DOI: 10.1109/MSP.2014.2312183.

[24] X. Shi, C. Siriteanu, S. Yoshizawa, Y. Miyanaga, "Realistic Rician Fading Channel based Optimal Linear MIMO Precoding Evaluation," IEEE International Symposium on Communications Control and Signal Processing (ISCCSP), 2012. DOI: 10.1109/ISCCSP.2012.6217780.

Cebrail ÇiFTLiKLi was born in K. Maras, Turkey, in 1961. He received the Ph.D. degree in electronics engineering from Erciyes University in 1990. In 2004, he joined Erciyes University Kayseri Vocational College as Professor where he is now principal. Prof. Dr. Ciftlikli's current research interests include spread spectrum communications, wireless ATM/LAN, signal processing, DSCDMA system engineering, RF power amplifier linearization for wireless communication systems. He works at Department of Electronics and Automation, Kayseri University, Kayseri, Turkey.

Musaab AL-OBAIDI was born in Bagdad, Iraq, in 1981. 2000-2004 B.Sc. in Department of Electrical Engineering, Al-Mustanseria University, Iraq. 2010-2013 M.Sc. in Electrical Engineering, Universiti Tenaga Nasional, Malaysia. Since 2014 he is Ph.D. student in Department of Electrical and Electronics Engineering, Erciyes University, Kayseri, Turkey.

Mohammed Fadhil received the B.Sc. degree in electrical engineering from AL-Mustansiria University, College of Engineering, Iraq in 2001 and the M.Sc. degree from University Tenaga National (UNITEN), Malaysia in 2013. He is currently Ph.D. candidate at Universiti Kebangsaan Malaysia (UKM), Kuala Lumpur, Malaysia. His research interests include wireless communication, with a focus on cooperative communication and beamforming.

Wael AL-OBAIDI was born in Bagdad, Iraq, in 1985. 2003-2007 B.Sc. in Department of Electrical Engineering, University of Technology (UOT), Iraq. He is currently M.Sc. candidate at Electrical and Electronics Engineering, Erciyes University, Kayseri, Turkey.

Polyphase Radar Signals with ZACZ Based on p-Pairs D-Code Sequences and Their Compression Algorithm

Roman N. Ipanov, *Member, IEEE*

***Abstract* — In modern synthetic-aperture radars, signals with the linear frequency modulation (LFM) have found the practical application as probing signals. Utilization of LFM-signals was formed historically since they were the first wideband signals, which found application in radar technology, and their properties have studied a long time ago and in detail. However, the LFM-signals have the "splay" ambiguity function, which results the ambiguity in range. The question of the probing signal choice is also relevant in connection with the problem of weak echoes detection, which are closed by the side lobes of ACF of the strong echoes. In this paper, the polyphase (*p*-phase, where *p* is the prime integer number) radar signal, which has an area of zero side lobes in a vicinity of the central peak of autocorrelation function, has been synthesized. It is shown that this signal represents a train from *p* coherent phase-code-shift keyed pulses, which are coded by complementary sequences of the *p*-ary D-code. The method of ensemble set formation of the *p*-ary D-code for signal synthesis is suggested. Correlation characteristics of the synthesized signal are discussed. The compression algorithm of this signal is considered including in its structure the combined algorithm of Vilenkin-Chrestenson and Fourier fast transform.**

***Index Terms* — Autocorrelation function, complementary sequences, polyphase signal, pulse train, Vilenkin-Chrestenson functions, zero autocorrelation zone.**

I. INTRODUCTION

For accurate determination of the distance (range) and speed of a variety of small-size space objects on the near-Earth orbit, for resolution of separate elements of complex space objects and also for resolution of small-size objects on the Earth surface, it is necessary to use the wideband probing signals, which have high resolution on the slant range $\Delta r = c/(2F_s)$, where F_s is the signal spectrum width, and c is the radial speed. To obtain the high angular resolution $\Delta\theta$ of Earth surface elements and targets located on this surface, radars are used, which are installed on the quickly-moved aircraft-space carriers with the direct aperture synthesis. High resolutions on the slant and transverse $\Delta r_\perp = r_0\Delta\theta$ ranges, where r_0 is the slant range to observing resolution element, permit to obtained of two-dimensional target patterns in distance. Ensuring of the high angular resolution of small-size space objects or elements of complex space objects is based on the effect of the inverse synthesis of the antenna aperture [1]. For resolution on the Doppler frequency equaled to $\Delta F_D = 1/T_s$, where T_s is the probing signal duration (time of coherent accumulation), the angular resolution $\Delta\theta = \lambda/(2V\sin\theta_0)\Delta F_D$ is provided, where V is the ground speed of object motion, θ_0 is the angle between the ground speed vector and the pointing direction. The transverse resolution is provided by turning of the target velocity vector with regard to the pointing direction and is realized by processing of the sequence of complex samples, which arrive from each target element resolved on the slant range.

It follows from the above-mentioned that for providing of high resolutions on the slant Δr and transverse $\Delta r_\perp$ ranges, it is necessary to use the probing signals with the wide spectrum and the long duration.

As research shows, for these purposes can use the train of linear-frequency-modulated (LFM) pulses with the high repetition frequency [2, 6]. Nevertheless, as we know, the LFM signals have the "splay" ambiguity function, which results the ambiguity in range. The ambiguity peaks are appeared on autocorrelation function (ACF) of the train of LFM pulses.

The question of the probing signal choice is also relevant in connection with the problem of weak echoes detection, which are closed by the side lobes of ACF of the strong echoes. To suppress the side lobes of ACF echoes, one can apply the intra-pulse and inter-pulse weighting [3, 4]. However, at that, the spreading of the main ACF lobe occurs together with the loss in SNR.

To solve the stated tasks, we can use the phase-code-shift keyed (PCSK) signals, which are free from shortcomings of FM and FSK signals. In [4 - 7], the radar PCSK signals are considered, which have the zero correlation zone in the region of the central peak of aperiodic ACF (Zero Autocorrelation Zone - ZACZ). These signals represent the periodic sequence from $M \gg 1$ coherent pulses coding (or phase-shift keyed) by the ensembles of complementary or orthogonal sequences. PCSK signals with ZACZ solve the problem of weak echo detection on the background of strong echoes. However, the relative ZACZ width of these signals is

$$\varepsilon = Z/L = (q-1)/(q(M-1)+1) \ll 1. \quad (1)$$

where Z is the ZACZ width; L is the signal duration [8].

In addition, at formation and processing of the PCSK signal with the large number of pulses in the train, it is

The reported study was funded by RFBR and MCESSM according to the research project № 19-57-44001.

R. N. Ipanov is with the Moscow Power Engineering Institute (National Research University), Moscow 111250, Russia (e-mail: iproman@ya.ru).

DOI: 10.36244/ICJ.2019.3.4

difficult enough to keep their coherence. The polyphase PCSK signals discussed in [4 - 7] (Frank or P4), also have the large alphabet of phases equaled to the number of contiguous time slices (each of duration T_0) in the pulse.

Recently there were considerably great attention attracted to reduction of the detection possibility of radar stations (RS) by the means of the radio-electronic reconnaissance and by the self-guided anti-radar missiles [9 - 11]. In RS with low probability of emission detection, the special measures are anticipated to increase of the RS operation secrecy. Among them: the low spectral density of emission, variation of probing signal parameters according the random law, operation in the wide frequency band, control of the emission power. Applied wideband probing signals – LFM signals or bi-phase PCSK signals – do not provide the RS operation secrecy. So, LFM signals can be easily recognized by means of reconnaissance on the phase variation speed; while bi-phase PCSK signals – with the help of quadratic detection circuits. The emission secrecy can be increased by a great extent through the utilization of the polyphase PCSK signals [11]. Polyphase pulse signals can be formed by the wide set of p-ary codes and differ by the low spectral density and the low level of ACF side lobes.

In this paper, to solve problems of high resolution of the variety of small-size space objects on the near-Earth orbit, the separate elements of the complicated space object, as well as the small-size objects on the Earth surface, the polyphase (p-phase, where p is the prime integer number) radar signal is synthesized, which has ZACZ. This signal represented the train from p coherent PCSK pulses coding by complementary sequences of the p-ary D-code [13, 14]. It has low pulse number p in the train, the small alphabet of phases equaled to p, and an approach to code formation allows usage of the fast transform algorithm for its compression in the matched filter.

II. THE SYNTHESIS OF THE P-ARY D-CODE AND THE POLYPHASE COHERENT ADDITIONAL SIGNAL

Sequences $\left\{d_n^1\right\},\left\{d_n^2\right\},...,\left\{d_n^i\right\},...,\left\{d_n^p\right\}$, $\left(n=1,2,...,N\right)$ of the length $N=p^k$, where $k\geq 2$ is the integer number, are called complementary [6, 12, 13] if

$$r_m^1+r_m^2+...+r_m^i+...+r_m^p=\begin{cases}pN;\ m=0,\\ 0;\ m=\pm 1,...,\pm\left(N-1\right),\end{cases} \tag{2}$$

where $r_m^i=r_m^{i,i}=\sum_{n=m+1}^{N}d_n^i d^{*i}_{n-m}$ is the aperiodic ACF of the sequence $\left\{d_n^i\right\}$, * is the complex conjugation operation.

N/p sets of complementary (additional) sequences with the N length satisfying to (2) form a matrix of p-phase additional sequences (MAS) with dimensions $N\times N$. In publications this matrix is called the ensemble of Golay complimentary sequences at $p=2$ [6, 12]. We introduce the generalized concept of the Golay sequences for $p>2$ [14].

Let $\tilde{\mathbf{D}}_N=\left\|\tilde{d}_{i,n}\right\|_1^N$ be a matrix of p-ary D-codes [13, 14], $\tilde{d}_{i,n}=0,1,...,p-1$; $N=p^k$, p is the prime number. Then MAS of the k-th order (dimensions $N\times N$) will have a form:

$$\mathbf{D}_N=\left\|d_{i,n}\right\|_1^N,\ \ d_{i,n}=\exp\left\{j\frac{2\pi}{p}\tilde{d}_{i,n}\right\}. \tag{3}$$

Let us call sequences $\mathbf{D}_{1,N}^i=\left\|d_{i,n}\right\|_{n=1}^N$ and $\mathbf{D}_{1,N}^j=\left\|d_{j,n}\right\|_{n=1}^N$ p-paired if

$$\left(i-1\right)_p\oplus\left(j-1\right)_p=\left(\Delta\right)_p,\ \ i,j=1,2,...,N, \tag{4}$$

where i, j are numbers of sequences in the D-code or numbers of MAS rows; $\left(a\right)_p$ is a number a in the p-ary form; $\oplus$ is the operation of adding modulo p; $\Delta=p^{k-1}$.

p-paired sequences are complimentary, i.e., for them (2) holds true.

Let $\mathbf{D}_N$ be MAS (3), and $\mathbf{H}_N=\left\|h_{i,n}\right\|_1^N$ be a matrix of the system of Vilenkin-Chrestenson-Kronecker (VC-Kronecker) functions [15]. It is known that the system of VC-Kronecker is multiplicative Abelian group [16]. Since the variety consisting of the MAS rows is the adjacent class in the sub-group, elements of which are rows of the VC-Kronecker matrix, and the first MAS row is the leader of the adjacent class, then we may write:

$$\mathbf{D}_N=\mathbf{H}_N\mathbf{d}_N, \tag{5}$$

where $\mathbf{d}_N=\mathrm{diag}\left\{d_{1,1},d_{1,2},...,d_{1,n},...,d_{1,N}\right\}$ is the diagonal matrix with elements from the first row of $\mathbf{D}_N$.

At $p=2$, the VC-Kronecker matrix is transformed into the Hadamard matrix [17].

It follows from (5) that to construct of MAS $\mathbf{D}_N$, it is necessary to form its first row $\mathbf{D}_{1,N}^1$.

Elements of the MAS first row are defined as follows [18]:

$$d_{1,y+1}=\exp\left\{j\frac{2\pi}{p}\sum_{i=1}^{k-1}y_{i+1}y_{l_i}\right\}, \tag{6}$$

where $y+1=n$ is a number of the MAS column; $\left(y\right)_p=\left(y_k\ \ y_{k-1}\ \ ...\ \ y_i\ \ ...\ \ y_1\right)$ is a number of the MAS column in the p-ary form; $y_i=0,1,...,p-1$; $y=0,1,...,p^k-1$; $l_i=1,2,...,i$; $i=1,2,...,k-1$; $l_{k-1}\neq l_{k-2}\neq\ldots\neq l_2$.

Adding in (6) is performed modulo p. This approach allows formation of 2^{k-2} ensembles of the D-code of k-th order. Let further γ - number of ensembles of the D-code of k-th order, i.e. $\gamma=2^{k-2}$.

A. Example formation of binary D-code

Consider an example of the formation of a binary D-code of size 16×16 [17]. The D-code of order $k=4$ has

$\gamma = 2^{k-2} = 4$ ensembles.

At $k = 4$, we obtain:

$$i = 1, 2, 3 \Rightarrow l_1 = 1; l_2 = 1, 2; l_3 = 1, 2, 3$$

$$y_1, y_2, y_3, y_4 = 0, 1;\ y = 0, 1, ..., 15;$$

$$(y)_2 = (y_4 \quad y_3 \quad y_2 \quad y_1)$$

In this case, the condition $l_3 \neq l_2$ must be satisfied.

Let us write the sum from (6) for four ensembles:

$$\tilde{d}_{1,y+1} = \sum_{i=1}^{3} y_{i+1} y_{l_i} = y_2 y_1 + y_3 y_1 + y_4 y_2;$$

$$\tilde{d}_{1,y+1} = \sum_{i=1}^{3} y_{i+1} y_{l_i} = y_2 y_1 + y_3 y_1 + y_4 y_3;$$

$$\tilde{d}_{1,y+1} = \sum_{i=1}^{3} y_{i+1} y_{l_i} = y_2 y_1 + y_3 y_2 + y_4 y_1;$$

$$\tilde{d}_{1,y+1} = \sum_{i=1}^{3} y_{i+1} y_{l_i} = y_2 y_1 + y_3 y_2 + y_4 y_3.$$

Having performed additions for all columns of the CSM, from (6) we obtain the first sequences of four D-code ensembles of order $k = 4$.

(0 0 0 1 0 1 0 0 0 0 1 0 0 1 1 1);
(0 0 0 1 0 1 0 0 0 0 0 1 1 0 1 1);
(0 0 0 1 0 0 1 0 0 1 0 0 0 1 1 1);
(0 0 0 1 0 0 1 0 0 0 0 1 1 1 0 1).

The remaining rows of the D-code matrix are obtained from the first row by element-wise modulo 2 addition with the corresponding rows of the Hadamard matrix.

B. Example formation of ternary D-code

Consider now an example of the formation of the ternary D-code of order $k = 3$ with the length of code words $N = 3^3 = 27$, which allows you to form a $\gamma = 2^{3-2} = 2$ ensembles of D-code using method (5) - (6) [18].

We form the first rows of two different matrices (ensembles) of the D-code of order $k = 3$. The remaining rows of the D-code matrix are obtained from the first row by element-wise addition modulo p with the corresponding rows of the VC-Kronecker matrix.

In this case, from (6) we obtain:

$$\tilde{d}_{1,y+1} = \sum_{i=1}^{2} y_{i+1} y_{l_i} = (y_2 y_{l_1} + y_3 y_{l_2});$$

$$(y)_3 = (y_3 \quad y_2 \quad y_1);\ y_1, y_2, y_3 = 0, 1, 2;\ y = 0, 1, ..., 26;$$

$$i = 1, 2; l_1 = 1; l_2 = 1, 2.$$

From where for two ensembles we obtain:

$$\tilde{d}_{1,y+1} = y_2 y_1 + y_3 y_1 \quad \text{and} \quad \tilde{d}_{1,y+1} = y_2 y_1 + y_3 y_2.$$

At $y = 0, 1, ..., 26$, for the first ensemble we obtain the following first row of the matrix of the D-code:

(0 0 0 0 1 2 0 2 1 0 1 2 0 2 1 0 0 0 0 2 1 0 0 0 0 1 2).

For the second ensemble, the first row of the D-code matrix is as follows:

(0 0 0 0 1 2 0 2 1 0 0 0 1 2 0 2 1 0 0 0 0 2 0 1 1 0 2).

C. Determination of coherent additional signal

Let us refer as the polyphase coherent additional signal (CAS) of the train of p PCSK pulses encoded by p-paired sequences of the D-code [14]. We call this signal "coherent" because the coherence of PCSK pulses must be maintained in the train. In addition, we call it "additional" because the pulses are encoded by complementary (additional) sequences.

The analytical expression of the complex envelope (CE) of CAS has a form:

$$\dot{S}(t) = \sum_{i=1}^{p} \sum_{n=1}^{N} S_0\left(t - \left(n + (i-1)Nq - 1\right)T_0\right) d_{i,n}, \tag{7}$$

where $S_0\left(t - (n-1)T_0\right) = \begin{cases} 1, (n-1)T_0 \le t \le nT_0 \\ 0, \text{at other } t \end{cases}$ is the envelope of the n–th slice of CAS; T_0 is the slice duration; $q \ge 2$ is the off-duty factor; $\left\| d_{i,n} \right\|_1^N = \mathbf{D}_{1,N}^i$ are elements of i-th p-paired sequence.

CE of CAS in the vector form will have the following form:

$$\mathbf{S}_{1,N((p-1)q+1)} = \left(\mathbf{D}_{1,N}^1 \quad \mathbf{0}_{1,N(q-1)} \quad \mathbf{D}_{1,N}^2 \quad \mathbf{0}_{1,N(q-1)} \quad ... \quad ... \quad \mathbf{D}_{1,N}^i \quad \mathbf{0}_{1,N(q-1)} \quad ... \quad \mathbf{D}_{1,N}^p\right), \tag{8}$$

where $\mathbf{0}_{1,N(q-1)} = \left(0_1 \quad 0_2 \quad ... \quad 0_n \quad ... \quad 0_{N(q-1)}\right)$ is the zero vector- row with length $N(q-1)$.

III. CORRELATION CHARACTERISTICS OF POLYPHASE COHERENT ADDITIONAL SIGNALS

An analysis of CAS correlation characteristics is performed in [14, 17].

The aperiodic cross-correlation function (CCF) of sequences $\{d_n^i\}$ and $\{d_n^j\}$ is defined as:

$$r_m^{i,j} = \sum_{n=m+1}^{N} d_n^i d^{*j}_{n-m} \ \text{ at } i \neq j;\ m = 0, \pm 1, ..., \pm(N-1), \tag{9}$$

where $r_m^{i,j} = 0$ at $m = 0$, because complimentary sequences built according to (5) – (6), are orthogonal.

In the vector form, ACF of the polyphase CAS will have a form [14]:

$$\mathbf{R}_{1,2N((p-1)q+1)-1}^s = \left(\sum_{i=1}^{p-(p-1)} \mathbf{R}_{1,2N-1}^{i+p-1,i} \quad .... \right.$$
$$... \quad \sum_{i=1}^{p} \mathbf{R}_{1,2N-1}^{i} \quad \mathbf{0}_{1,N(q-2)} \quad 0 \quad \sum_{i=1}^{p-1} \mathbf{R}_{1,2N-1}^{i,i+1} \quad ... \tag{10}$$
$$\left. ... \quad \sum_{i=1}^{p-j} \mathbf{R}_{1,2N-1}^{i,i+j} \quad \mathbf{0}_{1,N(q-2)} \quad 0 \quad ... \quad \sum_{i=1}^{p-(p-1)} \mathbf{R}_{1,2N-1}^{i,i+p-1} \right),$$

where $\mathbf{0}_{1,N(q-2)} = \left(0_1 \quad 0_2 \quad ... \quad 0_n \quad ... \quad 0_{N(q-2)}\right)$ is the zero vector-row with the length $N(q-2)$;

$$\mathbf{R}^{i,j}_{1,2N-1} == \left(r^{i,j}_{-N+1} \quad r^{i,j}_{-N+2} \quad ... \quad r^{i,j}_{-1} \quad r^{i,j}_{0} \quad r^{i,j}_{1} \quad ... \right.$$
$$\left. ... \quad r^{i,j}_{m} \quad ... \quad r^{i,j}_{N-2} \quad r^{i,j}_{N-1}\right).$$

For $i = j$, $\mathbf{R}^{i,j}_{1,2N-1} = \mathbf{R}^{i}_{1,2N-1}$ and according to (2):

$$\sum_{i=1}^{p} \mathbf{R}^{i}_{1,2N-1} = \left(0_{-N+1} \quad 0_{-N+2} \quad ... \quad pN \quad ... \quad 0_{N-2} \quad 0_{N-1}\right), \qquad (11)$$

and at $i \neq j$ $r^{i,j}_{0} = 0$.

It follows from (10) and (11) that the ZACZ width (from both sides of the central peak of ACF) of the polyphase CAS is equal to $2Z = 1 + N(q-2) + 2N - 1 - 1 + N(q-2) + 1 = 2N(q-1)$, and taking into account the slice duration T_0:

$$Z = NT_0(q-1). \qquad (12)$$

The relative width of ZACZ is defined as:

$$\varepsilon = Z/LT_0 = (q-1)/\left(q(p-1)+1\right), \qquad (13)$$

where $L = N\left((p-1)q+1\right)$ is the slices number in CAS.

It follows from (13) that

$$1/(2p-1) \le \varepsilon < 1/(p-1), \qquad (14)$$

and at $p = 2$, $1/3 \le \varepsilon < 1$ [17].

In (1), $M \ge N = p^k$, $k \ge 2$ is the integer number, therefore, for signals considered in [4 - 7], $\varepsilon \ll 1$.

The polyphase CAS can be considered as the signal formed by the sequence from the ZACZ-ensemble [8, 17] with parameters:

$$ZACZ(J, L, Z),$$

where $J = \gamma \dfrac{N}{p}$ is a number of sequences in the ensemble.

The set of sequences forming p CAS and formed from the adjacent sets of p-paired sequences of the D-code can be considered as the ZCZ-ensemble [17] with parameters:

$$ZCZ(p, L, Z).$$

Fig. 1 and 2 show, relatively, a part of the two-dimensional ambiguity function $|R(\tau, F)|$ of the three-phase CAS with the number of slices of $N = 243$ in the pulse and with the off-duty factor $q = 3$ and its section by the plane $F = 0$, i.e., ACF of CE of CAS at complete filter matching with echoes in frequency.

The width of CAS ZACZ with given parameters in relative units is $Z/T_0 = 486$. From Fig. 1 it is seen that in the region of the central peak, the ambiguity function has the clearly expressed rectangular region of zero correlation along the whole frequency axis F at $N - 1 < |\tau/T_0| \le N(q-1)$, which is caused by a presence of the vector $\mathbf{0}_{1,N(q-2)}$ in (10). The dimensions of this region does not depend on the law of the phase-shift keying and on mismatching in frequency, but depends only on the off-duty factor q. The region of zero correlation at $0 < |\tau/T_0| \le N - 1$ near the central peak of ACF, which is caused by the property of complementary sequences (2), takes a place only at complete filter matching with the echoes in frequency.

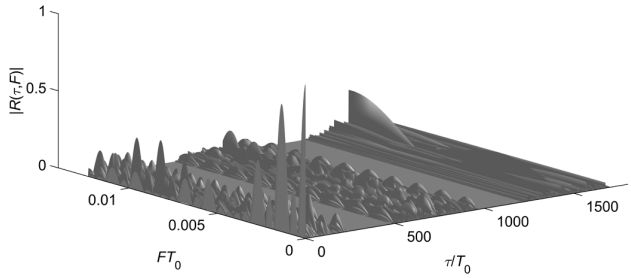

Fig. 1. Ambiguity function of the three-phase CAS

The ambiguity function section of CAS by the plane $\tau = 0$ has the envelope of the form $|\sin x/x|$ with the main lobe width on the zero level $2/(NT_0)$ and the internal comb structure. The spectrum combs are spaced from each other in F by the value $1/(qNT_0)$. The comb width on the zero level is $2/(pqNT_0)$, and the total number of combs within the main lobe of the amplitude-frequency spectrum envelope of the CAS CE square is equal to $2q-1$. The side lobes with the width $1/(pqNT_0)$ on the zero level occur between combs and the total number of side lobes is equal to $p-2$.

ZACZ exists only at complete filter matching with echoes in the Doppler frequency [14]. At mismatch ΔF in the frequency in ZACZ near the main ACF peak, the side lobed appear, the greatest of them is compared in the level with the maximal side lobe outside ZACZ at $\Delta F = 0.3/pqNT_0$.

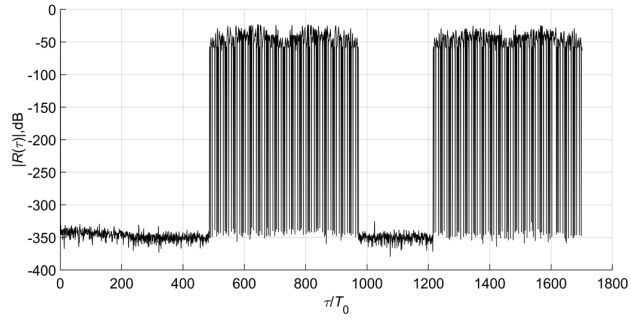

Fig. 2. Autocorrelation function of the three-phase CAS

CAS is assumed to use at radar target tracking in resolution modes for accurate measurements (specification) of the Doppler frequency, when the target rough estimation is already known from the preliminary target detection. At that, the compression device for CAS should be multi-channel in the Doppler frequency with the necessary channel width.

IV. THE COMPRESSION DEVICE OF POLYPHASE COHERENT ADDITIONAL SIGNALS

For compression of the coherent pulse sequence, the correlation-filtering processing is usually used, at which the reflected signal modulation is first removed and then, with the help of the fast Fourier transform (FFT), the Doppler frequency is defined [4, 6].

The structural circuit of the compression device for polyphase CAS is shown in Fig. 3 and represents the equivalent structural diagram of the matched filter of polyphase CAS at the known Doppler frequency or the equivalent structural diagram of the matched filter in the single frequency channel.

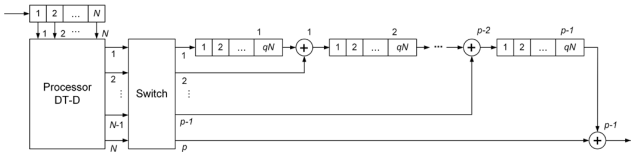

Fig. 3. Structural diagram of the single-channel compression device of CAS

The compression device consists of the input register on N memory cells, the processor of the discrete D-transform with N inputs and N outputs, the switching block, $p-1$ similar shift registers on qN memory cells and $p-1$ similar summation units of complex number, where q is the off-duty factor, $N = p^k$ is the D-code length.

The switching block performs connection of p from its N inputs with p outputs according to expression (4), i.e., in accordance with the row numbers, in which the p-paired D-codes are situated.

At $p = 2$, we obtain the compression device of bi-phase (binary) CAS.

The basing element of this device is the processor of discrete D-transform (the processor DT-D), which operation algorithm is described by the following mathematical expression:

$$\mathbf{G}_{N,1} = \mathbf{D}_N \mathbf{S}_{1,N}^T, \tag{15}$$

where $\mathbf{S}_{1,N}$ is the vector of input signal samples of the discrete D-transform; T is operation of the vector transposition.

Substituting (5) in (15), we obtain:

$$\mathbf{G}_{N,1} = \mathbf{H}_N \mathbf{d}_N \mathbf{S}_{1,N}^T. \tag{16}$$

It is known that the VC-Kronecker matrix can be factorized by the Good method [19], i.e., the discrete D-transform (16) can be reduced to FFT in the basis of VC-Kronecker function system (FTVC), which has the form:

$$\mathbf{G}_{N,1} = \mathbf{C}_{k_N} \mathbf{C}_{k-1_N} ... \mathbf{C}_{j_N} ... \mathbf{C}_{1_N} \mathbf{d}_N \mathbf{S}_{1,N}^T, \tag{17}$$

$$\mathbf{C}_{k_N} = \mathbf{E}_p \otimes \mathbf{1}_p \otimes ... \otimes \mathbf{1}_p;$$
$$\mathbf{C}_{k-1_N} = \mathbf{1}_p \otimes \mathbf{E}_p \otimes ... \otimes \mathbf{1}_p;$$
$$.....$$
$$\mathbf{C}_{j_N} = \mathbf{1}_p \otimes ... \otimes \mathbf{E}_p \otimes ... \otimes \mathbf{1}_p;$$
$$.....$$
$$\mathbf{C}_{1_N} = \underbrace{\mathbf{1}_p \otimes ... \otimes \mathbf{1}_p \otimes \mathbf{E}_p}_{k},$$

where $\otimes$ is the operation of the Kronecker product; $\mathbf{1}_p$ is the unitary matrix with dimensions $p \times p$; $\mathbf{E}_p$ is the matrix of discrete exponential functions (DEF) with dimensions $p \times p$.

From expression (17), it follows that the DT-D processor in the diagram in Fig. 3 can be replaced by the FTVC processor with addition of weight coefficients (the matrix $\mathbf{d}_N$ in expression) in the processor input, which are elements of the first row of MAS $\mathbf{D}_N$. Then the structural diagram of the compression device of the polyphase CAS will have the form presented in Fig. 4.

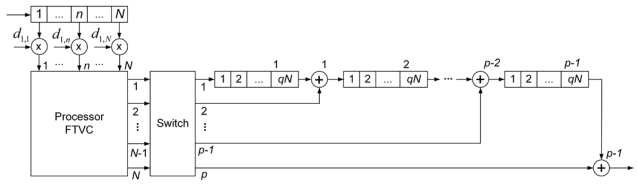

Fig. 4. Structural diagram of the single-channel compression device of CAS with FTVC

For $p = 2$, the compression algorithm of polyphase CAS presented in the form of the structural diagram in Fig. 4 is transformed into the compression algorithm of binary CAS, and the FTVC processor is transformed into the processor of the fast Walsh transform.

V. THE MULTI-CHANNEL COMPRESSION DEVICE OF POLYPHASE COHERENT ADDITIONAL SIGNALS

In [20] the multi-channel compression device for CAS is described, which allows simultaneous removal of the modulation of polyphase pulse signals encoded by complimentary sequences and determine the Doppler frequency in restricted Doppler frequency range according to preliminary target detection. This device consists of the processor of fast D-transform-Fourier (FT-D-F$_K$, K is a number of used frequency channels), using the combination of the FFT algorithms in basis-matrices of additional sequences and DEF by means of bit-by-bit multiplication of each MAS row with dimensions of $N \times N$. The MAS matrix here is the matrix of pulse characteristics of CAS pulses. The block matrix with dimension $NK \times N$ obtained at that represents the set of matrices of pulse characteristics on K different frequencies, i.e., rows of DEF matrix play the role of frequency channels. In the FT-D-F$_K$ algorithm, the MAS matrix itself is factorized.

The multi-channel compression device of CAS described in

[20], can be built on the base of FTVC using (5). The structural diagram of such a device is presented in Fig. 5. The controllable local oscillator of the radar receiving device, according to rough estimation of the Doppler frequency $\hat{F}_{\mathrm{D}}$ obtained in the mode of target detection, retunes its frequency so as the value $\hat{F}_{\mathrm{D}}$ falls in the frequency range, which is covered by frequency channels of the compression device of CAS. To CAS compression, the processor of fast Vilenkin-Chrestenson-Fourier (FTVC-F$_K$, K is a number of used frequency channels) using of combination of FFT algorithms in the basis of the VC-Kronecker and DEF function system by means of the bit-by-bit multiplication of each row of the VC-Kronecker matrix with dimension $N\times L$, $L=N\left((p-1)q+1\right)$ (the matrix rows are prolonged by repeating of each element or zero padding), by each from K rows of DEF matrix with dimension $L\times L$.

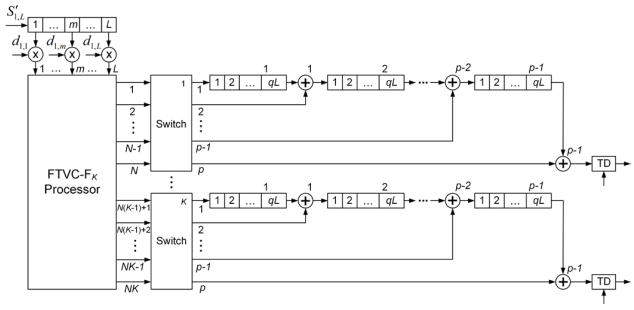

Fig. 5. Structural diagram of the multi-channel compression device of CAS with FTVC-F$_K$

CE of the signal reflected from the target can be written as:

$$\dot{S}\left(t,\hat{F}_{\mathrm{D}}\right)=\dot{S}(t)\exp\left(-j2\pi\hat{F}_{\mathrm{D}}t\right),$$

where $\dot{S}(t)$ is CAS CE (7). The signal is fed from the ADC outputs in the quadratic channels to the input shift register of the compression device. Having transferred from analog quantities to discrete ones, i.e., at $t\to t_n=(n-1)T_0$, $\hat{F}_{\mathrm{D}}\to\hat{F}_{\mathrm{D}_k}=(k-1)\Delta F$, $\Delta F=1/LT_0$ is the mismatch between frequency channels, $n=1,2,...,L$, $k=1,2,...,K$, we obtain the echo CE in the discrete form:

$$\dot{S}(n,k)=\dot{S}(n)\exp\left(-j\frac{2\pi}{L}(n-1)(k-1)\right).$$

Hence, the DEF matrix should have the dimension $L\times L$.

Because MAS has N columns, and a number of MAS and DEF columns should be equal, the rows of MAS matrix and CAS pulses need to be prolonged, for example, owing to repeat of each samples by $L/N=(p-1)q+1$ times or to use zero padding.

Then the discrete D-transform-Fourier (DT-D-F$_K$) has a form:

$$\mathbf{G}_{KN,1}=\mathbf{D}'_{N,L}\left(\mathbf{E}_{1_L}\quad\mathbf{E}_{2_L}\quad\ldots\quad\mathbf{E}_{k_L}\quad\ldots\quad\mathbf{E}_{K_L}\right)^T\mathbf{S}'^T_{1,L}=\mathbf{D}'_{N,L}\mathbf{E}_{KL,L}\mathbf{S}'^T_{1,L},\qquad(18)$$

where $\mathbf{S}'_{1,L}$ is the sample vector of the prolonged input signal; $\mathbf{E}_{k_L}=\mathrm{diag}\left\{W^{0(k-1)}\quad W^{1(k-1)}\quad\ldots\quad W^{(n-1)(k-1)}\quad\ldots\quad W^{(L-1)(k-1)}\right\}$, $W=\exp\left(-j2\pi/L\right)$, is a diagonal matrix with elements from the k-th row of the DEF matrix, which is included in the structure of the block matrix $\mathbf{E}_{KL,L}$; $\mathbf{D}'_{N,L}$ is MAS with prolonged rows.

Taking (5) into consideration, we obtain from (18) the discrete Vilenkin-Chrestenson-Fourier transform (DTVC-F$_K$):

$$\mathbf{G}_{KN,1}=\mathbf{H}'_{N,L}\mathbf{d}'_L\mathbf{E}_{KL,L}\mathbf{S}'^T_{1,L}=\mathbf{H}'_{N,L}\mathbf{E}_{KL,L}\mathbf{d}'_L\mathbf{S}'^T_{1,L},\qquad(19)$$

where $\mathbf{H}'_{N,L}$ is the VC-Kronecker matrix with prolonged rows; $\mathbf{d}'_L=\mathrm{diag}\left\{\mathbf{D}'^1_{1,L}\right\}$ is the diagonal matrix with elements from the first rows of the $\mathbf{D}'_{N,L}$ matrix.

From [19] we know that column repeating of the VC-Kronecker matrix with dimension $N\times N$, $N=p^k$, p^l times is equivalent to row decimation of the VC-Kronecker matrix with dimension $L\times L$, where $L=p^{k+l}$ to the rectangular matrix with dimension $N\times L$. In other words, in (19), the $\mathbf{H}'_{N,L}$ matrix can be replaced by the VC-Kronecker matrix with dimension $L\times L$, we can factorize it, and necessary values of the signal spectrum can be obtained from the known decimated row numbers.

Thus, from (19) we have the expression for FTVC-F$_K$:

$$\mathbf{G}_{KL,1}=\mathbf{H}_L\mathbf{E}_{KL,L}\mathbf{d}'_L\mathbf{S}'^T_{1,L}=\mathbf{C}_{k+l_L}\mathbf{C}_{k+l-1_L}\ldots\mathbf{C}_{j_L}\ldots\mathbf{C}_{1_L}\mathbf{E}_{KL,L}\mathbf{d}'_L\mathbf{S}'^T_{1,L},\qquad(20)$$

where $\mathbf{C}_{j_L}$ is the weakly-filled matrix from the Good factorization algorithm (17), $j=1,2,...,k+l$.

At $p=2$, FTVC-F$_K$ transforms into the fast Walsh-Fourier (FTW-F$_K$) and $L=N(q+1)$ [8]. To achieve the maximal FFT effectiveness, the DEF matrix dimension should be equal to the power of 2. For this, we introduce the quantity $l=\lceil\log_2(q+1)\rceil$, where $\lceil x\rceil$ is the operation of the number x rounding to the larger value. Then $L=2^lN=2^{k+l}$. The rectangular matrix in (19)

$$\mathbf{H}'_{N,L}=\left\|h_{i,\lfloor(m-1)/2^l\rfloor+1}\right\|_{i=1,m=1}^{N,L},$$

where $\left\|h_{i,n}\right\|_1^N=\mathbf{H}_N$ is the Hadamard matrix with dimension $N\times N$, $\lfloor x\rfloor$ is the operation of integer part extraction of the number x, which is obtained from the Hadamard matrix $\mathbf{H}_L$ with dimension $L\times L$ in (20) be means of its rows decimation. The diagonal matrix in (19) and (20) is

$$\mathbf{d}'_L=\mathrm{diag}\left\{d_{1,1}\quad d_{1,1}\quad\ldots\quad d_{1,\lfloor(m-1)/2^l\rfloor+1}\quad\ldots\quad d_{1,N}\quad d_{1,N}\right\},$$
$$m=1,2,...,L,$$

where $\left\|d_{1,n}\right\|_1^N=\mathbf{D}^1_{1,N}$. The processor FTW-F$_K$ has NK outputs

(decimated rows). The first N outputs represent the result of multiplication of the pulse characteristics matrix (MAS) by the processor input signal samples in the first frequency channel, the second N outputs – in the second frequency channel and so on, the last N outputs – in the K-th frequency channel. The switching block in each frequency channel performs the connection of two from its N inputs with two outputs in accordance with the rows number, in which the paired or adjacent sequences of the D-code are located. In adder of each channel, the summation of ACF samples of CAS pulses is performed owing to the samples delay of the ACF in the shift register by the repetition period of pulses qL. According to the number of the threshold device (TD in Fig. 5) ($k = 1,2,...,K$), in which the threshold is exceeded, the Doppler frequency shift ($\hat{F}_{D_k} = (k-1)\Delta F$) is determined.

VI. CONCLUSIONS

The method of polyphase radar signal with ZACZ is offered in this paper. At that, this signal represents the train of p PCSK pulses encoded by p-ary complementary sequences and is called the coherent additional signal. ZACZ takes place only at complete matching of the filter with echoes in the Doppler frequency. At mismatch in frequency, the level of the ACF main peak decreases and side lobes appear in ZACZ. The multi-channel compression device of this signal is studied. It is shown that the method of D-code formation allows utilization of algorithms of the fast transform for signal compression in the matched filter.

REFERENCES

[1] H. Wu and G. Y Delisle, "Precision tracking algorithms for ISAR imaging," *IEEE Trans. Aerosp. Electron.* Syst., vol. 32, no. 1, pp. 243–254, Jan. 1996, DOI: 10.1109/7.481266

[2] D. R. Wehner, *High Resolution Radar*, 2nd ed. Norwood, MA, USA: Artech House, 1994.

[3] A. Akbaripour and M. H. Bastani, "Range Sidelobe Reduction Filter Design for Binary Coded Pulse Compression System," *IEEE Trans. Aerosp. Electron. Syst.*, vol. 48, no. 1, pp. 348-359, Jan. 2012, DOI: 10.1109/TAES.2012.6129640

[4] E. Mozeson and N. Levanon, "Removing autocorrelation sidelobes by overlaying orthogonal coding on any train of identical pulses," *IEEE Trans. Aerosp. Electron. Syst.*, vol. 39, no. 2, pp. 583–603, Apr. 2003, DOI: 10.1109/TAES.2003.1207268

[5] R. Sivaswamy, "Digital and analog subcomplementary sequences for pulse compression," *IEEE Trans. Aerosp. Electron. Syst.*, vol. AES-14, no. 2, pp. 343–350, Mar. 1978, DOI: 10.1109/TAES.1978.308657

[6] N. Levanon and E. Mozeson, Radar Signals. Hoboken, NJ, USA: Wiley, 2004.

[7] D. Chebanov and G. Lu, "Removing autocorrelation sidelobes of phase-coded waveforms," in *IEEE Radar Conf.*, Washington, DC, USA, 2010, pp. 1428–1433, DOI: 10.1109/RADAR.2010.5494391

[8] R. N. Ipanov, A. I. Baskakov, N. Olyunin and M.-H. Ka, "Radar Signals With ZACZ Based on Pairs of D-Code Sequences and Their Compression Algorithm," *IEEE Signal Proc. Lett.*, vol. 25, no. 10, pp. 1560–1564, Oct. 2018, DOI: 10.1109/LSP.2018.2867734

[9] H. Wang, M. Diao and L. Gao, "Low probability of intercept radar waveform recognition based on dictionary leaming," in *10th Int. Conf. Wirel. Commun. and Signal Process.*, Hangzhou, China, 2018, pp. 1–6, DOI: 10.1109/WCSP.2018.8555906

[10] M. Zhang, L. Liu and M. Diao, "LPI radar waveform recognition based on time-frequency distribution," *Sensors*, vol. 16, no. 10, p. 1682, Oct. 2016, DOI: 10.3390/s16101682

[11] E. J. Carlson, "Low probability of intercept (LPI) techniques and implementations for radar systems," in I*EEE National Radar Conf., Ann Arbor*, MI, USA, 1988, pp. 56-60, DOI: 10.1109/NRC.1988.10930

[12] R. R. Durai, N. Suehiro and C. Han, "Complete complementary sequences of different length," *IEICE Trans. Fundam. Electron., Commun., Comput. Sci.*, vol. E90-A, no. 7, pp. 1428–1431, Jul. 2007.

[13] G. Welti, "Quaternary codes for pulsed radar," *IRE Trans. Inf. Theory*, vol. 6, no. 3, pp. 400–408, Jun. 1960, DOI: 10.1109/TIT.1960.1057572

[14] R. N. Ipanov, "Polyphase coherent complemented signals," *J. of Radio Electronics*, no. 1, Jan. 2017. Accessed on: January 23, 2017, http://jre.cplire.ru/jre/jan17/14/abstract_e.html

[15] H. F. Chrestenson, "A Class of generalized Walsh functions", *Pacific J. Math.*, vol. 5, pp. 17-31, 1955.

[16] H. A. Helm, "Group codes and Walsh functions," *IEEE Trans. Electromagn. Compat.*, vol. EMC-13, no. 3, pp. 78–83, Aug. 1971, DOI: 10.1109/TEMC.1971.303132

[17] R. N. Ipanov, "Pulsed Phase-Shift Keyed Signals with Zero Autocorrelation Zone," *J. of Commun. Techn. and Electron*, vol. 63, no. 8, pp. 895–901, Aug. 2018. DOI: 10.1134/S1064226918080077

[18] R. N. Ipanov, "The formation method of the ensemble variety of p-ary D-codes, RU Patent 2 670 773, Oct. 25, 2018.

[19] M. Zhou, X. Shi and Z. Liu, "Chrestenson transform and its relations with Fourier transform," in *3rd Int. Conf. Robot, Vision, Signal Process.*, Kaohsiung, Taiwan, 2015, pp. 212–215, DOI: 10.1109/RVSP.2015.57

[20] R. N. Ipanov, "Device of digital processing of polyphase additional phase-codes-shift keyed signals," RU Patent 2 647 632, Mar. 16, 2018.

Roman N. Ipanov was born in Kishinev City, Moldova, USSR, in 1974. In 1999 he graduated in the specialty radio-electronic systems the Military Space Academy named after A. F. Mozhaisky, Saint Petersburg. He received the Ph.D. in the specialty radiolocation and radio navigation at the Military Space Academy named after AF Mozhaisky in 2004. From 2004 to 2010 he was a lecturer and a senior lecturer in the department of radiolocation at the Military Space Academy named after AF Mozhaisky. From 2013 to 2010 he worked as a senior researcher in the Federal Government Institution Scientific and Production Association Special Equipment and Telecoms of the Ministry of Internal Affairs of the Russian Federation, Moscow. Currently working as an associate professor at the Department of Radio Engineering Devices and Antenna Systems at the Moscow Power Engineering Institute, studying in doctoral studies. He is the author of more than 50 scientific papers and three inventions. Research interests include the synthesis and digital processing of radar signals.

Synthesis and Analysis of Non-recursive Rejection Filters in the Transient Mode

Dmitrii I. Popov, Sergey M. Smolskiy, *Member, IEEE*[1]

***Abstract*— The non-recursive rejection filter (RF), which is improved with the purpose of transient acceleration at arriving of the passive interference edge caused by disturbing reflections from fixed or slow-moving objects, is synthesized by the state-variables method. The structural diagram is offered of the tunable RF in the transient with the purpose of improvement of signal extraction effectiveness from the moving targets on the background of the passive interference edge. The comparative analysis is performed of RF effectiveness for fixed and tunable structure in the transient according to the criterion of the normalized interference suppression coefficient and the improvement coefficient of the signal-to-interference ratio. The essential increase of the signal extraction effectiveness from the moving objects on the background on the interference edge for the wide class of the spectral-correlation characteristics at RF structure modification.**

***Index Terms*— effectiveness analysis, clutter edge, variable states, structure adjustment, transient mode, rejection filters**

I. INTRODUCTION

Radar systems (RS) found an application for solution of a wide circle of problems of civil and military character [1]. Modern multi-functional RSs allow detection and coordinate localization of various objects. The presence of the strong passive (correlated) interference from the fixed or slowly moved objects caused by disturbing reflections (so-called, a clutter) essentially disturbs the normal RS operation leading to receiver front-end overloading as well as signal masking and eventually to the moving target signal disappearing [2, 3]. The moving target signal detection on the background of passive interference is the one of relevant and complex tasks of received data processing, which is solved in RS of various application [1]. Methods of protection approaches against clutter and coordinate measurement for different types of radars and the used probing signal are described in a series of publications, in particular, in [1-5].

The clutter protection problem is most effectively solved in so-called pulse-Doppler RSs with the small of-duty factor of the probing signal or in RSs with quasi-continuous wave, in which the coherent pulses with high repetition frequency (up to several tens and even hundreds of kilohertz) are used [1, 2]. At that, the unambiguous measurement of the Doppler target velocity with high resolution and accuracy are achieved. However, the range measurement is ambiguous and to avoid this, the specific methods must be applied which complicate the signal processing [1, 5].

The unambiguous range measurement is achieved in coherent-pulse RSs at high duty-off factor of probing signals, which leads to wide application of such RSs in practice [1]. However, the low pulse repetition frequency does not provide the unambiguous Doppler frequency measurement for the relevant velocities of the wide class of radar objects [3, 4].

The low pulse repetition frequency chosen from the condition of unambiguous range measurement leads to the close location of comb spectral components, which complicates the moving object signal selection on the background of interference that exceeds in power. In this case, the main operation of received data processing is the rejection of interference spectral components. The rejection filter (RF) becomes the main unit of the appropriate processing system.

A problem of moving target selection on the clutter background, properties of the clutter, novel promising methods of the clutter rejection effectiveness growth and various aspects of this problems are permanently described in Russian and foreign scientific-engineering periodic journals [6-16]. Nevertheless, this scientific direction cannot be considered as fully studied. In this paper, we consider improvement of characteristics of rejection filters of the non-recursive type, which are widely used in the systems of echoes extractions from moving targets on the background of the intensive clutter [1-3]. When the clutter edge arrives to the input of such a RF, the complicated transient mode is observed at its output as far as this clutter is occupied all delay stages of the RF. In this case, non-compensated clutter residues produce a strong background, which masks the desired signal and leads to false alarms of a radar. To struggle against this situation at discrete scanning of the antenna beam we can use the strobbing (gating) of the RF output samples excluding thus the transient mode at the cost of appropriate number lack of the processed samples. In the mode of continuous scanning, in order to exclude the transient mode, is necessary to undertake the addition measures to determine the clutter edge position. Regardless of the scanning mode, reduction of the processed sequence at its restricted duration, in the case of the high coverage rate, is related to effectiveness losses of signal processing.

In above-cited books [1-5] and papers in the periodic editions [6-15], the problem of improvement of rejection filter characteristic with the purpose of transient reduction is not solved. The exclusion is the publication [16], in which the problem of transient acceleration is solved for the recursive rejection filters. This is achieved by means of switching of

Manuscript submitted on 16 April, 2018.

[1] Dmitrii I. Popov is with Ryazan State Radio Engineering University, Russia (e-mail: adop@mail.ru).

Sergey M. Smolskiy is with Moscow Power Engineering Institute (National Research University), Russia (e-mail: SmolskiySM@mail.ru).

DOI: 10.36244/ICJ.2019.3.5

recursive connections after achievement the steady-state mode in the non-recursive part of RF. At that, the structure of the non-recursive part is classical without acceleration of its transients.

In this connection, the improvement of the RF structure with the aim of its transients speeding-up and effectiveness improving of signal extraction on the background of clutter edge is the relevant research task. Exactly this task is considered in the present paper.

II. THE SYNTHESIS OF IMPROVED REJECTION FILTER

For the synthesis of the modernized RF structure in the transient mode, similar to [16], we use the method of state variables, which gives the adequate filter description in the time domain. Being a discrete system, the digital non-recursive RF of m-order in the k-th time moment can be described by some state vector $\mathbf{X}(k) = [x_n(k)]$, where $x_n(k)$ is the state variable corresponding to the output value of the n-th delay unit of the RF, $n = \overline{1, m}$. The difference matrix equation of the RF state has a view in the standard form [17]

$$\mathbf{X}(k+1) = \mathbf{A}\mathbf{X}(k) + \mathbf{B}u(k), \quad (1)$$

where $\mathbf{A}$ is the matrix of $m \times m$ dimension, which defines the connection between states in k-th and $(k+1)$-th time moments, $\mathbf{B}$ is a column vector of m dimension describing the dependence between state variables and the input impact $u(k)$.

The difference equation (1) solution, at known processed sample beginning, similar to [16], is the following vector

$$\mathbf{X}(k) = \mathbf{A}^k\mathbf{X}(0) + \sum_{l=0}^{k-1}\mathbf{A}^{k-1-l}\mathbf{B}\,u(l), \quad (2)$$

depending on filter parameters and the vector initial state $\mathbf{X}(0)$.

Modernization of the non-recursive RF structure with the aim of transient speeding-up assumes the formation of the initial state vector. A criterion of transient speeding-up is based on the condition of RF output constancy and hence, its state from the moments of clutter arrival

$$\mathbf{X}(k+1) = \mathbf{X}(k) = \mathbf{X}(0)$$

$$\text{or } \mathbf{X}(k+1) - \mathbf{X}(k) = 0 \text{ for } k \geq 0. \quad (3)$$

The squareness of the pulse train envelope, which takes place at discrete observation radar mode and in combination with known time of sample arrival, opens new possibilities of RF transient speeding-up and is the necessary condition of criterion (3) fulfillment. If the envelope shape differs from rectangular one, for example, at continuous scanning, then we must fix the moment of clutter arrival and perform the preliminary sample weighting to provide the envelope squareness.

Actual clutter samples represent a random process with definite fluctuation character, and we may imply the envelope squareness within the limits of the mean value of samples' sequence. On this account, we shall approximate a step at the clutter edge by the stepped input impact with constant amplitude. Then, a limitation superposable to the input sample takes a form

$$u(k+1) = u(k) = u(0)$$

$$\text{or } u(k+1) - u(k) = 0 \text{ for } k \geq 0. \quad (4)$$

The criterion (3) with relations (2) and (4) account leads to equation

$$\mathbf{A}^k(\mathbf{A} - \mathbf{I})\mathbf{X}(0) + \mathbf{A}^k\mathbf{B}\,u(0) = 0,$$

which solution is the vector of initial state

$$\mathbf{X}(0) = (\mathbf{I} - \mathbf{A})^{-1}\mathbf{B}\,u(0), \quad (5)$$

where $\mathbf{I}$ is the identity matrix.

Thus, a constancy of states and the RF output is provided upon condition that the initial state vector $\mathbf{X}(0)$ takes a value at the moment of clutter arrival, which is proportional, according to (5), to the first clutter sample.

Let us illustrate a synthesis of the improved RF in the transient mode on an example of non-recursive filter of the 3rd order ($m = 3$) for which

$$\mathbf{A} = \begin{bmatrix} 0 & 1 & 0 \\ 0 & 0 & 1 \\ 0 & 0 & 0 \end{bmatrix}, \qquad \mathbf{B} = \begin{bmatrix} 0 \\ 0 \\ 1 \end{bmatrix}.$$

In accordance to (5), we obtain

$$\mathbf{X}(0) = \begin{bmatrix} 1 & -1 & 0 \\ 0 & 1 & -1 \\ 0 & 0 & 1 \end{bmatrix}^{-1} \begin{bmatrix} 0 \\ 0 \\ 1 \end{bmatrix} u(0) =$$

$$= \begin{bmatrix} 1 & 1 & 1 \\ 0 & 1 & 1 \\ 0 & 0 & 1 \end{bmatrix} \begin{bmatrix} 0 \\ 0 \\ 1 \end{bmatrix} u(0) = \begin{bmatrix} 1 \\ 1 \\ 1 \end{bmatrix} u(0) = \begin{bmatrix} u(0) \\ u(0) \\ u(0) \end{bmatrix}. \quad (6)$$

The value of initial state vector $\mathbf{X}(0)$, which is obtained as a results of a synthesis, in contrast to [16] assumes the sample $u(0)$ arrival at outputs of all RF delay units at the moment of clutter edge appearance. Since in the classic RF diagram, the $u(0)$ sample does not pass to outputs of delay units and, accordingly, the vector $\mathbf{X}(0) = 0$, then, to satisfy the condition (6), we must require introduction of units, which perform the RF structure adjustment.

III. THE STRUCTURAL DIAGRAM OF THE IMPROVED RF

The structural diagram of the adjustable RF represented in Fig.1 contains the clutter detector CD, the synchronous generator SG, the switch SW, storage devices SD_T performing functions of delay units for samples processed over the period T of its repetition, adders (Σ) and weighting units $g(l)$, $l = \overline{0, m}$ [18]. The clutter detector (CD) contains the comparator performing the comparison of the received interference with the specified values, and logical elements for formation of the unitary single [18]. At coincidence of the antenna beam position during discrete scanning and the clutter

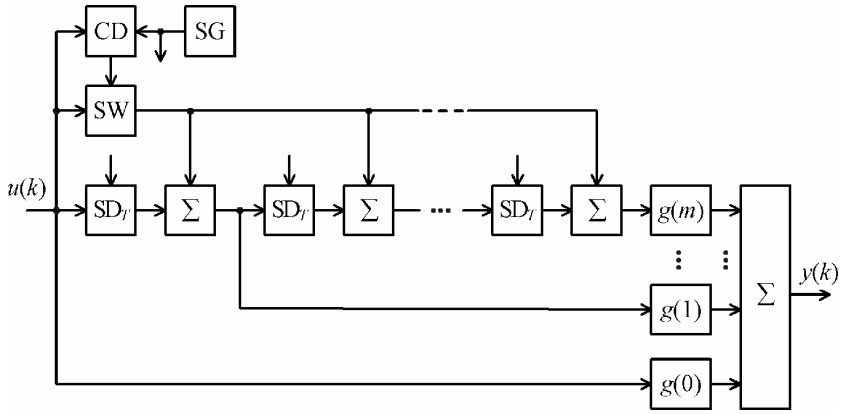

Fig.1. Structural diagram of the adjustable RF

"cloud" edge, the clutter detector CD produces the single voltage signal, and the switch SW, which was earlier in open state, is closed now. The digital sample of the first reflected pulse passes to the first SD_T input and, simultaneously, through the switch SW and adders, to inputs of subsequent SD_T. At that, the compensation of clutter component takes place. To the moment of the second reflected pulse arrival, the clutter detector CD opens the switch SW until reflections from the other clutter source begin to appear.

The further processing of samples of the signal and clutter mixture is fulfilled in conventional manner: samples arrive in sequence to the storage devices SD_T, weighting units $g(l)$ and the output adder. Samples of the signal mixture and decorrelated (for the received number of periods) interference remainders. Beginning from the first clutter sample, the compensation effectiveness for low-frequency components during the transient mode constantly grows. Echoes from moving targets, which differ from the narrowband clutter by the Doppler modulation, are not compensated and beginning from the second sample pass to RF output. As a whole, effectiveness of Doppler signal extraction on the clutter background in the transient mode increases sequentially from one pulse to the next achieving. After $(m+1)$-th clutter sample arrival, the steady-state value, which corresponds to maximal effectiveness for RF chosen order and parameters.

Synchronous information timing in the storage devices SD_T and the other units provides by the pulses of the synchronous generator SG, which follow with a period of time discretization of the input data. The specific realization of the clutter detector CD and description of its operation are given in [18].

At continuous observation mode, perfection of the RF structure with the aim of transient speeding-up has its own peculiarities caused by clutter pulse modulation at its edges by the antenna pattern. Detection of the front clutter edge is performed over all modulated pulses of edges till the moments of pulse arrival, which corresponds to the flat plateau of the clutter envelope [19]. Further, the delayed clutter edge samples are weighted with the aim of its squareness recovering, which allows effective extraction of Doppler signals at similar to Fig.1 processing, without waiting of pulses arrival for the envelope flat part. As well, at arrival and detection of the rear clutter edge by means of sample weighting, the recovering of its envelope squareness takes place. After the last pulse arrival, connection between storage devices breaks, which leads to cancellation of the information contained and thus to elimination of the RF transient mode (chink) from the clutter rear edge. Implementation and operation principle of edges detector for continuous observation are described in [19].

The problem of transient speeding-up in the adaptive RF can be solved in the same manner. This is achieved by addition of conventional adaptation units, which perform estimation of spectral-correlation clutter parameters and adjustment of RF characteristics. For this, we may introduce the similar to above-mentioned the detector of clutter edges and appropriate units, which eliminate transients from front and rear edges of the clutter [20].

IV. RF EFFECTIVENESS ANALYSIS IN THE TRANSIENT MODE

The analysis of RF effectiveness with adjustable structure (Fig. 1) in the transient mode, we perform in the similar manner using the method of state variables. The RF output, as it follows from the matrix equation of input–state–output type, equals

$$y(k) = \mathbf{C}\mathbf{X}(k) + du(k), \qquad (7)$$

where $\mathbf{C}$ is the vector-line of m-dimension describing a connection between RF state and the output value; d is a scalar characterizing a connection between input and output.

Taking (2) into consideration, equation (7) for RF output takes a form

$$y(k) = \mathbf{C}\mathbf{A}^k\mathbf{X}(0) + \mathbf{C}\sum_{l=0}^{k-1}\mathbf{A}^{k-1-l}\mathbf{B}\,u(l) + du(k). \qquad (8)$$

For RF with fixed structure, the vector $\mathbf{X}(0) \equiv 0$ and expression (8) is converted to the conventional form, which is a convolution of input impact and the weighting function $h(l)$ (pulse response) of RF

$$y(k) = \sum_{l=0}^{k-1} h(k-l)\,u(l) + du(k) = \sum_{l=0}^{k} h(k-l)\,u(l), \qquad (9)$$

where $h(k-l) = \mathbf{C}\mathbf{A}^{k-1-l}\mathbf{B}$ are coefficients of the RF pulse response coinciding with RF weighting coefficients, i.e., $h(k-l) = g(k-l)$.

For RF with adjustable structure, taking into account (5),

(8), and (9), we have

$$y(k) = \mathbf{C}\mathbf{A}^k(\mathbf{I}-\mathbf{A})^{-1}\mathbf{B}u(0) + \sum_{l=0}^{k-1} h(k-l)u(l) =$$

$$= q(k)u(0) + \sum_{l=0}^{k-1} h(k-l)u(l), \qquad (10)$$

where $q(k) = \mathbf{C}\mathbf{A}^k(\mathbf{I}-\mathbf{A})^{-1}\mathbf{B}$.

The term $q(k)u(0)$ defines a contribution to output value formation in the k-th time moment at the cost of RF structure adjustment, at that, $q(k) = 0$ for $k \geq m$.

The expression (10) can be written as a convolution (9), where coefficients $h(k-l)$ are determined according to the rule

$$h(k-l) = \begin{cases} g(k-l) & \text{for } l > 0, \\ g(k-l) + q(k) & \text{for } l = 0. \end{cases}$$

The RF effectiveness can be characterized by the normalized (relative the proper receiver noise) clutter suppression coefficient

$$\gamma_{cl} = (\sigma^2/\sigma^2_{RF})_{cl} \big/ (\sigma^2/\sigma^2_{RF})_n =$$

$$= (\sigma^2_{RF}/\sigma^2)_n \big/ (\sigma^2_{RF}/\sigma^2)_{cl},$$

where σ^2 and σ^2_{RF} are variances of the clutter or noise, accordingly, at RF input and output.

At zero mean value of initial processes (clutter and noise), the variance at the RF output relative to the $(k+1)$-th pulse of processed sequence is determined in the form $\sigma^2_{RF} = \overline{y^2(k)}$. As a result of statistical averaging, taking into account the formula (9) and correlation properties of the clutter and noise, we obtain

$$\gamma_{cl} = \sum_{j=0}^{k} h^2(j) \Big/ \sum_{j,l=0}^{k} h(k-j)h(k-l)\rho(j,l),$$

where $\rho(j,l)$ are coefficients of the inter-period correlation of the clutter.

Going over to the matrix form, we have

$$\gamma_{cl} = \mathbf{H}^{\mathrm{T}}\mathbf{H} \big/ \mathbf{H}^{\mathrm{T}}\mathbf{R}_{cl}\mathbf{H}, \qquad (11)$$

where $\mathbf{H} = [h(k-j)]$ is the K-dimension column vector of the RF weighting function, which elements are determined depending on the RF structure (fixed or adjustable); $K = k+1$ is a number of pulses processed in RF; the index "T" means the transposition operation; $\mathbf{R}_{cl} = [\rho(j,l)]$ is the clutter correlation matrix with $K \times K$ dimension.

As clutter spectral characteristics, we choose boundary approximations for a wide class of the clutter power spectra, which correspond to fast and slow spectrum falling and describing by Gaussian and resonant curves:

$$G_G(f) = \exp\{-2,8[(f-f_0)/\Delta f]^2\},$$

$$G_{res}(f) = \{1 + [2(f-f_0)/\Delta f]^2\}^{-1},$$

where f_0 is the central frequency, Δf is a spectrum width on a half-level.

Gaussian and exponential correlation functions correspond to these approximations, and coefficients of inter-period correlation have a view

$\rho_G(j,l) = \rho_G^{(j-l)^2}$, where $\rho_G = \exp[-\pi^2(\Delta fT)^2/2,8]$;

$\rho_{exp}(j,l) = \rho_{exp}^{|j-l|}$, where $\rho_{exp} = \exp(-\pi\Delta fT)$.

V. ANALYSIS RESULTS

Let us fulfill the RF effectiveness analysis in the transient operation mode for $K = 2, 3,$ and 4 on the example of non-recursive RF the 3rd order with binomial weighting coefficients $g(0) = -g(3) = 1$, $g(1) = -g(2) = -3$.

Values of processing vector $\mathbf{H}$ for different K and for both types of RF: fixed structure (FS) and adjustable structure (AS) are shown in Table 1. We see that RF structure adjustment leads to such values of pulse response coefficients, which correspond to compensation of constant amplitude samples that corresponds to sample decorrelation of the actual clutter at each step of the transient process.

Table 1. Values of the processing vector $\mathbf{H}$

RF type \ K	1	2	3	4
FS	$\begin{bmatrix} 1 \end{bmatrix}$	$\begin{bmatrix} -3 \\ 1 \end{bmatrix}$	$\begin{bmatrix} 3 \\ -3 \\ 1 \end{bmatrix}$	$\begin{bmatrix} -1 \\ 3 \\ -3 \\ 1 \end{bmatrix}$
AS	$\begin{bmatrix} 0 \end{bmatrix}$	$\begin{bmatrix} -1 \\ 1 \end{bmatrix}$	$\begin{bmatrix} 2 \\ -3 \\ 1 \end{bmatrix}$	$\begin{bmatrix} -1 \\ 3 \\ -3 \\ 1 \end{bmatrix}$

The specific expressions for γ_{cl} coefficient for both approximations of the clutter correlation functions, which are obtained by formula (11), are shown in Table 2.

Functions $\gamma_{cl}(K)$ for the RF fixed structure (dashed line) and for the RF adjustable structure (solid lines) calculated according to Table 2 expressions for $\rho_G = \rho_{exp} = 0,99$ are shown in Fig. 2. Characteristics with number 1 correspond to the Gaussian function of clutter correlation; characteristic with number 2 correspond to the exponential function. As we see, for adjustable structure of RF, the significant growth of clutter suppression effectiveness can be achieved.

Table 2. Specific expressions for γ_{cl} coefficient

K	RF type	Gaussian correlation function	Exponential correlation function
2	FS	$10/[4+6(1-\rho_G)]$	$10/[4+6(1-\rho_{exp})]$
	AS	$1/(1-\rho_G)$	$1/(1-\rho_{exp})$
3	FS	$19/[19(1-\rho_G)-5\rho_G(1-\rho_G^3)+\rho_G^4]$	$19/[(1-\rho_{exp})(19-5\rho_{exp})+\rho_{exp}^2]$
	AS	$14/[14(1-\rho_G)-4\rho_G(1-\rho_G^3)]$	$14/(1-\rho_{exp})(14-4\rho_{exp})$
4	FS and AS	$20/[20(1-\rho_G)-10\rho_G(1-\rho_G^3)+2\rho_G^4(1-\rho_G^5)]$	$20/(1-\rho_{exp})(20-10\rho_{exp}+2\rho_{exp}^2)$

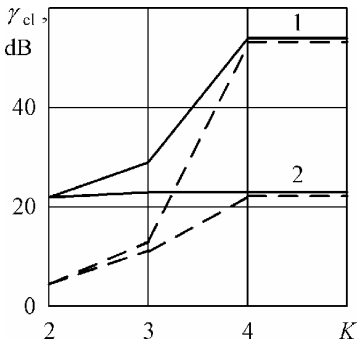

Fig. 2. Functions of the clutter suppression coefficient

For $K=2$ the benefit in γ_{cl} coefficient (compared to RF without adjustment) is 17 dB, for $K=3$–16 dB for the Gaussian function and 12 dB for the exponential function. If $K=4$, the steady-state mode of RF operation occurs. The suppression effectiveness of the clutter with fast spectrum decrease is shown essentially higher than with slow decrease. However, in the last case, during RF structure the steady-state mode of clutter suppression is achieved practically right away.

Let us consider the signal extraction effectiveness in the RF, which can be characterized by the improving coefficient of a signal/clutter ratio

$$\mu = \mathbf{H}^T\mathbf{R}_s\mathbf{H}/\mathbf{H}^T\mathbf{R}_{cl}\mathbf{H},$$

where $\mathbf{R}_s=[\rho_s(j,l)]$ is the correlation matrix of the RF input signal, $\mathbf{H}^T\mathbf{R}_s\mathbf{H}=\gamma_s$ is the signal transmission factor through RF.

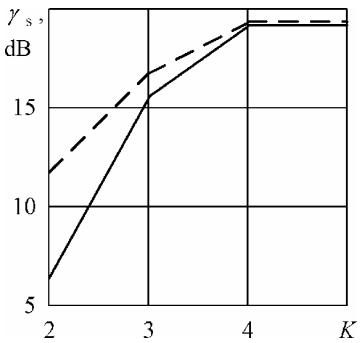

Fig. 3. Functions of signal transmission factor

Functions of $\gamma_s(K)$ and $\mu(K)$, respectively, are shown in Figs. 3 and 4 for the optimal target velocity, mutual signal fluctuations $[\rho_s(j,l)=(-1)^{j+l}]$ and former clutter characteristics (designations correspond to Fig. 2). It follows from Fig. 3 that under RF structure adjustment and $K=2$ and 3, the rather small loss in signal transmission through the RF takes place, which can be explained by differences in $\mathbf{H}$ vector elements for RF of both types (see Table 1). Resulting effectiveness of signal extraction on the background of clutter edge, as we see from Fig. 4, for the filter with adjustable

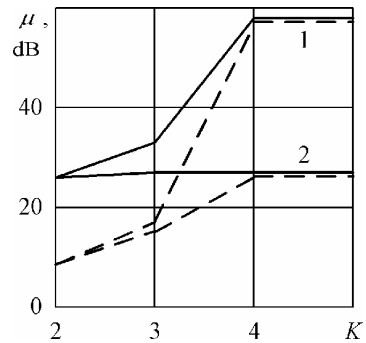

Fig. 4. Functions of improvement factor for signal/clutter

structure, is higher than effectiveness of conventional RF with the fixed structure by 12–17 dB.

VI. CONCLUSION

The improved non-recursive RF synthesized in this paper using the method of state variables allows performing speeding-up of the transient process by means of setting the initial RF state, which is proportional to the first clutter sample at the moment of its arrival.

RF modernization is achieved by its structure adjustment according to results of clutter edge detection, which leads to its effectiveness increase in the transient mode sequentially from one pulse to another.

The comparative RF analysis for fixed and adjustable structures performed by authors on the base of the state variables method shows that adjustment of RF structure ensures significant effectiveness growth in the transient mode for moving targets on the background of clutter edges for a wide class of spectral-correlation characteristics.

REFERENCES

[1] Radar Handbook / Ed. by M. I. Skolnik. – 3rd ed. – McGraw–Hill, 2008. – 1352 p.
[2] Melvin, W.L., Scheer, J.A. (Eds.). Principles of Modern Radar: Advanced Techniques. – New York: SciTech Publishing, IET, Edison, 2013. – 846 p.
[3] Richards, M.A. Fundamentals of Radar Signal Processing, Second Edition. – New York: McGraw–Hill Education, 2014. – 618 p.
[4] Digital signal processing in multi-functional radars. Methods. Algorithms. Equipment / under edition of G.V. Zaitsev (in Russian). – Moscow: Radiotekhnika Publ., 2015. – 376 p.
[5] Lozovskiy, I.F. Digital signal processing in surveillance radars (in Russian). – Novosibirsk: NSTU Publ., 2016. – 270 p.
[6] Cui, Y., Yamaguchi, Y., Kobayashi, H. Yang, J., Singh, G., Park, S.-E. On Semiparametric Clutter Estimation for Ship Detection in Synthetic Aperture Radar Images // IEEE Transactions on Geoscience and Remote Sensing. – 2013. – Vol. 51. – No 5. – P. 3170-3180. DOI: 10.1109/TGRS.2012.2218659.
[7] Bezruk, V.M., Tykhonov, V.A., Kudriavtseva, N.V. Clutter Suppression Using Additive Linear Prediction Filters // Telecommunications and Radio Engineering. – 2013. – Vol. 72. – No 9. – P. 819-828. DOI: 10.1615/TelecomRadEng.v72.i9.70.
[8] Zhang, L.-Z., Lu, B.-Y., Zhou, Z.-M., Sun, X. The Clutter Suppression Based on Factor Analysis and Image Contrast in Through-the-wall Application // Dianzi Yu Xinxi Xuebao. – 2013. – T. 35. – No 11. – P. 2686-2692. DOI: 10.3724/SPJ.1146.2013.00063
[9] Rodionov V.V. Noise-immunity of adaptive pulse-Doppler detectors on the clutter background (in Russian). // Antennas. – 2014. – No 1 (200). – P. 023-029.
[10] Gordeev A.Yu., Yatsyshen V.V. Promising methods of effectiveness increase for clutter suppression by systems of moving target selection. (in Russian). // Electromagnetic waves and electronic systems. – 2015. – Vol. 20. – No 3. – P. 40-52.
[11] Kutepov V.E. Doppler filtering 0f clutter and disturbing reflections on the super-scale range (in Russian). // Uspekhi covremennoi radioelectroniki. – 2016. – No 2. – P. 104-107.
[12] Gracheva, V., Ender, J. Multichannel Analysis and Suppression of Sea Clutter for Airborne Microwave Radar Systems // *IEEE Transactions on Geoscience and Remote Sensing*. – 2016. – Vol. 54. – No 4. – P. 2385-2399.
DOI: 10.1109/TGRS.2015.2500918
[13] Dmitrii I. Popov and Sergey M. Smolskiy, "Estimation of the Clutter Correlation Coefficient in Radar Systems", Infocommunications Journal, Vol. VIII, No 3, September 2016, pp. 8-12.
[14] Dmitrii I. Popov and Sergey M. Smolskiy, "Optimization of the digital rejection filter", Infocommunications Journal, Vol. IX, No 2, June 2017, pp. 1-5.
[15] Ananenkov A.E., Marin D.V., Nuzhdin V.M., Rastorguev V.V. Estimation of clutter suppression level in radar for detection of small-size flying vehicles (in Russian). // Electrosviaz. – 2017. – No 11. – P. 54-57.
[16] Popov, D.I., Smolskiy, S.M. Signal processing in recursive rejection filters in the transient mode // Turkish Journal of Electrical Engineering & Computer Sciences, 26, No 1, 2018, pp. 194-203. DOI: 10.3906/elk-1705-215.
[17] Director, S.W.; Rohrer, R.A. Introduction to Systems Theory, McGraw-Hill Book Company, New York, 1972. – 464 p.
[18] Guskov, S.V.; Popov, D.I. Device for interference suppression. SU Patent No. 1083367. MKP H04B 1/10. *Byull. Izobret*., n. 12, 1984. Claimed 06.01.1982. Published 30.03.1984.
[19] Guskov, S.V.; Ivanov, V.A.; Popov, D.I. Rejection filter. SU Patent No. 1679874. MKP G01S 13/52. *Byull. Izobret*., n. 23, 1999. Claimed 16.01.1984. Published 20.08.1999.
[20] Popov, D.I.; Gerasimov, S.V.; Mataev, E.N. Device for adaptive suppression of interference. SU Patent No. 1802616. MKP G06F 17/17, H03H 21/00. *Byull. Izobret*., n. 22, 1996. Claimed 19.04.1990. Published 10.08.1996.

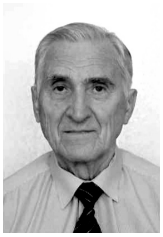

Dmitrii I. POPOV, born in 1939, in Ryazan, Ph.D. in Engineering, Dr. Sc. in Engineering, full professor of Radio Engineering Systems Department in Ryazan State Radio Engineering University (RSREU). Graduated from RSREU in 1961 on specialty "Designing and manufacture of radio equipment". Ph.D. from 1967, Dr. Sc. from 1990.
PhD thesis in specialty "Radar and Radio Navigation Technologies" on theme "Research of detection systems effectiveness for fluctuating signals on the clutter background". Dr. Sc. thesis in specialty "Radar and Radio Navigation Technologies" on theme "Synthesis and analysis of adaptive systems for moving target selection". The active member of International Academy of Informatization.
Author of about 350 scientific publication and patents. Field of research: theory and technique of radar signals processing against noises.

Sergey M. SMOLSKIY, born in 1946, Ph.D. in Engineering, Dr. Sc. in Engineering, full professor of Department of Radio Signals Formation and Processing of the National Research University "MPEI". After graduation of Ph.D. course and defense of Ph.D. thesis in 1974 he worked in Department of Radio Transmitting Devices of MPEI, where was engaged in theoretical and practical problems of development of transmitting cascades of short-range radar. In 1993 defended the Doctor of Science thesis and now he works as a professor of Radio Signals Formation and Processing Dept. Academic experience - over forty years. The list of scientific works and inventions contains over three hundreds of scientific articles, 15 books, three USSR copyright certificates on invention. The active member of International Academy of Informatization, International Academy of Electrotechnical Sciences, International Academy of Sciences of Higher Educational Institutions. The active member of IEEE.

Methods for Predicting Behavior of Elephant Flows in Data Center Networks

Aymen Hasan Alawadi [1], Maiass Zaher [2], and Sándor Molnár [3]

Abstract—**Several Traffic Engineering (TE) techniques based on SDN (Software-defined networking) proposed to resolve flow competitions for network resources. However, there is no comprehensive study on the probability distribution of their throughput. Moreover, there is no study on predicting the future of elephant flows. To address these issues, we propose a new stochastic performance evaluation model to estimate the loss rate of two state-of-art flow scheduling algorithms including Equal-cost multi-path routing (ECMP), Hedera besides a flow congestion control algorithm which is Data Center TCP (DCTCP). Although these algorithms have theoretical and practical benefits, their effectiveness has not been statistically investigated and analyzed in conserving the elephant flows. Therefore, we conducted extensive experiments on the fat-tree data center network to examine the efficiency of the algorithms under different network circumstances based on Monte Carlo risk analysis. The results show that Hedera is still risky to be used to handle the elephant flows due to its unstable throughput achieved under stochastic network congestion. On the other hand, DCTCP found suffering under high load scenarios. These outcomes might apply to all data center applications, in particular, the applications that demand high stability and productivity.**

Index Terms— **Elephant flow, SDN, Risk analysis, Value-at-Risk, Flow scheduling, Congestion control.**

I. INTRODUCTION

Nowadays, many enterprises leverage data center fabrics to manage highly-demanded bandwidth applications. Applications like Hadoop [1] and MapReduce [2] rely on hundreds or thousands of servers to provide high availability and scalability; therefore large data is transferred through the data center network to achieve these requirements. However, other types of data center applications such as regular web services are hosted inside the data center as well, due to the guaranteed availability and reliability. Because of these substantial requirements, many data center topologies evolved like hyperx [3], flattened butterfly [4], and fat-tree [5]. On the other hand, many traffic management techniques emerged, like throughput-based forwarding and load balancing [6]. Typically, the applications of data center produce two types of flows which are mice and elephant flows [6]. Mice flows are known as the smallest and shortest-lived TCP flows in the network and more sensitive to the communication delay. Whereas the most massive and long-lived TCP flows, elephant flows, are more affected by the residual link bandwidth [6].

Department of Telecommunications and Media Informatics, Budapest University of Technology and Economics, Hungary, 1117 Budapest, Magyar Tudosok krt. 2.
[1] aymen@tmit.bme.hu, [2] zaher@tmit.bme.hu,
[3] molnar@tmit.bme.hu

The number of elephant flows in data centers is fewer than that of mice flows, but they carry the most, e.g., 80%, of the transferred data [7]. Some applications, like data mining, machine learning, and data analysis [8] [9] generate such flows since they demand intensive data transmission. These flows must be forwarded through appropriate routes following their requirements. Static forwarding techniques like ECMP [10] could yield network congestions where bottlenecks would stem from collides on a specific switch port due to static hashing [11] [12]. Hence, enhancing flow scheduling in data center networks would improve throughput and Flow Completion Time (FCT).

In today's data centers, SDN plays a vital role in network resource allocation, traffic monitoring, and classification [14]. The paradigm has significantly employed by the research community for flow scheduling, and traffic load balancing [15] [16] since the implementation of real-time applications is delicate without adequate resource and traffic management [2]. The standard design of a data center network includes multi-rooted trees that have multiple paths between every pair of hosts [12]. As a result, the challenge is to identify the suitable path for flows according to the current load of the paths and to avoid network congestion. However, most of the existing flow scheduling solutions like Hedera [12] forward both flow types on the same paths; hence, flow competitions and bottlenecks are inevitable [17]. Furthermore, rerouting the elephant flows might yield delay, packet reordering, and retransmission.

In this paper, we evaluate and predict the performance of ECMP, Hedera, and DCTCP. Particularly, we empirically investigate the performance and efficiency of the algorithms to answer the following questions:

1. What is the predicted loss rate of elephant flows using different algorithms?
2. What are the risk factors of implementing these algorithms regarding the elephant flow preserving?
3. How could the FCT and throughput of mice and elephant flows be under different algorithms?

Therefore, our main contributions are:

1. Implementing a wide range of workloads to estimate the probability distribution of the algorithms' performance.
2. Conducting stochastic performance analysis instead of deterministic one to explore the minimum and maximum value of elephant flows loss rate.
3. Predicting the future performance of the different algorithms based on the stochastic evaluation and

DOI: 10.36244/ICJ.2019.3.6

demonstrate their impact on data center applications in terms of the expected productivity.

The rest of the paper is organized as follows. In section II, we present related works. We describe the proposed model in section III. In section IV, we describe the simulations, results and, discussions. We finally conclude in Section V.

II. RELATED WORKS

Liu et al. [18] present a framework to enable adaptive multipath routing of elephant flows in data center networks under changing load conditions; however, this solution employs NOX controller which has some negative effects on the performance. Similar to Mahout [15], it detects elephant flows at end-hosts, but it monitors TCP socket buffer at end-host to mark flows exceed a predefined threshold so that elephant flows are forwarded based on a weighted multipath routing algorithm which results in installing better paths in switches. Besides, like Hedera, mice flows are delivered based on ECMP by default. However, it employs link load as the only metric for rerouting decisions. Devoflow [19] provides a flow control mechanism in data center networks by rerouting elephant flows whose sizes are more significant than 1 MB.

Similarly, authors in [20] employ group feature of OpenFlow to implement a framework for managing the routes in data center networks by checking links load so that the framework distributes flows among different paths to balance the loads. This framework provides no distinguishing between elephant and mice flows, but when the congestion occurs on a link, the framework selects a backup flow with most considerable traffic demand, which means in practice most probably it will be an elephant flow, but it does not provide any measurements about the impact on mice flows. Wang et al. in [21] present TSACO, which detects elephant flows by OpenFlow and sFlow then forwards them according to an adaptive multi-path algorithm and handles mice flows differently. TSACO computes the available bandwidth and delay of paths and splits an elephant flow over multiple paths, which have considerably enough free bandwidth to balance the load whereas it sends mice flows on the remaining computed flows whose delay characteristics are suitable. As a result, TSACO provides better throughput for elephant flows, and shorter delay for mice flows in comparison with ECMP and weighted ECMP.

III. EXPERIMENTAL METHODOLOGY

In this section, we describe our experimental methodology, including our system setup, network setup, and applications workloads employed in our empirical study.

A. System setup

K-4 fat-tree data center topology was built by using Mininet 2.2.2 SDN emulator installed on Ubuntu 16.04 machine provided with Intel Core i5-8400 CPU 2.80 GHz with 16 GB of RAM.

B. Flow scheduling algorithms

1. **Hedera**: estimates the demand for elephant flows then reroute them to a path with sufficient bandwidth by installing new flow entries on the switches. Particularly, flows will be forwarded through one of the equal-cost paths by applying a static hashing based technique as in ECMP until they grow beyond the predefined threshold which is 10% of the link capacity [12].
2. **Equal-Cost Multi-Path (ECMP)**: switches are statically configured with several forwarding paths for different subnets. The forwarding is based on the hash value of specific fields of packets header modulo the number of paths for spreading the load across many paths [10].
3. **DCTCP**: employs Explicit Congestion Notification (ECN) to estimate the fraction of bytes that encounter congestion rather than directly detecting that congestion has occurred. Then, DCTCP scales the size of the TCP congestion window accordingly. This method provides low latency and high throughput with shallow-buffered switches where they can be used in large data centers to reduce the capital expenditure. In typical DCTCP deployments, the marking threshold in the switches is set to a deficient value to reduce queueing delay, and a relatively small amount of congestion will cause the marking. During the blockage, DCTCP will use the fraction of marked packets to reduce the size of the congestion window more gradually than that in case of conventional TCP [22].

DCTCP and Hedera algorithms are implemented and tested as SDN applications by using Ryu controller whereas, ECMP is implemented statically in switches.

C. Collecting and normalizing the data

In this section, we present the conducted experiment to evaluate the results of the proposed evaluation model. In this paper, fat-tree topology is used since it is considered one of the essential topologies for building efficient, scalable, and cost-effective data centers. Fat-tree topology constructed from three main layers of connected switches located in core, aggregate, and edge layers. However, *K*-4 fat-tree data center topology has been built in Mininet with 10 Mbps links for each as shown in Figure 1.

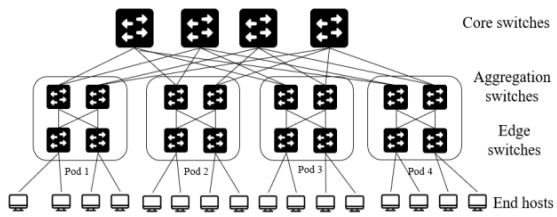

Fig. 1 K-4 fat-tree data center.

The conducted scenarios have two patterns; the first one generates connections that span all topology layers while the second one generates connections span the switches in edge and aggregation layers only as depicted in Figure 2. In these patterns, all of the end hosts in each rack employed to generate the traffic for each of the proposed scenario. To generate the required elephant and mice flows, we employed *iperf* for generating elephant flows, whereas the traffic of mice flows was generated by requesting specific files whose sizes are 10 Kbyte by applying an Apache server repeatedly in a random fashion as reported in [7].

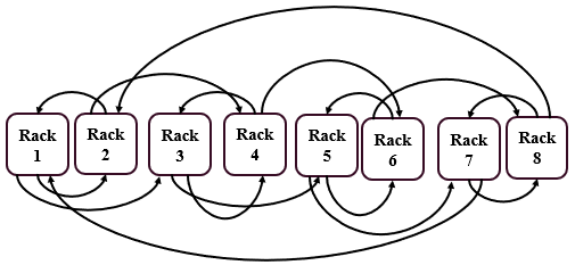

Fig. 2 The traffic pattern.

However, the performance of the proposed model will be evaluated under high load scenarios where the mice flows are synchronized with the elephant flows to introduce congestion in the network. The evaluation process includes three different scenarios with different workloads, a mix of elephant and mice flows, whose time span are varied from 1 to 15 seconds in case of elephant flows to evaluate the investigated algorithms with different sizes of elephant flows. In the first scenario, 1:1 ratio, we generated 120 concurrent connections, so mice and elephant flows have an equal proportion, e.g., 60:60, respectively. In the second scenario, the 1:2 ratio, where we increased the number of the elephant flows to 80, and reduced mice flows to 40. Finally, in the third scenario, 2:1 ratio, where we have 40 elephant flows to 80 mice flows. However, each scenario has been executed twenty-five times, and during each repetition, the throughput has been measured between hosts 1 and 16 by creating a 20 seconds connection using *iperf* to reflect the impact of different algorithms on the throughput of a specific elephant flow, and we built our risk analysis based on it. To obtain the risk factor of the error in throughput measurements, we utilized the arithmetic sample standard deviation. The maximum value of the calculated standard deviation is considered since it indicates a more significant value than the sample mean for the worst-case evaluation.

D. Goodness of fit

The goodness of fit test performed to find the proper probability distribution functions of the throughputs and errors. Therefore, we adopted EasyFit professional [23], which is a specialized statistical tool to test the collected data. Since the collected data is in the discrete domain, we chose to use the Kolmogorov Smirnov statistic test (KS) as a hypothesis test to assess the distribution of the data [24]. KS test is a non-parametric test mainly used to compare the distance between the empirical data samples and a specific class of well-known reference probability distributions as in equation 1 [25].

$$D_n = \sup_x |F_n(x) - F(x)| \quad (1)$$

Where F_n is the cumulative distribution function of the observed samples in comparison with the reference distribution functions F of an ordered data.

A null hypothesis testing has been performed to accomplish this kind of testing, where H_0 is identified when the tested data specify the distribution, and H_1 is recognized when the data does not follow the distribution. To come up with the desired distribution, KS assumes a significance level α (0.01, 0.05, etc.) and compares the tested statistics (D_n) with some of the critical values of the well-known distribution. The hypothesis of the measured distribution will be discarded if the value of D_n exceeds the critical value at a significant level.

P-value based on the KS test helps to identify the level when the null hypothesis is rejected. This value indicates a threshold for the significant level (H_0) to accept all values less than the P-value. For instance, when the P-value = 0.025, the null hypothesis will take all the significance levels less than the P-value, i.e., 0.01 and 0.02, and reject the higher levels [26].

Table 1 shows the results of conducting KS null hypothesis testing on the throughput measurements of the algorithms. The throughput of both Hedera and ECMP followed the Geometric distribution (G-D) based on P-value, and the acceptable critical value was 0.02. However, G-D is recognized as a discrete probability distribution that represents the probability of the success number of independent trials, i.e., Bernoulli trials [27].

TABLE I. KS TEST VALUES FOR THE AVAILABLE THROUGHOUT.

Algorithm	*KS accepted values (critical values)*	*P-Value*	*Distribution*
Hedera	0.05	0.07077	Geometric
ECMP	0.02	0.03	Geometric
DCTCP	Rejected	0.008	-

We got rejection as a result of DCTCP distribution testing for all of the significance levels, as appeared in Table 1. Therefore, we used another normality test called the Anderson-Darling (AD) test. However, the AD test followed the null hypothesis testing and defined as A^2.

$$A^2 = -N - S \quad (2)$$

Where S:

$$S = \sum_{i=1}^{N} \frac{(2i-1)}{N} [\ln F(Y_i) + \ln(1 - F(Y_N + 1 - i))] \quad (3)$$

Where F is the cumulative distribution function of the observed samples and Y_i are the ordered data.

The testing shows that the throughput of DCTCP followed G-D with an acceptable critical value equals 0.02. Hence, we utilized probability mass function of G-D to generate samples required for Monte Carlo simulation model by applying equation 4 where Hedera, ECMP, and DCTCP have different probability values.

$$P_r(A) = (1-p)^{r-1} p \quad (4)$$

Where A is the random variable of the throughput, r is the number of failures with p probability.

Besides, we repeated the same procedure, to identify the distribution of measurement errors, i.e., error factors, as shown in Table 2.

TABLE II. KS TEST VALUES FOR ERROR FACTOR.

Algorithm	*KS accepted values (critical values)*	*P-Value*	*Distribution*
Hedera	0.05	0.86674	Discrete uniform
ECMP	0.05	0.2179	Negative binomial
DCTCP	0.05	0.76964	Poisson

In the case of Hedera, the testing of Hedera algorithm showed that it was following the Discrete Uniform distribution (D-U). Therefore, to generate the required samples of the error factor, we used equation 5.

$$P_r(E_{rH}) = \frac{1}{n} \tag{5}$$

Where E_{rH} is the random variable of the error factor for Hedera algorithm and n is the number of samples generated for the error factor.

On the other hand, the error factor of the ECMP algorithm followed Negative binomial distribution (N-B). N-B is a discrete probability distribution mainly describes the number of successes in a series of independent Bernoulli trials until arriving the defined number of non-random failures occurs. Hence, to generate its sample values for error factor, we utilized equation 6.

$$P_r(E_{rE}) = \binom{r+c-1}{c} p^c (1-p)^r \tag{6}$$

Where E_{rE} is the random variable of the error, r is the number of failures with $1-p$ probability, c is the number of success or failure and, p is the probability of success.

Similarly, the error factor for DCTCP followed a Poisson distribution (P-D) function. However, P-D mostly used to express the probability of occurring certain events within the sample space or fixed interval of time [28]. The probability mass function of the P-D, i.e., equation 7, was used to generate its required samples of the error factor.

$$P_r(E_{rD}) = e^{-k} \frac{\lambda^k}{k!} \tag{7}$$

Where E_{rD} is the random variable of the error factor, λ is the average number of errors recorded per the whole sample, e is the Euler's number 2.71828, and k is the number actually observed occurrences.

E. Monte Carlo Simulation

Monte Carlo approach is a technique used to reproduce the stochastic behavior of a system or to assess a set of uncertainty input of a deterministic model. Typically, it is not possible to predict and determine all possible outcomes of a black box system [29]. Hence, the Monte Carlo simulation process utilized to generate multiple predicted scenarios by estimating the probability distribution of the stochastic input parameters. Consequently, this process recurred hundreds or thousands of times to produce possible scenarios or solutions with different probabilities.

However, we address the impact of the algorithms by calculating the value at risk of the elephant flows. For this purpose, we used the generated samples of throughput and error factor as inputs of the Monte Carlo simulation model. Our fundamental equation, i.e., equation 8 that forms Monte Carlo simulation based on simulating various sizes and volumes of elephant flows along with the risk values.

$$Pre\ (V, S, A, E) = B_m = V_i \times (S_j - (A_k + E_l)) \tag{8}$$

Where B_m is the predicted loss rate, V_i is the different volumes of the evaluated elephant flows, S_j is the sizes of the elephant flows, as shown in Table 3, A_k is the available throughput factor, and E_l is the error factor variables.

TABLE III. ELEPHANT FLOW PARAMETERS.

Elephant flow	*Size S*	*Volume V*
Large	1.25 MByte	100
Normal 1	0.75 MByte	85
Normal 2	0.5 MByte	65
Small	0.12 MByte	45

The assumed values for the size *S* varies from the maximum bandwidth the physical link can handle, i.e., 10 Mbps, to the minimum elephant flow size, i.e., 10% of link capacity, as defined by Al-Fares et al. [12]. The volume parameter *V* represents the amount of the flow within a specific path.

IV. RESULTS AND DISCUSSIONS

The proposed model performed on the algorithms to investigate how they will preserve the elephant flows. The primary expected outcome from this analysis is a histogram represents the probability distribution of the predicted loss rate of elephant flows resulted from employing each algorithm. Therefore, equation 8 repeated one million times. On the upcoming subsections, we will address and compare the results of the investigated algorithms.

A. Throughput of the elephant flow

In Figure 3, we compare the achieved throughput of the algorithms under different scenarios by tracking the connection between hosts 1 and 16. Furthermore, to measure the stability of each algorithm, we calculated the second central moment, e.g., error variance. Results show that Hedera achieved the highest variance, 25.5, in comparison with ECMP, 21.74, while DCTCP had 17.17.

B. Loss rate distribution

Monte Carlo simulation provided the whole estimation for the tested data, as shown in Table 4. However, it is clear that the DCTCP algorithm achieved the worst loss rate due to the fact that DCTCP does not provide any special handling for elephant flows. Furthermore, Hedera and ECMP have layer-4 flow control mechanisms and scheduling capabilities as well.

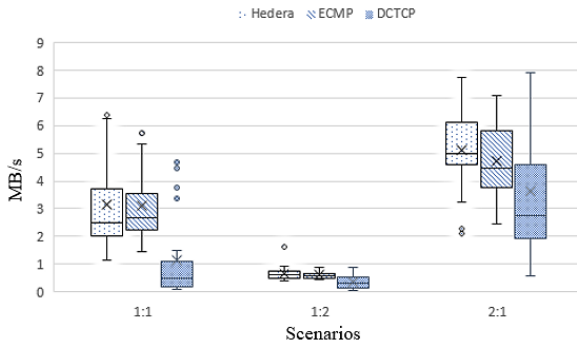

Fig. 3 Throughput achievement of the different scenarios.

TABLE IV. DISTRIBUTION STATISTICS OF THE TESTED ALGORITHMS.

Algorithm	*Loss rate*
Hedera	64%
ECMP	68%
DCTCP	77%

C. *Distribution shape analysis*

To implement the value at risk (VaR) analysis for the obtained result, we should present the histogram of loss rate for each algorithm to figure out the variations of the values. Figures 4, 5, and 6 depict the histograms for Hedera, ECMP, and DCTCP, respectively. The current histograms do not follow a particular type of known probability distributions, but we can indicate that they have a heavy left-hand tail and unsteady proceed to the long right-hand tail. Nevertheless, the yielded histograms may plot almost the same behavior regarding the shape, since the input values (S and V) are the same. Considering the first raw moment of the mean value, blue line, and median value, red line, for such samples may not present the exact expected value of the loss rate [30] since the prediction depends on the merging of the risk values of different samples. Consequently, since we have the sufficient number of samples and for better understanding of the behavior of the loss rate, common distribution shape measurements were calculated, like skewness and kurtosis, as shown in Table 5.

Skewness is the third central moment, and it used for measuring the symmetry of the distribution, and it has two values; positive and negative. The positive value, i.e., right skew, indicates that the mean value is higher than the median value, while the negative value, left skew, suggests the opposite.

Equation 9 describes the skewness degree calculation for the observed distributions.

TABLE V. MEAN, MEDIAN, SKEWNESS, KURTOSIS, AND NUMBER OF SAMPLES FOR THE ALGORITHMS.

Algorithm	*Mean*	*Median*	*Skewness*	*Kurtosis*	*Samples*
Hedera	48.11	39.95	0.55	-0.97	640385
ECMP	48.96	40.80	0.55	-0.97	678761
DCTCP	51.14	43.35	0.49	-1.09	770154

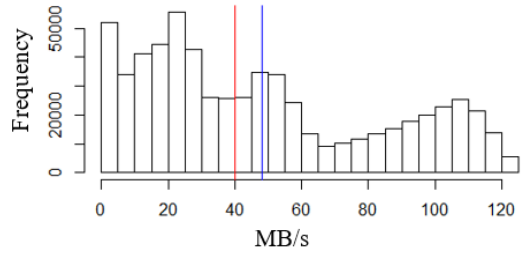

Fig. 4. Histogram of Hedera for the blocked rate.

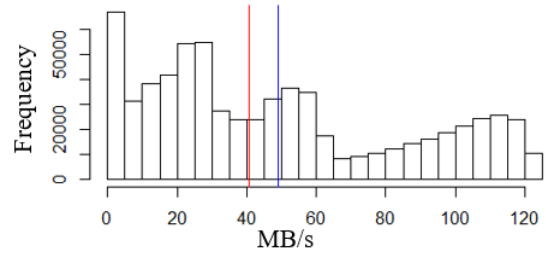

Fig. 5. Histogram of ECMP the blocked rate.

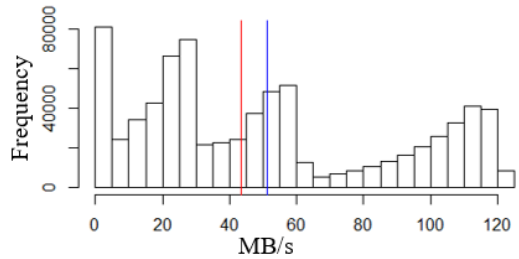

Fig. 6. Histogram of DCTCP for the blocked rate.

$$skew = \frac{\frac{1}{n}\sum_{i=1}^{n}(x_i-\bar{x})^3}{(\frac{1}{n}\sum_{i=1}^{n}(x_i-\bar{x})^2)^{\frac{3}{2}}} \quad (9)$$

Where x_i holds n observations and $\bar{x}$ is the mean values of the observations.

Kurtosis, as shown in equation 10, is the fourth central moment, and it is another essential shape measurement utilized for describing the distribution tail thickness compared to the Normal distribution. Typically, there are three types of Kurtosis, which are mesokurtic, leptokurtic, and platykurtic distributions. Mesokurtic distribution has the same characteristics of the Normal distribution concerning the extreme tail values, while leptokurtic has higher tail values due to the long tail, as for the platykurtic type, it has a precise tail with fewer outliers [31].

$$Kurtosis = \frac{\frac{1}{n}\sum_{m=1}^{n}(B_m-\overline{B_m})^4}{\left(\frac{1}{n}\sum_{m=1}^{n}(B_m-\overline{B_m})^2\right)^2} - 3 \quad (10)$$

Where B_m holds n observations of the predicted blocked rate and $\overline{B_m}$ is the mean values of the observations.

The calculated values indicate that all of the algorithms follow positive and semi-identical symmetry, but they are right-skewed since the mean values precede the median values. However, the degree of the skewness shows that the skews are

moderate, which are between 0.5 and 1 [32]. In this case, the right-hand tail of the histograms will be longer than the left-hand tail, which means most of the data will be on the left-hand tail. But the length of the tail may affect the considering of the average value as the expected value of the loss rate [30]. However, we obtained kurtosis degrees for each algorithm to identify which one has the propensity to produce more outlier results. We found that the prediction distribution for the algorithms follows the platykurtic distribution since the kurtosis is negative compared with the Normal distribution. Therefore, the expected behavior for the algorithms is to produce fewer extreme values for the outliers at their tails, but it is clear that Hedera and ECMP have a higher degree of kurtosis, i.e., 0.79, in comparison with DCTCP what makes their highest loss rate not so trusted. Back to the histograms of ECMP and DCTCP in Figures 5 and 6, we noticed that the error rate to present its lowest values in the rage of 65 – 75 MB/s. However, these centrally located values may happen due to the throughput outliers' effects achieved from scenario 1:1 and 1:2 for both algorithms (Figure 3).

D. Value at Risk (VaR) analysis

Even though, the histogram and the statistics provide comparative information about the behavior of the model and the loss rate prediction, Value at Risk (VaR) analysis could provide more deep analysis based on some confidence [33]. The Monte Carlo simulation model considered as one of the three common types of VaR. In this research and for better generalizability, the chosen confidence level was 95%, since outlier results would appear with a more significant percentage, especially for Hedera and ECMP. Note that we calculated the probability of the confidence level by considering the quantile function, as in equation 11 [33].

$$VaR = -\mu_n + \emptyset^{-1}(1-u)\sigma_n \qquad (11)$$

Where μ_n is the mean of the values of the prediction, $\emptyset$ is the function of the standard Normal distribution, σ_n is the standard deviation of the values and $(1-u)$ used for the chosen confidence level.

This kind of investigation presents a dynamic interpretation of how the elephant flows will be handled while employing such flow scheduling or congestion control algorithms. However, we depicted a broad examination of various confidence levels for the analysis in Figure 7. The loss rate in the case of Hedera is lowest with 112 MB/s for the total number of tested elephant flows appeared in Table 3. The loss of the others, i.e., ECMP and DCTCP, were 116 and 117 MB/s, respectively. Mainly, these values represent the maximum value that will be under risk of losing.

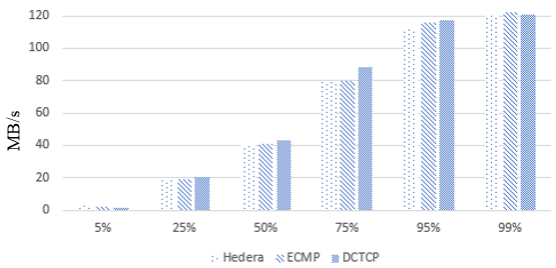

Fig. 7 Different confidence levels of VaR analysis.

5. The probability distribution of the whole overload

In this section, we present the probability distribution of the entire workload, i.e., 120 connections of each scenario for all algorithms. We evaluate the performance of DCTCP, ECMP, and Hedera in terms of throughput of elephant flows and flow completion time of mice flows. All figures show the fact that Hedera and ECMP have very similar performance regarding flow completion time of mice flows and the throughput of elephant flows. Where Hedera employs ECMP for forwarding the mice flows, and ECMP performs well when there are no collide on switch ports what makes its performance in terms of elephant flows throughput closely approaches that of Hedera as shown in Figure 8(a), 8(b), 8(c). On the other hand, figures 9(a), 9(b), 9(c) depict the performance of DCTCP where its FCT of mice flows is more significant than that of Hedera and ECMP because of that DCTCP employs shallow threshold to trigger the marking event. Consequently, the transmission rate will be mitigated by sources where mice flow is delay-sensitive traffic, as well as elephant flows, have worse throughput than that of ECMP and Hedera where DCTCP provides flow control mechanisms, but it does not provide scheduling technique.

In a nutshell, Hedera achieved a lower loss rate than ECMP as expected, but with higher variance for the error factor. We can infer that this factor makes the Hedera does not much outperform over ECMP. As for the response time, Hedera and ECMP achieved better flow completion time due to the static hashing between every source and destination on the network. In the case of flow congestion control in DCTCP, it has achieved its best in the 2:1 scenario whereas it has many outlier results in the 1:1 scenario as depicted in Figure 3. This indicates that the algorithm suffers in case of high elephant flow loads. Regarding data center applications that demand high bandwidth and low latency, every TCP loss causes bursty retransmission and that what makes queues length of the data center switches bloat frequently. Therefore, applications like MapReduce cannot make incremental progress without limiting the number of contending flows.

Therefore, we suggest that some fairness should be considered by providing a balance between link utilization, congestion control. As for the performance evaluation methods of new algorithms that handle traffic flows, we recommend considering the uncertainty behaviors of the tested network and predict their loss rates. To the best of our knowledge, most of the developed heuristic algorithms for flow scheduling are evaluated using the average values for the obtained data without employing the probability distribution function. Note that the expected value for random variables does not exist for some distributions that have a long tail [30]. Consequently, considering the average for any sample of the data may not actually describe the expected value of the measured data, especially if the number of samples is limited. Such as in the case of Hedera [12] and Mahout [15] where the average value is taken for different performance evaluation objectives without identifying the proper probability distribution. Nevertheless, the essence of the prediction produced by independent and random variables relies on current observations to predict future performance. Accordingly, the model and assumptions need to be accurate enough.

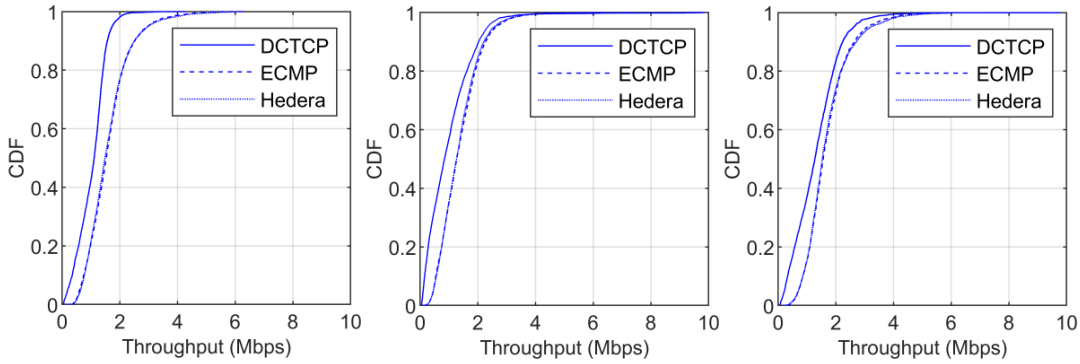

Fig. a Scenario 1:1 Fig. b Scenario 1:2 Fig. c Scenario 2:1

Fig. 8 Throughput of elephant flows.

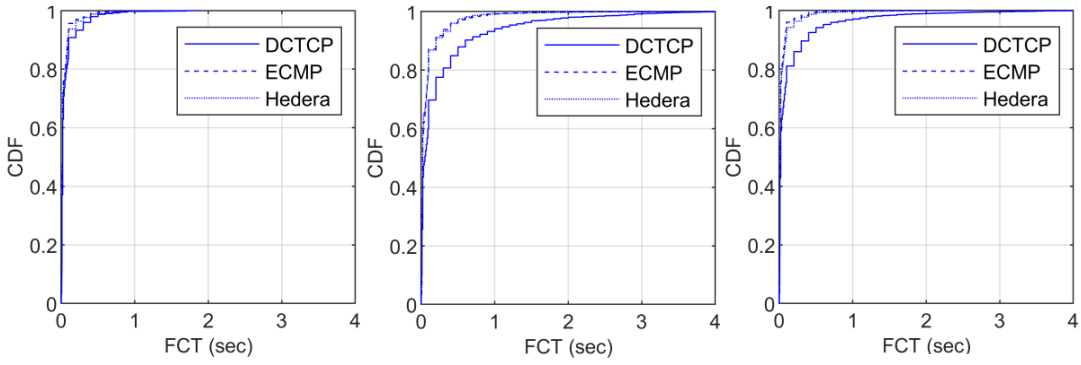

Fig. a Scenario 1:1 Fig. b Scenario 1:2 Fig. c Scenario 2:1

Fig. 9 Flow Completion Time.

V. CONCLUSIONS

In this paper, we empirically designed, implemented, and analyzed a new performance evaluation model for flow scheduling and flow congestion control algorithms used in data center networks based on multiple stochastic workloads to predict the value at risk of the elephant flows loss rate. The evaluation considers the proper probability distribution functions for the proposed risk factors of the loss rate for Hedera, ECMP, and DCTCP. The proposed evaluation model has been built based on Monte Carlo simulation as a value at risk analysis model. The evaluation included an estimation of the probability distribution for risk factors based on Kolmogorov Smirnov and Anderson-Darling tests. Finding the probability distribution of such algorithms helps further mathematical analysis regarding elephant flow handling without conducting more practical experiments. The results of Hedera show that 64% of the evaluated TCP elephant flows are exhibited to be lost 112 MB/s with 95% of the confidence level, while ECMP lost 67.8% with 116 MB/s at risk, and DCTCP lost 77% with 117 MB/s. However, the throughput achieved by Hedera is not permanent due to the stochastic behavior of the traffic congestion. These risks have a direct influence on the status of data center applications in terms of flow completion time and throughput. However, the development of the flow scheduling techniques needs to have proper awareness in terms of flow risk analysis instead of accepting the simple average values of the results, especially when the samples are not large enough. Finally, further study is needed to evaluate more complicated data center workloads with real traces from data center applications to analyze more complex bottlenecks cases.

REFERENCES

[1] 'Apache Hadoop'. [Online]. Available: http://hadoop.apache.org/.

[2] J. Dean and S. Ghemawat, 'MapReduce: simplified data processing on large clusters', *Commun. ACM*, vol. 53, no. 1, pp. 107–113, Jan. 2008.

[3] J. H. Ahn, N. Binkert, A. Davis, M. McLaren, and R. S. Schreiber, 'HyperX: topology, routing, and packaging of efficient large-scale networks', in *Prof. of Conf. on High Performance Computing Networking, Storage and Analysis*, 2009, p. article no. 41. DOI: 10.21276/ijre.2018.5.5.4

[4] J. Kim, W. Dally, and D. Abts, 'Flattened butterfly: a cost-efficient topology for high-radix networks', *ACM SIGARCH Comput. Archit. News*, vol. 35, no. 2, pp. 126–137, Jun. 2007. DOI: 10.1145/1273440.1250679

[5] M. Al-Fares, A. Loukissas, and A. Vahdat, 'A scalable, commodity data center network architecture', *Proc. ACM SIGCOMM 2008 Conf. Data Commun. - SIGCOMM '08*, p. 63, 2008. DOI: 10.1145/1402958.1402967

[6] J. A. Rashid, 'Sorted-GFF: An efficient large flows placing mechanism in software defined network datacenter', *Karbala Int. J. Mod. Sci.*, vol. 4, no. 3, pp. 313–331, 2018. DOI: 10.1016/j.kijoms.2018.06.003

[7] T. Benson, A. Akella, and D. A. Maltz, 'Network traffic characteristics of data centers in the wild', in *Proceedings of the 10th annual conference on Internet measurement - IMC '10, 2010*, p. 267. DOI: 10.1145/1879141.1879175

[8] T. Mori, S. Naito, R. Kawahara, and S. Goto, 'On the characteristics of Internet traffic variability: Spikes and elephants', in *Proceedings - International Symposium on Applications and the Internet,* 2004, pp. 99–106. DOI: 10.1109/saint.2004.1266104

[9] S. Yu, X. Lin, and J. Misic, 'Networking for big data: Part 2 [Guest Editorial]', *IEEE Netw.*, vol. 29, no. 5, pp. 4–5, 2015. DOI: 10.1109/MNET.2015.7293297

[10] C. E. Hopps, *Analysis of an Equal-Cost Multi-Path Algorithm*. RFC 2992 (Informational), 2000. doi :10.17487/rfc2992

[11] A. Greenberg et al., 'VL2', in *Proceedings of the ACM SIGCOMM 2009 conference on Data communication - SIGCOMM '09*, 2009, vol. 39, no. 4, p. 51. DOI: 10.1145/1592568.1592576

[12] M. Al-Fares, S. Radhakrishnan, B. Raghavan, N. Huang, and A. Vahdat, 'Hedera: dynamic flow scheduling for data center networks', *Proceedings of the 7th USENIX conference on Networked systems design and implementation*. pp. 19–19, 2010. [Online]. Available: https://raghavan.usc.edu/papers/hedera-nsdi10.pdf

[13] N. McKeown et al., 'OpenFlow: enabling innovation in campus networks', *ACM SIGCOMM Comput. Commun. Rev.*, vol. 38, no. 2, p. 69, Mar. 2008. DOI: 10.1145/1355734.1355746

[14] A. Chhabra and M. Kiran, 'Classifying Elephant and Mice Flows in High-Speed Scientific Networks', in 4*th International Workshop on Innovating the Network for Data Intensive Science (INDIS)*, 2017. [Online]. Available: https://scinet.supercomputing.org/workshop/sites/default/files/Chabbra-classifying_flows.pdf

[15] A. R. Curtis, W. Kim, and P. Yalagandula, 'Mahout: Low-overhead datacenter traffic management using end-host-based elephant detection', in *2011 Proceedings IEEE INFOCOM*, 2011, pp. 1629–1637. DOI: 10.1109/infcom.2011.5934956

[16] C. Wang, B. Hu, S. Chen, D. Li, and B. Liu, 'A Switch Migration-Based Decision-Making Scheme for Balancing Load in *SDN', IEEE Access*, vol. 5, pp. 4537–4544, 2017. DOI: 10.1109/access.2017.2684188

[17] F. Tang, H. Zhang, L. T. Yang, and L. Chen, 'Elephant Flow Detection and Differentiated Scheduling with Efficient Sampling and Classification', *IEEE Trans. Cloud Comput.*, pp. 1–1, 2019. DOI: 10.1109/tcc.2019.2901669

[18] J. Liu, J. Li, G. Shou, Y. Hu, Z. Guo, and W. Dai, 'SDN based load balancing mechanism for elephant flow in data center networks', in 2014 International Symposium on Wireless Personal Multimedia Communications (WPMC), 2014, vol. 2015-Janua, pp. 486–490. DOI: 10.1109/WPMC.2014.7014867

[19] P. Sharma, A. R. Curtis, J. Tourrilhes, S. Banerjee, J. C. Mogul, and P. Yalagandula, 'DevoFlow: scaling flow management for high-performance networks', in SIGCOMM '11 Proceedings of the ACM SIGCOMM 2011 conference, 2011, vol. 41, no. 4, pp. 254–265. DOI: 10.1145/2018436.2018466

[20] Y. C. Wang and S. Y. You, 'An Efficient Route Management Framework for Load Balance and Overhead Reduction in SDN-Based Data Center Networks', IEEE Trans. Netw. Serv. Manag., vol. 15, no. 4, pp. 1422–1434, Dec. 2018. DOI: 10.1109/tnsm.2018.2872054

[21] C. Wang, G. Zhang, H. Chen, and H. Xu, 'An ACO-based elephant and mice flow scheduling system in SDN', in 2017 IEEE 2nd International Conference on Big Data Analysis (ICBDA), 2017, pp. 859–863. DOI: 10.1109/icbda.2017.8078760

[22] M. Alizadeh, A. Greenberg, D. A. Maltz, J. Padhye, P. Patel, B. Prabhakar, S. Sengupta, and M. Sridharan, 'Data center TCP (DCTCP)', ACM SIGCOMM Comput. Commun. Rev., vol. 41, no. 4, pp. 63–74, 2011. DOI: 10.1145/1851182.1851192

[23] A. Drokin, 'Easyfit - Distribution fitting software'. p. www.mathwave.com, 2010. Available: www.mathwave.com, 2010.

[24] D. S. Dimitrova, V. K. Kaishev, and S. Tan, 'Computing the Kolmogorov-Smirnov Distribution when the Underlying cdf is Purely Discrete, Mixed or Continuous', Nov. 2017. DOI: 10.18637/jss.v039.i11

[25] H. M. Abachi, S. Hosseini, M. A. Maskouni, M. Kangavari, and N. M. Cheung, 'Statistical discretization of continuous attributes using kolmogorov-smirnov test', in Lecture Notes in Computer Science 2018, vol. 10837 LNCS, pp. 309–315. DOI: 10.1007/978-3-319-92013-9_25

[26] A. Drokin, 'EasyFit - Kolmogorov-Smirnov Test'. [Online]. Available: http://www.mathwave.com/help/easyfit/html/analyses/goodness_of_fit/kolmogorov-smirnov.html.

[27] A. N. Philippou, C. Georghiou, and G. N. Philippou, 'A generalized geometric distribution and some of its properties', Stat. Probab. Lett., vol. 1, no. 4, pp. 171–175, Jun. 1983. DOI: 10.1016/0167-7152(83)90025-1

[28] E. Brooks, 'Statistics The Poisson Distribution', University of Massachusetts at Amherst, 2007. [Online]. Available: http://www.umass.edu/wsp/resources/poisson/index.html.

[29] J.-C. Walter and G. T. Barkema, 'An introduction to Monte Carlo methods', Phys. A Stat. Mech. its Appl., vol. 418, no. 1, pp. 78–87, Jan. 2015. DOI: 10.1016/j.physa.2014.06.014

[30] R. W. Hamming, The Art of Probability for Engineers. Addison-Wesley, 1991. DOI: 10.1201/9780429492952-1

[31] Investopedia, 'Kurtosis'. [Online]. Available: https://www.investopedia.com/terms/k/kurtosis.asp.

[32] B. McNeese, 'Are the Skewness and Kurtosis Useful Statistics? | BPI Consulting', SPC Excel, 2008. [Online]. Available: https://www.spcforexcel.com/knowledge/basic-statistics/are-skewness-and-kurtosis-useful-statistics#skewness.

[33] C. K. Thim, M. Nourani, and Y. V. Choong, 'Value-at-risk and conditional value-at-risk estimation: A comparative study of risk performance for selected malaysian sectoral indices', in ICSSBE 2012 - Proceedings: 'Empowering Decision Making with Statistical

Aymen Alawadi Obtained his B. Sc. in 2006-2007 in the Computer Engineering from the University of Technology in Baghdad - Iraq. In 2007, he joined the University of Kufa in Najaf -Iraq as IT Engineer. From 2010 to 2012 he got M.Sc. in Computer Science from Universiti Sains Malaysia. Since 2017, he is a PhD student in the Department of Telecommunication and Media Informatics, Budapest University of Technology and Economics, Hungary.

Maiass Zaher Obtained his B. Sc. in 2008 in the Computer Networks and Systems Engineering from Tishreen University, Syria. In 2013-2016 he got M.Sc. in Information Technology Engineering, Damascus University, Syria. Since 2016, he is a Ph.D. student in the Department of Telecommunication and Media Informatics, Budapest University of Technology and Economics, Hungary.

Sándor Molnár received his MSc, PhD and Habilitation in Electrical Engineering and Computer Science from the Budapest University of Technology and Economics (BME), Budapest, Hungary, in 1991, 1996 and 2013, respectively. In 1995 he joined the Department of Telecommunications and Media Informatics, BME. He is now an Associate Professor and the principal investigator of the tele traffic

Deep Web Data Source Classification Based on Text Feature Extension and Extraction

Yuancheng Li, Guixian Wu, and Xiaohan Wang

***Abstract*—With the growth of volume of high quality information in the Deep Web, as the key to utilize this information, Deep Web data source classification becomes one topic with great research value. In this paper, we propose a Deep Web data source classification method based on text feature extension and extraction. Firstly, because the data source contains less text, some data sources even contain less than 10 words. In order to classify the data source based on the text content, the original text must be extended. In text feature extension stage, we use the N-gram model to select extension words. Secondly, we proposed a feature extraction and classification method based on Attention-based Bi-LSTM. By combining LSTM and Attention mechanism, we can obtain contextual semantic representation and focus on words that are closer to the theme of the text, so that more accurate text vector representation can be obtained. In order to evaluate the performance of our classification model, some experiments are executed on the UIUC TEL-8 dataset. The experimental result shows that Deep Web data source classification method based on text feature extension and extraction has certain promotion in performance than some existing methods.**

***Index Terms*—Deep Web, Classification, Attention mechanism, Feature extension.**

I. INTRODUCTION

OVER the past decade, the number of web pages has grown exponentially with the popularity of the Internet [1]. At present, Surface Web refers to resources that can be accessed through static hyperlinks, usually static HTML pages [2]. Such resources can be crawled by web crawlers and are also visible to search engines. Whereas Deep Web refers to resources that are not hidden in the Web database and cannot be crawled by the web crawler. These resources are invisible to the search engine, users who want to get data in it must fill out the form and submit it according to actual needs to dynamically obtain Deep Web resources [3]. Fig. 1 shows an example of the Deep Web. According to statistic, Deep Web has the following advantages compared to Surface Web [4]-[6] (1) Information in Deep Web is 700 to 800 times that of Surface Web information. It includes a large amount of information that traditional search engines cannot find, and its growth rate is much higher than Surface Web; (2) The information contains in Deep Web is of higher quality than the information contained in the Surface Web. Moreover, Deep Web contains information in all areas. In the field of integration, structured data has a higher value, and the Deep Web contains information that is typically structured data. (3) Everyone has access to more than 90% of the Deep Web information, and we can get it for free, which greatly facilitates the interconnection of information. Therefore, research on Deep Web information acquisition has higher practical significance and practical value. To make better use of the information in the Deep Web, it is necessary to classify data sources based on content [7]-[8].

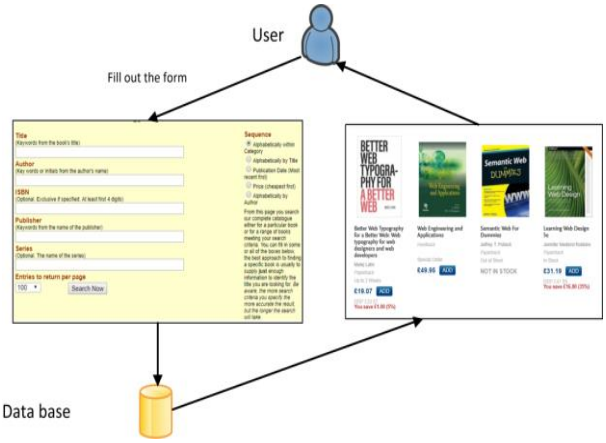

Fig. 1. An example of Deep Web data source.

In recent years, scholars all over the world have propose many kinds of intelligent methods for the classification of data sources. Reference [9] combines the two methods to get the similarity of the search interface and implement classification. The first one is based on vector space. Classic TF-IDF statistics are used to obtain similarities between search interfaces. The other is to use HowNet to calculate the semantic similarity between two pages. Reference [10] proposes a " one hot encoding" method to classify news headlines and summary information collected on the Deep Web. A content-based classification model is proposed in [11], which uses machine learning to filter unwanted information. Word2Vec word embedding tool is used to establish the classification model and classify the selected data set. Reference [12] proposes a new probabilistic subject model to realize text extension and enrich feature description. The deep architecture of the LSTM is applied to Web service recommendations and predictions for more accurate service recommendations. A text categorization network model based on human conditioned reflex (BLSTM) is proposed in [13]. The receptor obtains context information through BLSTM, the nervous center obtains important information of sentences through attention mechanism, and the effector obtains more key information through CNN.

Yuancheng Li , Guixian Wu and Xiaohan Wang are with School of Control and Computer Engineering, North China Electric Power University, Beijing, China. (e-mail: yuancheng@ncepu.cn).

DOI: 10.36244/ICJ.2019.3.7

Reference [14] proposes a coordinated CNN-LSTM-Attention model(CCLA). The semantic and emotional information of sentences and their relationships are adaptively encoded into vector representations of documents. Softmax regression classification is used to determine the emotional tendency in the text. For short text feature extension, there are two main methods at present [15]-[16]: (1) Using topic models such as potential Dirichlet allocation (LDA), Latent Semantic Analysis (LSA), and pLSA. (2) Using search engines and external knowledge bases like WordNet, HowNet, and Wikipedia.

This paper propose a Deep Web data source classification method based on text feature expansion and extraction. In the feature extension stage, We choose extension words through the N-gram model which is easy to train and does not require an external corpus when during feature extension. Then, in the classification stage, we propose a classification method based on Attention-based Bi-LSTM. LSTM is an improvement on traditional RNN. Based on the RNN model, LSTM adds a cell control mechanism to solve the long-term dependence problem and the gradient explosion cause by excessive sequence length [17]-[18]. However, The LSTM model can only utilize the preceding part of the text and does not use the information below, so some semantic information will be lost. To solve this problem, we replace LSTM with Bi-LSTM, which can use both the above and below information simultaneously. Moreover, it is clear that each word in the text contributes differently to the characteristic representation of the text, so whether using the average output of each neuron in the network output layer or the output value of the last neuron, the vector representation of the text cannot be accurately obtained. Therefore, the best way is to use a weighted average to process the output of each neuron in the output layer. To achieve a weighted average, we use the Attention mechanism to handle the output of the Bi-LSTM network. In summary, we propose the deep Web data source classification model based on N-gram and Attention-based Bi-LSTM. Then we conducte multiple sets of comparative experiments on the UIUC TEL-8 dataset. The experimental results show that the Deep Web data source classification method based on n-gram and Attention-based Bi-LSTM has better performance than existing methods.

II. MATERIALS AND METHODS

A. N-gram language model

The N-gram language model plays a pivotal role in natural language processing. Especially in many NLP tasks such as machine translation, syntactic analysis, phrase recognition, part-of-speech tagging, handwriting recognition, and spelling correction.

For a sentence S consisting of n words, the probability of its appearance is:

$$\begin{aligned} \mathrm{P(S)} &= P(w_1, w_2, \cdots, w_n) \\ &= \mathrm{P}(w_1) * \mathrm{P}(w_2|w_1) * \cdots * \mathrm{P}(w_n|w_1 w_2, \cdots, w_{n-1}) \\ &= \prod_{i=1}^{n} \mathrm{P}(w_i|w_1 w_2, \cdots, w_{i-1}) \end{aligned} \quad (1)$$

The probability that (1) represents the ith word is determined by the previous i-1 words. However, a serious problem with this calculation method is that as the length of the sentence increases, the number of parameters that need to be trained will increase exponentially. To solve this problem, according to the Markov hypothesis, supposing that the appearance of the ith word is only related to the first n-1 words. Then, the probability of the sentence $\mathrm{S} = \mathrm{w_1 w_2 \cdots w_n}$ is:

$$\begin{aligned} \mathrm{P(S)} &= P(w_1, w_2, \cdots, w_n) \\ &= \mathrm{P}(w_1) * \mathrm{P}(w_2|w_1) * \cdots * \mathrm{P}(w_n|w_1 w_2, \cdots, w_{n-1}) \\ &= \prod_{i=1}^{n} \mathrm{P}(w_i|w_1 w_2, \cdots, w_{i-1}) \\ &\approx \prod_{i=1}^{n} \mathrm{P}(w_i|w_{i-N+1} w_{i-N+2}, \cdots, w_{i-1}) \end{aligned} \quad (2)$$

The above is the N-gram model. When N = 2, it is assumed that the appearance of each word is only related to one of the previous words, called Bi-gram, as shown in (2).

$$P(S) \approx \prod_{i=1}^{n} \mathrm{P}(w_i|w_{i-1}) \quad (3)$$

In (3),

$$\mathrm{P}(w_i|w_{i-1}) = \frac{c(w_{i-1} w_i)}{c(w_{i-1})} \quad (4)$$

Where $\mathrm{c(w_{i-1} w_i)}$ refers to the number of occurrences of the word sequence $\mathrm{w_{i-1} w_i}$ in the training set, and $\mathrm{c(w_{i-1})}$ refers to the number of occurrences of the word $\mathrm{w_{i-1}}$.

The performance of the models is different when choosing different N. The Bi-gram model is widely used in NLP. The larger N is, the more constraints appear on the next word, and the stronger the recognition ability of the language model, but the higher the complexity of model training, the more sparse the parameters. Conversely, if N is smaller, the language model is easier to train, and the parameters obtain from the corpus will be more, and the statistical information of the corpus can be better utilized. In the research and practical application of natural language processing, the Bi-gram model is the most used.

B. Bidirectional Long Short-Term Memory Network

Long short-term memory (LSTM) is an improvement of the recurrent neural network (RNN), which effectively solves the problem of disappearing gradients. LSTM solves the disappearing gradient problem in RNN by adding a gating function to the general recursive neural network [19]-[20]. Fig. 2 shows the structure of the LSTM cell.

As shown in Fig. 2, The LSTM cell is mainly composed of three parts: the input gate, the forgotten gate, and the output gate. Each gate consists of a sigmoid layer and a vector operation. The probability value of the sigmoid layer output is between 0 and 1, which describes how much each part can pass. The input gate allows the input signal to change the state of the memory unit or block it. Besides, the output gate allows the state of the memory cell to affect other neurons or block it. Finally, the forgotten gate allows the unit to remember or forget its previous state [21].

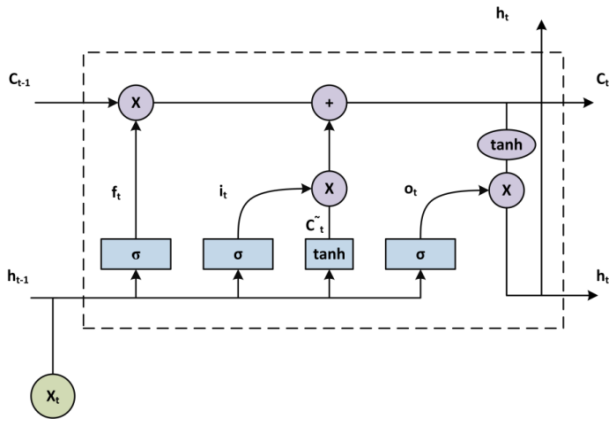

Fig. 2. The structure of a LSTM cell.

The calculation process of a LSTM memory cell is described as follow:

Let vector sequence $X = \{x_1, x_2, \ldots, x_t, \ldots, x_n\}$ is the input of LSTM network, vector sequence $H = \{h_1, h_2, \ldots, h_t, \ldots, h_n\}$ is the output of hidden layer of LSTM network and C_i, $i = 0,1, \ldots, t, \ldots n$ is the state of the i-th memory cell.

1. Decide how much to forget from the state of last memory cell, the calculation process is as follows.

$$f_t = \sigma\left(W_f \cdot [h_{t-1}, x_t]_f + b_f\right) \tag{5}$$

In (5), σ is sigmoid function, W_f and b_f are respectively weights and bias of forget gate, $f_t \in (0,1)$.

2. Decide what to add to the cell state, the calculation process is as follows.

$$i_t = \sigma\left(W_f \cdot [h_{t-1}, x_t] + b_i\right) \tag{6}$$

$$\tilde{C}_t = \tanh\left(W_C \cdot [h_{t-1}, x_t] + b_C\right) \tag{7}$$

In this step $\tilde{C}_t$ is the update candidate who calculates by output of last cell and input of current cell, and $i_t \in (0,1)$ decide which part of the candidate value is added to the state of the cell.

3. Update cell state

Update C_{t-1} to C_t according to (8).

$$C_t = f_t * C_{t-1} + i_t * \tilde{C} \tag{8}$$

Firstly, multiply the old state by f_t to discard some information in old state. Then, add new candidate value to old state.

4. Calculated output

$$o_t = \sigma\left(W_o \cdot [h_{t-1}, x_t] + b_o\right) \tag{9}$$

$$h_t = o_t * \tanh\left(C_t\right) \tag{10}$$

In (9), σ is sigmoid function, W_o and b_o is respectively weights and bias of output gate, and the result of (10) h_t is the output of current memory cell.

Bidirectional LSTM (Bi-LSTM) is a combination of two layers of LSTM networks [22]. In Fig. 3, the boxes are the LSTM cells, where representes as the output of the memory unit at the forward time t and are the output of the memory model in the backward direction at time t. A contextual semantic representation of the text can be obtained by concatenating the output of the forward sequence and the backward sequence.

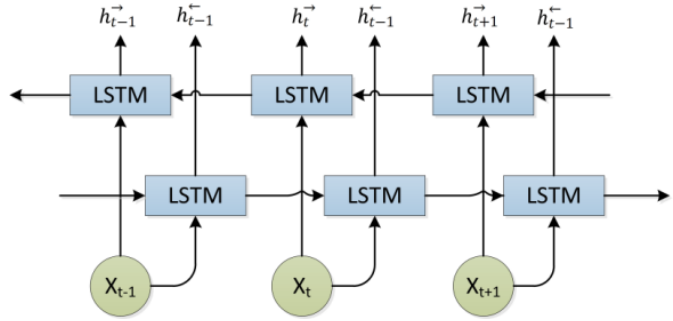

Fig. 3. Bidirectional LSTM.

C. Attention mechanism

We can take the average of the output at all times or the output at the last moment as a characteristic representation as to the output of the network [23]-[24]. However, all words contribute differently to the meaning of the sentence. Moreover, if the output of the last moment is taken as a feature representation, the previous semantic information will be lost. Therefore, to give higher weight to words that are more important to the meaning of the text, it is best to use a weighted average approach to process network output. To achieve this goal, We use the Attention mechanism to extract and aggregate words that are important to the meaning of the web page to form a text vector. Fig. 4 is a schematic diagram of the Attention mechanism. In the picture, we can see that the key to Attention mechanism is an attention matrix [25]-[26]. The calculation process of attention weights is shown in (11) (12) (13).

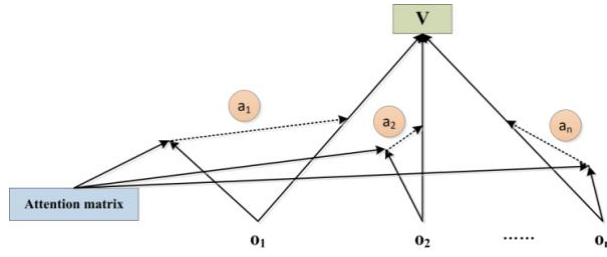

Fig. 4. Attention mechanism.

$$u_i = \tanh\left(W_o o_i + b_o\right) \tag{11}$$

$$a_i = \frac{\exp\left(u_i \cdot W_a\right)}{\sum_{i=1}^{n} \exp\left(u_i \cdot W_a\right)} \tag{12}$$

$$V = \sum_{i=1}^{n} o_i a_i \tag{13}$$

Firstly, We feed the word vector representation o_i through a one-layer MLP to get as a hidden representation of o_i according to (11). Then, as shown in (12), We use the softmax

function to obtain the standardized weight a_i of importance. Finally, according to the weight calculated in the previous step, we calculate the text vector V as the weight of each word vector. Since words that are closer to the text topic are assigned higher weights, the text vector obtains through the Attention mechanism can better express the semantics of the text.

D. Deep Web Data Source Feature Extension

Since some data sources contain a few words, feature extension is required first. Firstly, we need to extract keywords from the Deep Web data source. Generally speaking, in a sentence, verbs, and nouns usually express the meaning of sentences. Although adjectives and adverbs have no practical meaning, they appear in conjunction with nouns and verbs. Therefore, we choose these four types of words as the starting point for feature expansion [15].

Firstly, the N-gram model is used to build a feature extension library in this paper. Starting from word w_A, we can get conditional probability $P(w_B|w_A)$ of word sequence w_Aw_B, if $P(w_B|w_A) > P$, add w_B to the extension library and continue the process with w_B as the starting point until the maximum number of extensions M is reached. Detailed description is as follows:

Algorithm 1: Feature extension for Deep Web data source

Input: Original text of data source W
Threshold P of conditional probability

Extension library W_E={}
Set starting point word set W_S=W
while: Number of extensions <= M
  Starting point set of the next round of extension W'={}
  for: each word w_i in W
    for: each word sequence $w_i w_{next}^i$
      if $P(w_{next}^i|w_i) > P$
        Add w_{next}^i to the extension set W_E
        Add w_{next}^i to W'
      else
        Continue
    end for
  Number of extensions plus 1
  $W_S = W'$
  $W' = \{\}$
  end for
end while
end

Output: extension library W_E

E. Deep Web Data Source Classification Based on Attention-based Bi-LSTM

After feature extension, we solved the problem of the sparseness of feature. Then, our goal is to achieve accurate classification of data sources.

Through observation, we found that the structural difference of the data source is not very obvious and some data sources maybe only contain one or two html controls, which leads to bad performance of data source classification based on structural information. In addition, there is currently no large-scale Deep Web data source dataset that can be used to train deep networks. Based on the above questions, in this paper, we classify data by text in the Deep Web page, which not only can accurately classify the data source with simple structure but also can use large-scale text classification data set in the training phase. The core of our model present in this paper is an Attention-based Bi-LSTM model, its network structure is shown in Fig. 5. Our classification model is consist of a word embedding layer, input layer, a forward LSTM, a backward LSTM, an attention layer, a fully connected layer and a softmax classifier.

Let word sequence $W = \{w_1, w_2, \dots, w_n\}$ is all text of a Deep Web data source. Firstly, we convert W to word vector sequence $X = \{x_1, x_2, \dots, x_n\}$ by word2vec. Then, we use X as the input of forward LSTM and backward LSTM. The output sequence of the two layers of LSTM is $H^{\rightarrow} = \{h_1^{\rightarrow}, h_2^{\rightarrow}, \dots, h_n^{\rightarrow}\}$ and $H^{\leftarrow} = \{h_1^{\leftarrow}, h_2^{\leftarrow}, \dots, h_n^{\leftarrow}\}$ respectively, and the output sequence of Bi-LSTM network is $O = \{o_1, o_2, \dots, o_n\}$, in which, $o_i = [h_t^{\rightarrow}, h_t^{\leftarrow}]$. Next, we compute the weight sum of sequence O as the output of the Attention-based Bi-LSTM. Finally, obtain the classification label by fully connected layer and a softmax classifier.

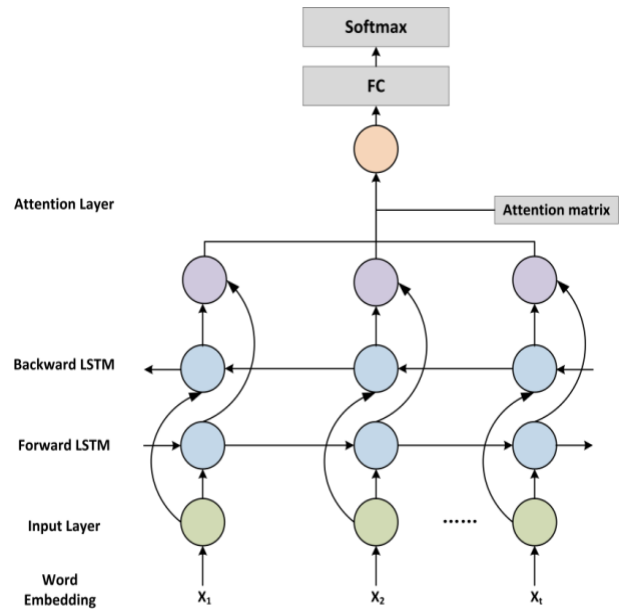

Fig. 5. Attention-based Bi-LSTM for Deep Web data source classification.

The main process of the proposed method is shown in Fig. 6 and described as follows:

(1) Since the data source of the deep web is the <form> tag in the html page, the first step is to parse the html and locate the <form> tag. In order to deal with non-standard html code and mismatched tags, we use Jsoup to parse the html code, which can fills in missing tags automatically. Moreover, in some <form> tags, some drop-down menus have hundreds of options. These drop-down menus are generally noises that do not help the classification (e.g. country, state). Therefore, drop-down menus with options greater than 30 are not used as feature.

(2) Next, we get all text between <form> tag through XML parsing and carry out some pretreatment (e.g. lemmatization, tokenize) by Stanford's CoreNLP and natural language toolkit (NLTK) [27]-[29].

(3) Then, we convert them into word vectors via Google word2vec.

(4) Build our Attention-based Bi-LSTM Deep Web data source classification.

(5) Training and test the classification model.

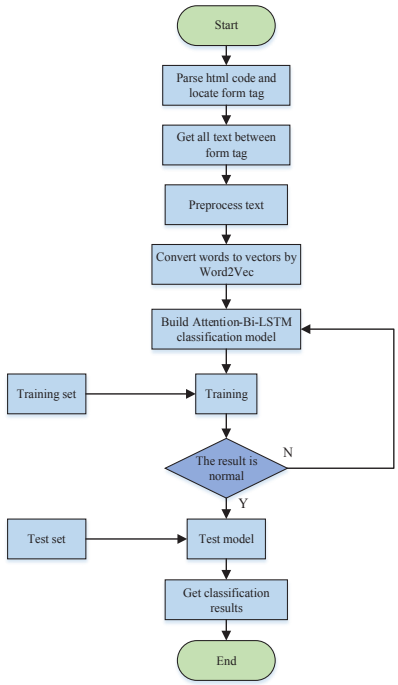

Fig. 6. The flow of our classification method.

III. EXPERIMENT AND DISCUSSION

A. DataSets

We experiment on UIUC TEL-8 datasets and evaluate the performance of our model. The UIUC TEL -8 dataset contains the original query interface of 447 Deep Web sources from 8 representative domains and its manually extract query functions. The 8 areas are further divided into three groups:(1) In the Travel group: Airfares, Hotels, and Car Rentals; (2) In the Entertainment group: Books, Movies, and Music Records; (3) In the Living group: Jobs and Automobiles.

B. Result and Analysis

1) Experiment for feature extension

In experiment for feature extension, we illustrate the effect of the feature extension process to the data source classification effect.

First of all, due to the sparseness of the data, smoothing techniques are needed in the process of training Bi-grams. We tried 4 smoothing algorithms: Add-one smoothing; Good-Turing smoothing; Interpolation; Kneser-Key smoothing. The evaluation index of the N-gram model is the perplexity, and its calculation method is as follows:

For the sentences $S = \{w_1 w_2 \cdots w_n\}$ in the test set, the perplexity is calculated as (14).

$$\begin{aligned} \mathrm{PP}(S) &= P(w_1 w_2 \cdots w_n)^{-\frac{1}{n}} \\ &= \sqrt[n]{\frac{1}{P(w_1 w_2 \cdots w_n)}} \\ &= \sqrt[n]{\prod_{i=1}^{n} \frac{1}{P(w_1 | w_1 w_2 \cdots w_{i-1})}} \end{aligned} \quad (14)$$

For Bi-gram,

$$\mathrm{PP}(S) = \sqrt[n]{\prod_{i=1}^{n} \frac{1}{P(w_i | w_{i-1})}} \quad (15)$$

The perplexity of model when using different smoothing algorithm is shown in Table I.

It can be seen from the above results that the selection of the smoothing algorithm is very important. According to the experimental results, we choose the Kneser-Key smoothing as the smoothing algorithm of our method.

TABLE I
THE PERPLEXITY OF MODEL WHEN USING DIFFERENT SMOOTHING ALGORITHM

Smoothing algorithm	Perplexity
Add-one smoothing	4253
Good-Turing smoothing	754
Interpolation	568
Kneser-Key smoothing	532

In the process of feature extension, the parameters that need to be manually selected are P and M. Firstly, we set M=3 and carry out text feature extension of Deep Web data source text with different P and use the Attention-based Bi-LSTM network

for feature extraction and classification. The experimental results are shown in Fig. 7.

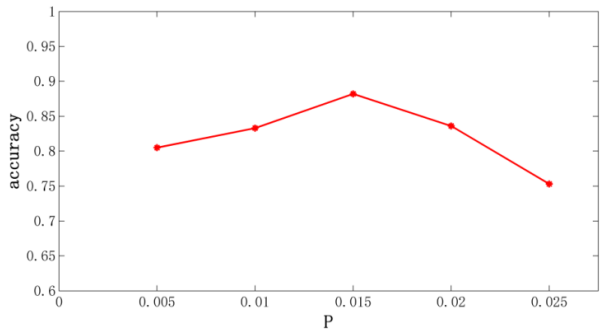

Fig. 7. The influence of the threshold P.

From the Fig.7 we can see that with the increase of P, the classification precision shows a trend of rising first and then decreasing. This is because when P is bigger, the restriction on feature extension is larger, and the fewer extension words are added to original text, so that the problem of feature sparseness cannot be solved. And when P is smaller, more extension words will be added, but the semantic difference between these words and the original text will be larger, which will bring noisy. When P=0.015, the best classification performance can be obtained.

Secondly, we set P=0.015 and change the value of M, respectively 0,1,2,3,4,5,6, where M=0 means no feature extension is performed. The results are shown in Fig. 8.

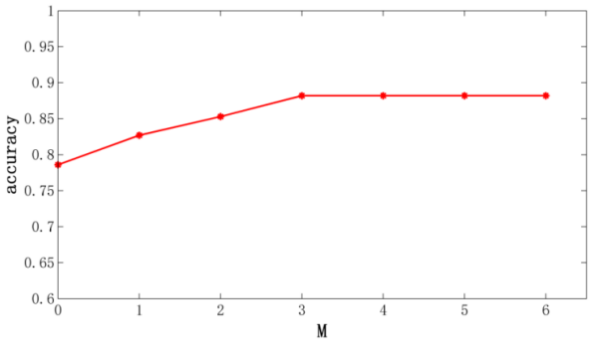

Fig. 8. The influence of maximum number of extension M.

As we can see in Fig. 8, the precision first increases with the increase of M, and then basically does not change when M>=3. Since the increase of M will increases the consumption of time, setting M=3 is the optimal choice.

Finally, we experiment to compare the performance of the classification model with and without feature expansion. The results are shown in Fig. 9.

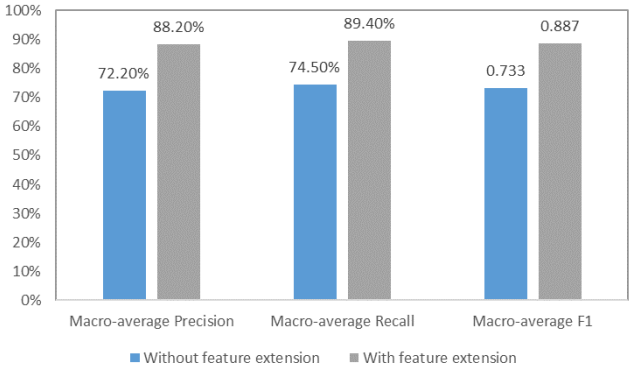

Fig. 9. Advantage of the feature extension.

Obviously, adding feature extension process can significantly improve performance of classification model.

2) Experiment for data source classification

In the second set of experiments, The performance of the Attention-based Bi-LSTM feature extraction and classification method is evaluated by comparison with existing methods. We compare our approach with the methods widely used for text classification. We choose the term frequency-inverse document frequency and support vector machine based(TF-IDF+SVM), latent dirichlet allocation and support vector machine-based(LDA+SVM), convolutional neural network (CNN) based Deep Web data source classification method as baselines. In this experiment, all results are obtained after the feature extension. The result of our experiments is shown in Fig.10.

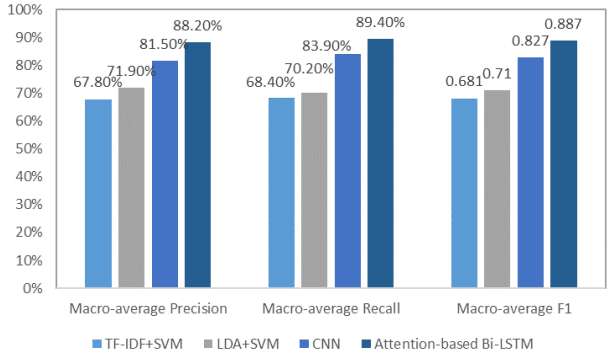

Fig. 10. The performance of different Deep Web data source classification method.

We use precision, recall and F-measure as evaluation indexes. Compare with two shallow learning methods based on SVM, our model outperforms them in precision by 20.4% and 16.3% respectively and in recall by 21.0% and 19.2%. Meanwhile, Attention-based Bi-LSTM classification model is 6.7% higher than CNN based method in precision and 5.5%

higher in recall. From Fig. 10 we can clearly see that our classification method has the best performance among the four methods.

Besides, we experiment to prove the optimization effect of the Attention mechanism on the classification model. The experimental results are shown in Fig. 11, where AVG indicates averaging and MAX indicates max-pooling.

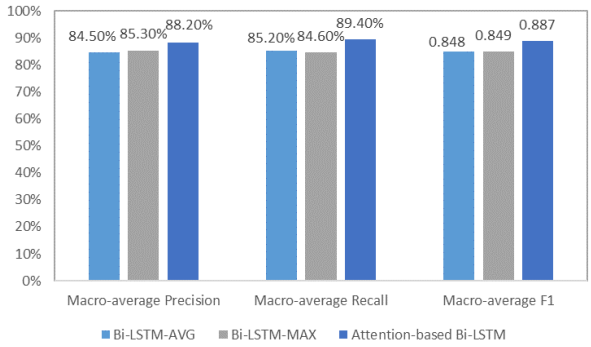

Fig. 11. Advantage of the attention mechanism.

Using the Attention mechanism to process the output at each time can obtain a more accurate vector representation of the text, thus achieving a more accurate classification of Deep Web data source. The model with Attention mechanism is 3.7% and 2.9% higher in precision and 4.2% and 4.8% higher in recall than models using averaging and max-pooling, respectively.

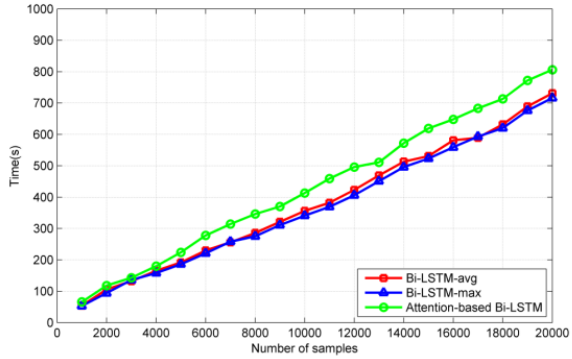

Fig. 12. Comparison of cost of time in training stage.

Finally, to prove that our classification method is feasible, we compare the network training time before and after adding the Attention mechanism when the network parameters and the number of samples are the same. In Fig. 12 we can see that the training time of model with Attention mechanism is longer than models that are not using it. However, the increase in training time is not significant. Therefore, the method we propose is completely feasible.

As can be seen from the above experimental results that the propose method is higher in precision than the existing method, and at the same time, there is no great increase in time consumption during the training stage.

IV. CONCLUSIONS

In this paper, we propose a Deep Web data source classification method based on text feature extension and extraction. In text feature extension stage, to solve the problem of feature sparseness, we built the feature extension using the N-gram model. In the Deep Web data source classification stage, we build a classification model based on Attention-based Bi-LSTM. Moreover, the Attention mechanism can give greater weight to words that are more relevant to the category of text, so that more accurate text vector representation can be obtained. The experimental results not only show that our model has significant advantages over the previous method, especially for Deep Web data sources with less text content, but also prove that the use of the Attention mechanism can improve the precision without a huge increase in the cost of training time. In conclusion, the Deep Web data source classification method based on text feature extension and extraction is a high performance and feasible method.

REFERENCES

[1] Lopez-Sanchez, Daniel, Gonzalez Arrieta, Angelica, Corchado, Juan M, "Visual content-based web page categorization with deep transfer learning and metric learning," NEUROCOMPUTING, pp. 418-431, 2019. DOI: 10.1016/j.neucom.2018.08.086.

[2] Feng Zhao, Jingyu Zhou, Chang Nie, Heqing Huang, Hai Jin, "SmartCrawler: A Two-Stage Crawler for Efficiently Harvesting Deep-Web Interfaces," IEEE Transactions on Services Computing, vol. 9, no. 4, pp. 608-620, 2016. DOI: 10.1109/TSC.2015.2414931.

[3] Marin Castro, Heidy Marisol, Sosa Sosa, Victor, Nuno Maganda, "Automatic construction of vertical search tools for the Deep Web," IEEE Latin America Transactions, 2018, vol. 16, no. 2, pp. 574-584, Feb. 2018. DOI: 10.1109/TLA.2018.8327415.

[4] Hernandez, Inma, Rivero, Carlos R, Ruiz, David, "Deep Web crawling: a survey," WORLD WIDE WEB-INTERNET AND WEB INFORMATION SYSTEMS, pp. 1577-1610, 2019. DOI: 10.1007/s11280-018-0602-1.

[5] Yuan, Jing, et al, "Result Merging for Structured Queries on the Deep Web with Active Relevance Weight Estimation," Information Systems, 64:93-103, 2017. DOI: 10.1016/j.is.2016.06.005.

[6] Barrio, Pablo, L. Gravano, "Sampling strategies for information extraction over the deep web," Information Processing & Management, 53.2:309-331, 2017. DOI: 10.1016/j.ipm.2016.11.006.

[7] Prafful Mishra, "Accuracy Crawler: An Accurate Crawler for Deep Web Data Extraction," 2018 International Conference on Control, Power, Communication and Computing Technologies (ICCPCCT), 2018. DOI: 10.1109/ICCPCCT.2018.8574286.

[8] Ye Hongfan, Cao Buqing, Peng Zhenlian, "Web Services Classification Based on Wide & Bi-LSTM Model," IEEE ACCESS, 43697-43706, 2019. DOI: 10.1109/ACCESS.2019.2907546.

[9] Z. Wang, Z. Qu, "Research on Web text classification algorithm based on improved CNN and SVM," 2017 IEEE 17th International Conference on Communication Technology (ICCT), Chengdu, pp. 1958-1961, 2017. DOI: 10.1109/ICCT.2017.8359971.

[10] Fatih Ertam, "Deep learning based text classification with Web Scraping methods," 2018 International Conference on Artificial Intelligence and Data Processing (IDAP), 2018. DOI: 10.1109/IDAP.2018.8620790.

[11] Serkan Ballı, Onur Karasoy, "Development of content-based SMS classification application by using Word2Vec-based feature extraction," IET Software, Volume: 13, Issue: 4, 2019. DOI: 10.1049/iet-sen.2018.5046.
[12] Shi M, Tang Y, Liu J, "Functional and Contextual Attentionbased LSTM for Service Recommendation in Mashup Creation," IEEE Transactions on Parallel and Distributed Systems, pp:1-1, 2018. DOI: 10.1109/TPDS.2018.2877363.
[13] Yanliang Jin, Can Luo, Weisi Guo, Jinfei Xie, Dijia Wu, Rui Wang, "Text Classification Based on Conditional Reflection," IEEE Access, Volume: 7, pp: 76712-76719, 2019. DOI: 10.1109/access.2019.2921976.
[14] Yangsen Zhang, Jia Zheng, Yuru Jiang, Gaijuan Huang, Ruoyu Chen, "A Text Sentiment Classification Modeling Method Based on Coordinated CNN-LSTM-Attention Model," Chinese Journal of Electronics, volume 28, pp: 120-126, 2019, DOI: 10.1049/cje.2018.11.004.
[15] B. Sun, P. Zhao, "Feature extension for Chinese short text classification based on topical N-Grams," 2017 IEEE/ACIS 16th International Conference on Computer and Information Science (ICIS), Wuhan, pp. 477-482, 2017. DOI: 10.1109/ICIS.2017.7960039.
[16] Xinwei Zhang, Bin Wu, "Short Text Classification based on feature extension using The N-Gram model," 2015 12th International Conference on Fuzzy Systems and Knowledge Discovery (FSKD), Zhangjiajie, pp. 710-716, 2015. DOI: 10.1109/FSKD.2015.7382029.
[17] Yang, Zichao, et al, "Hierarchical Attention Networks for Document Classification," Conference of the North American Chapter of the Association for Computational Linguistics: Human Language Technologies, 1480-1489, 2017.DOI: 10.18653/v1/n16-1174.
[18] Ullah, J, Ahmad, K, Muhammad, M. Sajjad, S. W. Baik, "Action Recognition in Video Sequences using Deep Bi-Directional LSTM With CNN Features," IEEE Access, vol. 6, pp. 1155-1166, 2018. DOI: 10.1109/ACCESS.2017.2778011.
[19] L. Gao, Z. Guo, H. Zhang, X. Xu, H. T. Shen, "Video Captioning With Attention-Based LSTM and Semantic Consistency," IEEE Transactions on Multimedia, vol. 19, no. 9, pp. 2045-2055, 2017. DOI: 10.1109/TMM.2017.2729019.
[20] K. Fu, J. Jin, R. Cui, F. Sha, C. Zhang, "Aligning Where to See and What to Tell: Image Captioning with Region-Based Attention and Scene-Specific Contexts," IEEE Transactions on Pattern Analysis and Machine Intelligence, vol. 39, no. 12, pp. 2321-2334, 2017. DOI: 10.1109/TPAMI.2016.2642953.
[21] Y. Wang, P. Yu, H. Li, H. Li, "Research on the Recognition of Offline Handwritten New Tai Lue Characters Based on Bidirectional LSTM," International Conference on Network, Communication, Computer Engineering, 2018. DOI: 10.2991/ncce-18.2018.189.
[22] Kim B, Chung K, Lee J, Seo J, Koo M.-W, "A Bi-LSTM memory network for end-to-end goal-oriented dialog learning," Computer Speech & Language, 53, 217-230, 2019. DOI: 10.1016/j.csl.2018.06.005.
[23] W. Du, Y. Wang, Y. Qiao, "Recurrent Spatial-Temporal Attention Network for Action Recognition in Videos," IEEE Transactions on Image Processing, vol. 27, no. 3, pp. 1347-1360, 2018. DOI: 10.1109/TIP.2017.2778563.
[24] F. Fahimi, C. Guan, W. B. Goh, K. K. Ang, C. G. Lim, T. S. Lee F. Fahimi, "Personalized features for attention detection in children with Attention Deficit Hyperactivity Disorder," 2017 39th Annual International Conference of the IEEE Engineering in Medicine and Biology Society (EMBC), Seogwipo, pp. 414-417, 2017. DOI: 10.1109/EMBC.2017.8036850.
[25] Zhang Y, Gao X, Peng X, Ye J, Li X, "Attention-Based Recurrent Temporal Restricted Boltzmann Machine for Radar High-Resolution Range Profile Sequence Recognition," Sensors, 18, 1585, 2018. DOI: 10.3390/s18051585.
[26] Shen C, Huang T, Liang X, Li F, Fu K, "Chinese Knowledge Base Question Answering by Attention-Based Multi-Granularity Model," Information, 9, 98, 2018. DOI: 10.3390/info9040098.
[27] M. Ali, S. Khalid, M. H. Aslam, "Pattern-Based Comprehensive Urdu Stemmer and Short Text Classification," IEEE Access, vol. 6, pp. 7374-7389, 2018. DOI: 10.1109/ACCESS.2017.2787798.
[28] N. Kumar Nagwani, "A Comment on "A Similarity Measure for Text Classification and Clustering," IEEE Transactions on Knowledge and Data Engineering, vol. 27, no. 9, pp. 2589-2590, 2015. DOI: 10.1109/tkde.2015.2451616.
[29] C. Liu, W. Hsaio, C. Lee, T. Chang, T. Kuo, C. Liu, "Semi-Supervised Text Classification With Universum Learning," IEEE Transactions on Cybernetics, vol. 46, no.

Yuancheng Li, received the Ph.D degree from University of Science and Technology of China, Hefei, China, in 2003. From 2004 to 2005, he was a postdoctoral research fellow in the Digital Media Lab, Beihang University, Beijing, China. Since 2005, he has been with the North China Electric Power University, where he is a professor and the Dean of the Institute of Smart Grid and Information Security. From 2009 to 2010, he was a postdoctoral research fellow in the Cyber Security Lab, college of information science and technology of Pennsylvania State University, Pennsylvania, USA.

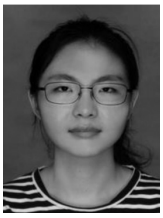

Guixian Wu was born in 1994 in guizhou Province, China. Since 2018, she has been a master's student in computer science and technology at north China electric power university in Beijing, China. Her research interests include text processing and artificial intelligence applications.

Xiaohan Wang was born in 1993 in Beijing, China. He received B.S. degree in information security from North China Electric Power University, Beijing, in 2016. Since 2016, he is a M.S. candidate in computer science and technology at North China Electric Power University. His research interests include natural language

The International Federation for Information Processing (IFIP) Networking 2020 Conference (NETWORKING 2020) will be held in Paris, France. This is the 19th event of the series, sponsored by the IFIP Technical Committee on Communication Systems (TC6). Accepted papers will be published in the IFIP Digital Library and submitted to the IEEE Xplore Digital Library. High quality papers will be recommended for fast track publications in selected journals.

The main objective of Networking 2020 is to bring together academic and industrial experts of the networking community to discuss the most recent advances in networking, to highlight key issues, identify trends, and develop a vision of the future Internet from a design, deployment and operation standpoints. Networking 2020 technical sessions will be structured around the following yet non limitative areas:

- Network Architectures, Applications and Services
- Network Modeling, Analysis and Operation
- Network Security and Privacy
- Wireless Networking

SUBMISSION GUIDELINES

The technical program committee welcomes paper submissions on all topics related to computer and communication networks. All submitted papers will be judged based on their quality and relevance through single-blind peer review. Only original papers that have not been published or submitted for review elsewhere will be considered. Submitted papers should be written in the English language, with a maximum length limit of 9 printed pages, including all the figures, references, and appendices. Papers longer than 9 pages will not be reviewed. All papers must be submitted in the Portable Document Format (PDF) electronically using EDAS. When submitting the paper, the title, all co-authors, and a concise abstract of up to 200 words should be provided to EDAS: https://edas.info/N25747 as the metadata of the paper. The metadata should be provided before the abstract registration deadline.

An author of an accepted paper is required to register for the conference at the full (member or non-member) rate and the paper must be presented by an author of that paper at the conference unless the TPC co-chairs grant permission for a substitute presenter before the conference. Non-refundable registration fees must be paid prior to uploading the final correctly formatted, publication-ready version of the paper. Accepted and presented papers will be published in the IFIP Digital Library and IEEE Xplore Digital Library.

To ensure appropriate consideration of conflicts of interest during the review process, changes to the list of authors are prohibited once a paper has been submitted for review. Should a paper be accepted, the complete list of authors, including the ordering of authors, must remain identical as the EDAS metadata in the final camera-ready manuscript.

IMPORTANT DATES

Title/Abstract submission: Dec 31, 2019
Full paper submission: Jan 7, 2020
Notification of acceptance: Apr 1, 2020
Camera-ready version: May 7, 2020
Full Event (Conference & workshops): June 22-26, 2020
IFIP Networking Conference: June 23-25, 2020

ORGANIZATION COMMITTEE

GENERAL CHAIR:
Guy Pujolle, Sorbonne University, France
Raouf Boutaba, University of Waterloo, Canada

PROGRAM CHAIRS:
Xiaoming Fu, U. Göttingen, Germany
Silvia Giordano, SUPSI, Switzerland
Christian Jacquenet, Orange Labs, France

STEERING COMMITTEE:
Robert Bestak, Czech Technical University in Prague, Czech Republic
Jordi Domingo-Pascual, UPC, Spain
Andrea Passarella, IIT-CNR, Italy
Henning Schulzrinne, Columbia University, USA
Burkhard Stiller, University of Zurich, Switzerland
Joerg Widmer, IMDEA Networks, Spain

Homepage: https://networking.ifip.org/2020

region 8 IEEE

IEEE Italy Section

UNIVERSITÀ DEGLI STUDI DI PALERMO

MELECON 2020 is a major international forum presenting design methodologies, techniques and experimental results in emerging electro-technologies. It is one of the flagship conferences of the IEEE Region 8 with participants from all over the world. It is expected to bring together researchers and practitioners from different fields of Electrical Engineering. The technical program will include plenary sessions, regular technical sessions, special sessions, poster sessions and tutorials. Prospective authors are invited to submit their manuscripts reporting original work as well as proposals for special sessions (6-8 papers) and tutorials in the mentioned areas.
For this edition, topics of interest include but are not limited to:

TRACK 1: Smart Mobility
Chairs
Rosario Miceli, University of Palermo.
Alberto Reatti, University of Firenze

1.1. Electric vehicle transportation systems and their environmental impact, charging infrastructure and grid integration

1.2. Transportation electrification, electric & hybrid vehicle, interconnected cities

1.3. Business models and technical solutions for smart mobility of people and goods

1.4. Public Transportation and shared mobility networks and their management, rail traffic management

1.5. Water transportations, infrastructures, vessel traffic management and shipboard electrical power systems

1.6. Air transportation, avionics and aerospace, more electric aircrafts

TRACK 2: Industry 4.0
Chairs
Giovanni Stea, University of Pisa
Rosario Sorbello, University of Palermo

2.1 Security, Privacy and Data Openness

2.2 Cloud-based Systems and Applications

2.3 Industrial Internet, 5G and Internet of Things

2.4 Wireless sensor nodes and energy harvesting

2.5 Artificial Intelligence and Big Data Analytics

2.6 Robotics, Automation and Advanced Manufacturing

2.7 Embedded and Cyber-physical systems

TRACK 3: Smart Healthcare
Chairs
Sergio Cerutti, Politechnic of Milano
Costantinos Pattichis, University of Cyprus

3.1. Services, Applications and Solutions to Challenging Problems in Smart Healthcare

3.2. Big Data Integration and IoT for Smart HealthCare

3.3. E-Health and Personalised Medicine

3.4. Neural and Cognitive Engineering

3.5. Advances in Medical Informatics for HealthCare Applications

3.6. Biotechnolgies: advanced Devices and Sensors

3.7. Bio-electromagnetic modelling

TRACK 4: Smart Grids
Chairs
Gaetano Zizzo, University of Palermo
Samuele Grillo, Politechnic of Milano

4.1. Smart and sustainable islands

4.2. Net zero energy systems

4.3. The Mediterranean energy hub

4.4. Demand response and prosumers' aggregation

Prospective Authors of papers are invited to submit a paper (typically 4-6 pages in standard IEEE two-column format) via EDAS by suggesting the related Track and Technical Session. The paper should contain a complete description of the proposed contribution along with results, suitably framed in the related state of the art. Each paper will be reviewed in terms of relevance with respect to the scope of the event, originality and quality of the technical content, overall organization and writing style. Papers must be prepared according to the Author's instructions reported on the MELCON2020 Website: **http://www.melecon2020.org**
Submission of papers implies intention to register and present the related content at the conference. Proceedings papers presented at the Conference will be submitted for inclusion in the IEEE Xplore Digital Library.

IMPORTANT DATES

Deadline for Submission of Special Session Proposalas	2 December 2019
Deadline for submission of Tutorials	16 December 2019
Deadline for Submission of papers	16 December 2019
Notification of acceptance	17 February 2020
Deadline for submission of camera-ready papers	25 March 2020
Early registration	17 April 2020

Honorary Chair
Magdalena Salazar Palma - IEEE R8 Director

General Chairs
Guido Ala, University of Palermo
Bernardo Tellini, IEEE Italy Section Chair
Tiziana Tambosso, IEEE Italy Section Past-Chair

Steering Committee
Ermanno Cardelli, University of Perugia
Dario Petri, University of Trento
Margaretha Eriksson, Past-Director Region 8
Costas Stasopoulos, Past-Director Region 8
Antonio Luque, Director-Elect Region 8
Peter Nagy, R8 Conference Coordinator
Mike Hinchey, UK&Ireland Session Chair
Yuval Beck, Israel Section Chair
Mohamme El Mohajir, Melecon2018 General Chair
C. S. Pattichis, Melecon2016 General co-Chair
E. Kyriakides, Melecon2016 General co-Chair
Salvatore Favuzza, University of Palermo
Adriano Fagiolini, University of Palermo

Technical Program Committee Chair
Giambattista Gruosso, Politecnico di Milano
Technical Program Committee co-Chair
Gaetano Zizzo, University of Palermo

Publication Chair
Pietro Romano, University of Palermo

Professional Activities and Tutorial Chair
Salvatore Favuzza, University of Palermo

Publicity Chair
Elisa Francomano – University of Palermo
Salvatore Favuzza, University of Palermo

Special Meeting and Exhibition for innovative start up and entrepreneurship
Vincenzo Piuri (IEEE Italy Section Entrepreneurship Coordinator)
Fabio Montagnino (Consorzio ARCA)

Women in engineering event
Dajana Cassioli, IEEE Italy Section WIE-AG Chair

Student and Young Professional Activity
Paolo Maresca, IEEE Italy Section SAC Coordinator
Fabio Viola, University of Palermo

Treasurer
Sergio Rapuano IEEE Italy Section Treasurer

Local Organization Committee
Guido Ala, Pietro Romano, Fabio Viola, Rosario Miceli, Salvatore Favuzza, Gaetano Zizzo, Elisa Francomano, Ciro Spataro, Valentina Cosentino, Graziella Giglia, Patrizia Livreri, Antonino Imburgia, Giuseppe Schettino, Dario Di Cara, Filippo Pellitteri, Massimo Caruso, Rossano Musca, Giuseppe Rizzo

Secretariat
Pietro Romano, University of Palermo
Fabio Viola, University of Palermo

Webmaster
Antonio Virdis, University of Pisa

Contact: fabio.viola@unipa.it

Guidelines for our Authors

Format of the manuscripts

Original manuscripts and final versions of papers should be submitted in IEEE format according to the formatting instructions available on

https://journals.ieeeauthorcenter.ieee.org/
Then click: "IEEE Author Tools for Journals"
- "Article Templates"
- "Templates for Transactions".

Length of the manuscripts

The length of papers in the aforementioned format should be 6-8 journal pages.
Wherever appropriate, include 1-2 figures or tables per journal page.

Paper structure

Papers should follow the standard structure, consisting of *Introduction* (the part of paper numbered by "1"), and *Conclusion* (the last numbered part) and several *Sections* in between.
The Introduction should introduce the topic, tell why the subject of the paper is important, summarize the state of the art with references to existing works and underline the main innovative results of the paper. The Introduction should conclude with outlining the structure of the paper.

Accompanying parts

Papers should be accompanied by an *Abstract* and a few *index terms (Keywords)*. For the final version of accepted papers, please send the short cvs and *photos* of the authors as well.

Authors

In the title of the paper, authors are listed in the order given in the submitted manuscript. Their full affiliations and e-mail addresses will be given in a footnote on the first page as shown in the template. No degrees or other titles of the authors are given. Memberships of IEEE, HTE and other professional societies will be indicated so please supply this information. When submitting the manuscript, one of the authors should be indicated as corresponding author providing his/her postal address, fax number and telephone number for eventual correspondence and communication with the Editorial Board.

References

References should be listed at the end of the paper in the IEEE format, see below:

a) Last name of author or authors and first name or initials, or name of organization
b) Title of article in quotation marks
c) Title of periodical in full and set in italics
d) Volume, number, and, if available, part
e) First and last pages of article
f) Date of issue
g) Document Object Identifier (DOI)

[11] Boggs, S.A. and Fujimoto, N., "Techniques and instrumentation for measurement of transients in gas-insulated switchgear," IEEE Transactions on Electrical Installation, vol. ET-19, no. 2, pp.87–92, April 1984. DOI: 10.1109/TEI.1984.298778

Format of a book reference:

[26] Peck, R.B., Hanson, W.E., and Thornburn, T.H., Foundation Engineering, 2nd ed. New York: McGraw-Hill, 1972, pp.230–292.

All references should be referred by the corresponding numbers in the text.

Figures

Figures should be black-and-white, clear, and drawn by the authors. Do not use figures or pictures downloaded from the Internet. Figures and pictures should be submitted also as separate files. Captions are obligatory. Within the text, references should be made by figure numbers, e.g. "see Fig. 2."
When using figures from other printed materials, exact references and note on copyright should be included. Obtaining the copyright is the responsibility of authors.

Contact address

Authors are requested to submit their papers electronically via the EasyChair system. The link for submission can be found on the journal's website:

www.infocommunications.hu/for-our-authors

If you have any question about the journal or the submission process, please do not hesitate to contact us via e-mail:

Pál Varga – Editor-in-Chief:
pvarga@tmit.bme.hu

Rolland Vida – Associate Editor-in-Chief:
vida@tmit.bme.hu

Special Issue

of the **Infocommunication Journal**

Call for Papers

"Cognitive Infocommunications Theory and Applications"

Cognitive infocommunications (CogInfoCom) investigates the link between the research areas of infocommunications and cognitive sciences, as well as the various engineering applications which have emerged as the synergic combination of these sciences. The primary goal of CogInfoCom is to provide a systematic view of how cognitive processes can co-evolve with infocommunications devices so that the capabilities of the human brain may not only be extended through these devices, irrespective of geographical distance but may also be blended with the capabilities of any artificially cognitive system. This merging and extension of cognitive capabilities are targeted towards engineering applications in which artificial and/or natural cognitive systems are enabled to work together more effectively.

This special issue collects the latest results emerging on the field of Cognitive Infocommunications.

Guest Editor:

Prof. Peter Baranyi DSc.,
Budapest University of Technology and Economics

Important dates:

Submission deadline: **30th of December, 2019**
Notification of the first review: **1st of March, 2020**
Deadline for revision is **1st of April 2020**
Camera Ready submission is **10th of May, 2020**

Regarding manuscript submission information, please visit:
https://www.infocommunications.hu/for-our-authors

SCIENTIFIC ASSOCIATION FOR INFOCOMMUNICATIONS

Who we are

Founded in 1949, the Scientific Association for Infocommunications (formerly known as Scientific Society for Telecommunications) is a voluntary and autonomous professional society of engineers and economists, researchers and businessmen, managers and educational, regulatory and other professionals working in the fields of telecommunications, broadcasting, electronics, information and media technologies in Hungary.

Besides its 1000 individual members, the Scientific Association for Infocommunications (in Hungarian: Híradástechnikai Tudományos Egyesület, HTE) has more than 60 corporate members as well. Among them there are large companies and small-and-medium enterprises with industrial, trade, service-providing, research and development activities, as well as educational institutions and research centers.

HTE is a Sister Society of the Institute of Electrical and Electronics Engineers, Inc. (IEEE) and the IEEE Communications Society.

What we do

HTE has a broad range of activities that aim to promote the convergence of information and communication technologies and the deployment of synergic applications and services, to broaden the knowledge and skills of our members, to facilitate the exchange of ideas and experiences, as well as to integrate and harmonize the professional opinions and standpoints derived from various group interests and market dynamics.

To achieve these goals, we…

- contribute to the analysis of technical, economic, and social questions related to our field of competence, and forward the synthesized opinion of our experts to scientific, legislative, industrial and educational organizations and institutions;
- follow the national and international trends and results related to our field of competence, foster the professional and business relations between foreign and Hungarian companies and institutes;
- organize an extensive range of lectures, seminars, debates, conferences, exhibitions, company presentations, and club events in order to transfer and deploy scientific, technical and economic knowledge and skills;
- promote professional secondary and higher education and take active part in the development of professional education, teaching and training;
- establish and maintain relations with other domestic and foreign fellow associations, IEEE sister societies;
- award prizes for outstanding scientific, educational, managerial, commercial and/or societal activities and achievements in the fields of infocommunication.

Contact information

President: **GÁBOR MAGYAR, PhD** • *elnok@hte.hu*

Secretary-General: **ERZSÉBET BÁNKUTI** • *bankutie@ahrt.hu*

Operations Director: **PÉTER NAGY** • *nagy.peter@hte.hu*

International Affairs: **ROLLAND VIDA, PhD** • *vida@tmit.bme.hu*

Address: H-1051 Budapest, Bajcsy-Zsilinszky str. 12, HUNGARY, Room: 502

Phone: +36 1 353 1027

E-mail: *info@hte.hu*, Web: *www.hte.hu*